Modeling Piston Skirt Lubrication in Internal Combustion Engines

by

Dongfang Bai

M.Sc., Automotive Engineering
Tsinghua University, 2007

and

B.Sc., Automotive Engineering
Tsinghua University, 2004

Submitted to the Department of Mechanical Engineering in Partial Fulfillment of the Requirements for the Degree of Doctor of Philosophy in Mechanical Engineering

at the

Massachusetts Institute of Technology

June 2012

Signature of Author .....
Department of Mechanical Engineering
May 04, 2012

Certified by .....
Tian Tian
Principle Research Engineer, Department of Mechanical Engineering
Thesis Supervisor

Certified by .....
Wai Cheng
Professor, Department of Mechanical Engineering
Committee Chair

Accepted by .....
David E. Hardt
Chairman, Department Committee on Graduate Studies
Department of Mechanical Engineering

Modeling Piston Skirt Lubrication in Internal Combustion Engines

by

Dongfang Bai

Submitted to the Department of Mechanical Engineering
on May 04, 2012, in partial fulfillment of the
requirements for the degree of
Doctor of Philosophy in Mechanical Engineering

Abstract

Ever-increasing demand for reduction of the undesirable emissions from the internal combustion engines propels broader effort in auto industry to design more fuel efficient engines. One of the major focuses is the reduction of engine mechanical losses, to which the friction of the piston skirt is one important contributor. Yet there lacks a sufficient understanding of the skirt lubrication behavior to effectively optimize the piston skirt system in practice.

The ultimate goal of this work is to develop a comprehensive model to advance the predictability of the skirt friction while integrating all the dynamic behavior of the piston secondary motion and the structural deformation of the piston skirt and cylinder liner. Major contributions of this work are analysis of and development of a model for the oil transport and exchange of the piston skirt region and its surroundings. The new oil transport model is composed with two elements. First, the oil scraped into the chamfer region by the oil control ring during a down-stroke is tracked and its accumulation and release to the skirt region are modeled. Second, oil separation and re-attachment are allowed in the skirt region, breaking conventional full-attachment assumption in lubrication studies. The new oil transport model together with hydrodynamic and boundary lubrication model were coupled with piston secondary motion and structural deformation of the piston skirt and cylinder liner. For numerical efficiency and physics clarity, we used different discretization for the lubrication from the structural deformation.

The final model is robust and efficient. The discussion of the model results is focused mainly on the oil transport. There exist a general pattern in available oil for skirt lubrication, namely, skirt tends to be starved when it travels at the upper portion of a stroke. Comparison with visualization experiment for oil accumulation patterns show consistency between model prediction and observation.

This work represents a major step forward to realistically predicting skirt friction and the influence of all the relevant design and operational parameters. However, oil supply to the region below the piston skirt can largely influence the outcome of the friction prediction and its mechanism is system dependent. Additionally, simple

treatment of the oil transport in the current model is merely a first step to modeling the complex fluid problems involved. Improvements of this model based on application and further analysis will make it a more powerful engineering tool to optimize the skirt system to minimize its undesirable outputs.

Thesis Supervisor: Tian Tian
Title: Principle Research Engineer, Department of Mechanical Engineering

Acknowledgments

There are many people who I would like to thank for their contributions to this research, and to my time at MIT. In particular I would like to thank my supervisor Dr. Tian Tian and the rest of my thesis committee members, Prof. Wai Cheng and Prof. Douglas P. Hart, for their support and guidance throughout my PhD. Their depth of knowledge and experience has significantly contributed to this research and to my learning experience at MIT. I would also like to thank my peer worker Ralf, Eric B. Senzer and Dallwoo Kim, who helped to support my model work through lab experiments. I absorbed numerous knowledge and ideas through the intense and inspiring discussions with them. I couldn't have finished the work without their continuous help in these entire five years.

I would also like to take this opportunity to thank our research sponsors, Daimler, Mahle, PSA, Renault, Toyota, Volkswagen, Argonne National Lab and Volvo for their financial and more specifically, their representatives, Hans-Jurgen Fuesser, Matthias Martin, Rolf-Gerhard Fiedler, Eduardo Tomanik, Remi Rabute, Bengt Olson, Fredrick Stromstedt, Gabriel Cavallaro, James Labiak, Max Maschewske, Randy Lunsford, Bernard laeer, Paulo Urzua Torres, Tom Shieh, Yeongching Lin, Guilleaume Mermazrollet and others for their continued encouragement over the years, and for sharing their extensive experience with me.

My appreciation also goes to members of MIT Sloan Automotive Lab for the opportunity to develop friendships and knowledge. In particular I would like to thank Steve Przesmitzki, Fiona McClure, Ke Jia, YinChun Wang, Haijie Chen, Camille Baelden, Dian Xu, Justin Ketterer, Kai Liao, Yujun Wang and Yong Li for their help to make the stressful time more fun.

Finally, I also would like to thank my parents and family for support throughout my time here.

Contents

List of Figures

List of Tables

Chapter 1

Introduction

1.1 Project Motivations

Internal combustion engines are widely used for propulsion in vehicles. Due to the huge amount of vehicles on road, the use of IC engines contributes significantly to air pollution and fossil fuel consumption. As a result, there is ever-increasing demand for improving fuel efficiency and reducing engine emission, while achieving proper control of noise and oil consumption. As these concerns are strongly affected by the piston skirt-cylinder liner interactions, a good understanding of the skirt-liner interaction is required.

The purpose of this study is to model and better understand piston secondary motion and piston skirt lubrication of internal combustion engines. The piston secondary motion is an important phenomenon in internal combustion engine. The mutual dependence between the piston motion and the skirt lubrication significantly impact almost all the major concerns in engine design, such as frictional loss, oil consumption, wear and seizure, and engine noise.

It is estimated that mechanical friction loss accounts for around 10% of the total energy in the fuel for a diesel engine. And $40 - 55\%$ of the friction losses are due to the power cylinder system, made up of the piston($25 - 47\%$), ring-pack($28 - 45\%$) and connecting-rod bearings($18 - 33\%$). Since the amount of friction loss generated at the piston skirt-liner interface can be about 40% of total piston assembly friction,

there is a large potential in improving the engine efficiency by reducing the friction between the piston skirt and the cylinder liner.

The piston skirt-liner interaction also affects engine noises. Piston secondary motion causes piston slap, which is a short duration impulsive type of sound that can be detected by human ear. The piston slap also excites the engine components such as cylinder block resulting in engine noise. Sliding contacts between piston skirt and cylinder liner also affect wear, piston seizure and liner damage due to cavitation from the coolant side in heavy duty engines with wet liners.

The skirt-liner interface also determines the boundary condition for the oil control ring. It serves as the first step oil control. The amount of oil that can accumulate below the oil control ring affects eventually how much oil can pass the oil ring. So the skirt-liner interaction affects oil consumption.

The design criteria for piston are often conflicting in nature. For example, in order to reduce engine friction, smaller skirt-liner clearance is favorable as tighter clearance gives less dynamics. On the other hand, small clearance may cause larger frictional losses.

Due to the complex nature of the system, a sufficiently accurate model of the system is needed in order to provide better understanding of the system and help engine design.

1.2 Introduction to Power Cylinder System and Skirt Lubrication

Figure 1-1 shows the power cylinder system of internal combustion engines, which is the system to be studied. The power cylinder system can be considered to be made up of ring pack, piston, wrist pin, connecting rod, crankshaft and cylinder bore. During engine operation, the chemical energy in the fuel is converted to kinetic energy and transmitted through the piston, wrist pin and connecting rod to the crankshaft. The crank-slider mechanism allows the linear motion of the piston to be converted to the

rotation of the crankshaft. Ideally, the piston has only one degree of freedom, allowing a reciprocating motion along the cylinder axis, which is commonly referred to as its primary motion. More realistically, due to the clearance between piston and cylinder liner and the connecting rod angle variation, the piston can have both transverse and rotational motion, which is called secondary motion.

For a working engine, the top two rings seal the gases in the combustion chamber to minimize energy loss and blow by. The oil ring controls oil consumption while providing proper oil film for the top two ring lubrication. Although the ring pack is not the objective of this thesis work, the piston dynamics can significantly impact the ring pack, and an accurate model of the piston motion is required as an input for ring pack analysis.

The piston skirt supports the side force and guides the motion of the whole system. Due to the connecting rod angle, there is a side force acting on piston from the pin, causing lateral motion. The side force can be quite significant, resulting in friction, wear or even surface failure if the skirt-liner interface is not lubricated properly. For example, the side force can reach 20,000 Newton for heavy duty diesel engine.

In order to reduce friction and wear, the skirt lubrication problem need to be analyzed. As the piston skirt slides over the liner under the side force, hydrodynamic pressure will be generated between the two surfaces to support the side force. The length scales in the sliding direction and circumferential direction are in the order of 10-100 mm while the length scale of the clearance between the skirt and liner is in the order of 1-100um. So the film thickness is significantly small relative to the length scales along the other two dimensions even when assuming there is full of oil between the skirt and liner. Then the inertia terms in the Navier-Stokes equation can be neglected and the Navier-Stokes equation can be simplified to the Reynolds equation.

Intuitively, if the side force is relatively high and there is not sufficient oil between the skirt and liner, solid-solid contact might occur. Hence one important factor of skirt lubrication is the amount of lubricant oil available between the skirt-liner interface. To answer this question, we need to know how the oil enters and leaves the system.

The lubrication oil for the piston may come from the oil sump by means of splash. In some engines, oil is also sprayed to the inside of the piston mainly for cooling purpose. The oil can then be transported to the skirt-liner interface. The oil may return to the oil sump through the drain holes or being scraped down by the bottom of the skirt. Some of the oil may go across the oil ring to the land region, contributing to oil consumption and emission. Not only the total amount of oil is important, how the oil is distributed and transported within the system also plays a significant role. Within the system, the oil is far from uniformly distributed. Solid-solid contact may still occur due to limited oil locally with big oil puddle unused somewhere else. The distribution of oil within the system also changes with time. There can be oil transport between piston skirt and liner due to couette flow and poiseuille flow, and oil transport along the skirt surface due to inertia driven flow. The complex nature of the oil transport requires a detailed model capturing the major physical phenomenon and describing the oil distribution within the system.

Another important factor playing an important role is the geometry of the two surfaces, which includes the thermal expansions of the skirt and liner, the elastic deformation of the two surfaces and piston dynamics. Due to piston secondary motion, the side force acting on piston is changing with time. While the piston slides over the liner, the two surfaces also move towards or leave each other. So the dynamics of the piston couples with the skirt-liner lubrication, making the lubrication problem more complex. Also, due to the force generated between the skirt-liner interface, both surfaces will deform accordingly. Hence the lubrication also depends on the structural compliance of the surfaces.

1.3 Previous Modeling Work

There has been lot of research activities going on in piston secondary motion and skirt lubrication using both analytical models and experimental studies.

Dursunkaya and Keribar[6] described the general model for the analysis of secondary motion in conventional and articulated piston assemblies. Motions of the

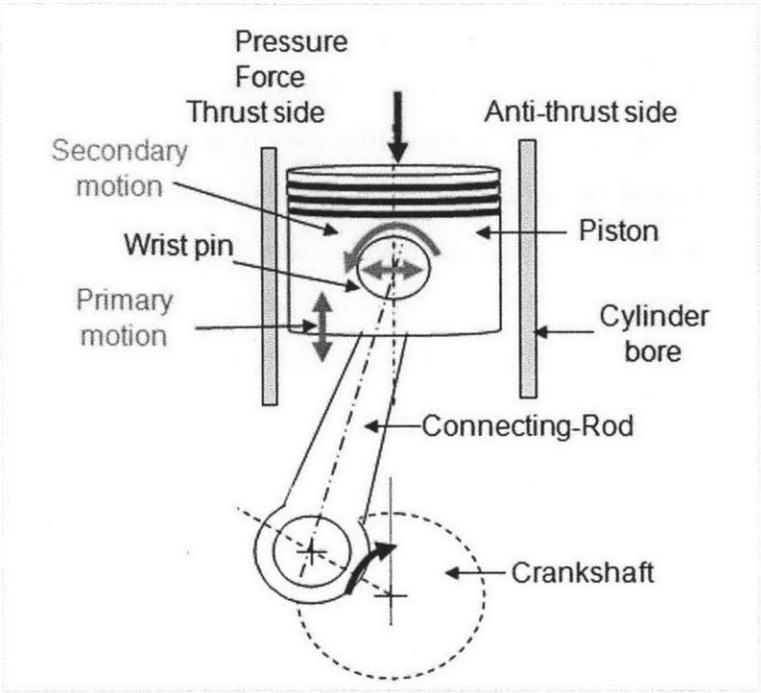

Figure 1-1: Power Cylinder System

piston, pin, and connecting rod were separately calculated by integrating equations of motion for individual components and dynamics degrees of freedom. Detailed sub models of skirt and piston pin lubrication were utilized to calculate the effects of lubrication oil film. Hydrodynamic bearing analysis was used to calculate the forces/torques transmitted at the piston pin bearings. Dursunkaya et al. developed an elastohydrodynamic skirt lubrication model. The piston secondary dynamics, skirt lubrication and skirt elastic deformations were solved simultaneously. Skirt deformations were calculated using a skirt compliance matrix derived from a finite element model of the piston.

Patir and Cheng[3] have developed an average Reynolds equation to model the oil film in lubrication region. Dong Zhu[4] [5] developed a mathematical model for mixed lubrication considering the effect of piston skirt waviness and roughness as well as the solid-to-solid asperity contact when the hydrodynamic pressure alone is insufficient to support the side load on piston.

Up to now, most of the important features, including mixed lubrication, skirt and

cylinder liner deformation, piston dynamics, simple assumption on availability of oil in this system, have been recognized and a lot of simulation models have been developed to predict secondary motion and friction. However, one important phenomenon those models fail to capture is the oil transport within the system. The oil film boundary condition in various studies is either assumed to be fully-flooded, or specified as a mass flux term (usually assumed to be in some simple form) at inlet boundary. Although it is meaningful to assume certain types of oil film boundary condition in term of parametric study, the actual oil film boundary conditions in real engines are much more complex and deserve a thorough study.

1.4 Scope of the Thesis Work

From the introductions presented in the previous sections, we can see the skirt lubrication performance depends on several entangled factors. The design of piston usually needs to consider the trade-offs between different goals. A robust and physics based model can help gain fundamental understanding of the system and help engine design. The ultimate objective of this thesis work is to develop such a model. Besides other significant factors, the oil transport between the skirt and its surroundings determines the amount of lubricant available. This factor plays a central role, but is not fully studied in previous research activities. This thesis project will try to capture the major oil transport within the system to provide a more realistic description of the oil film distribution.

The thesis work also get supports from experimental side. Here at MIT Sloan automotive lab, several graduate students (Eric Senzer, Ralf Hiller, Steve Przesmitski, reference internal consortium reports) have analyzed oil accumulation patterns in the piston skirt on a single cylinder engine with a visualization window on the liner using Two-Dimensional Laser-Induced Fluorescence (2D LIF) technique (please refer to the thesis of Przesmitzki Steve[24], Vokac[36] and Benoist Thirouard[35]). The 2D LIF results are analyzed extensively to better understand the oil transport within the system. A floating liner engine has also been set up in order to measure the friction

force of piston and piston rings.

The second chapter of this thesis introduces the dynamics and kinematics of the piston, which solves the necessary parameters used for skirt lubrication. It also describes the overall numerical solution method.

The third chapter then focuses on the skirt-liner interface. The major factors including the geometry, oil transport, separation and cavitation are analyzed. The model accounts for the oil exchange between piston skirt and its surroundings such as the skirt chamfer and the liner below the skirt.

The fourth chapter illustrates the solving method of the skirt lubrication problem. This model starts from the classical Reynolds' Equation. In order to track the oil transport more accurately, the model has considered the phenomena of oil separation and reattachment, and the corresponding inertia driven oil transport on the piston skirt surface. By doing so, the model can provide more realistic boundary condition for the skirt lubrication region. Furthermore, by keeping track of the oil mass on piston skirt and skirt liner separately, the model avoids the artificial oil mass transfer introduced by Reynolds' Equation when separation happens.

The fifth chapter shows some of the model results. The two-dimensional LIF observations are compared with the model prediction and the results are analyzed to gain deeper understanding of the system. Parametric studies of certain interesting parameters have also been carried out to show the strength and validity of the model.

The last chapter summarizes and concludes the thesis work and suggests potential future work on this topic.

Chapter 2

System Dynamics and Kinematics

This chapter describes the dynamics and kinematics of the power cylinder system. The main purpose is to determine the following parameters that are important for skirt-liner interaction:

- Driving force of piston lateral motion. Newton's second law says the acceleration a of the piston is parallel and directly proportional to the net force F and inversely proportional to its mass m. For the piston, the net force F can be decomposed into two parts, the driving part and the reacting part. Due to the connecting rod angle, both the combustion chamber pressure force and the inertia terms may lead to lateral force acting on the piston from the pin that will try to move piston laterally. Due to piston tilt angle, the combustion pressure force may also contribute a lateral force component. These are the driving force for piston lateral movement. Under the driving force, the piston moves laterally within the cylinder and interacts with the cylinder liner. The lateral force generated between the skirt-liner interface can be viewed as the reacting part. The driving force will be balanced by piston inertia and the reacting force generated between the skirt-liner interface. In the model, the driving force is determined by the dynamics and kinematics of the power cylinder system and is easier to solve. On the other hand, the force generated between the skirt-liner interface depends on the hydrodynamic pressure generation in the interface and

is more complex.

- Driving moment of piston tilt. Similar to the side force, the moment acting on the piston can also be divided into two parts, the driving part which comes from the wrist pin or directly from combustion pressure force, and the reacting part which comes from the skirt-liner interface. The net moment then gives piston angular acceleration. In the model, the driving moment will be solved from the system dynamics and kinematics.

- Other parameters related to piston primary motion that will be needed in solving the skirt-liner interaction. The first one is the piston sliding speed. The sliding speed affects how effective the hydrodynamic pressure can be generated. At hydrodynamic lubrication regime, with other parameters unchanged, higher sliding speed is more effective in generating hydrodynamic pressure. The second one is the piston acceleration along its sliding direction. As will be shown later, one mechanism that drives oil puddle in piston chamfer to move down to skirt lubrication region is the inertia term.

2.1 System Definition and Major Assumptions

During engine operation, the pistons, wristpins, connecting rods and crankshaft comprise the mechanism which captures a portion of the energy released by combustion and transforms that energy into useful rotary motion, as shown in Figure 2-1.

The coordinate system is defined in the figure, Z-axis is the cylinder axis, Y-axis is the thrust axis and X-axis is the wrist pin axis. Ideally, the piston only has a reciprocating motion along the cylinder axis (Z-axis), which is called the piston primary motion. This motion determines the instantaneous piston sliding speed at each crank angle, which is an important parameter for lubrication calculation. The primary motion also determines the lateral force acting on piston from the pin at each crank angle, providing the driving force for piston secondary motion. The piston lateral motion is along the Y-axis and the rotational motion of piston is around the

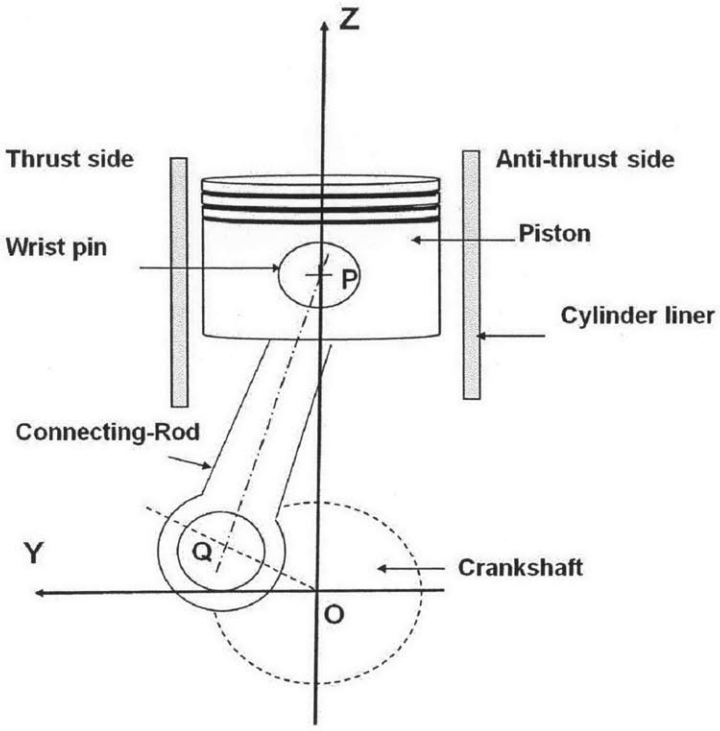

Figure 2-1: Power Cylinder System

X-axis. In the figure, point O is the center of crankshaft bearing, point Q is the center of connecting-rod large end bearing, and point P is the center of wrist pin bearing.

In order to solve for the driving force and driving moment acting on piston, the dynamics and kinematics of the power cylinder system is solved. In the thesis project, the following assumptions are made to simplify the calculation:

- The connecting rod big end bearing is frictionless. That is, the two components can rotate freely relative to each other without resisting friction generation.

- The wrist pin bearing is frictionless. This assumption greatly simplifies the calculation. Otherwise, a pin bearing lubrication model may be needed, which itself is quite complex. Further treatment can be asking the model user to supply the friction moment generated in the pin bearing, if the user has some knowledge of that.

- The connecting rod, wrist pin and piston are all rigid, with distributed mass. It

should be note that in the skirt-liner interface, the skirt structural deformation and the liner structural deformation, which are of the order of 100um, are considered. In the interface, this is a big number since the clearance profile between the skirt and liner is of the same order. However, when solving the dynamics and kinematics of the piston, these deformations can be neglected.

- Engine speed is assumed to be constant for now although extension to varying engine speed is straightforward.
- The wrist pin center of gravity is assumed to be at point P.

Given the large amount of symbols used in this chapter, a guideline for nomenclature is shown in Table 2.1.

2.2 System Dynamics

This section describes the equations describing the dynamics of each component. These information are needed in order to solve the force balance and moment balance for the system. Note that all the parameters in this section except ϕ,$\dot{\phi}$,$\ddot{\phi}$ and $a_{py}$are known at given crank angle. These four parameters depend on the piston secondary motion and will be solved iteratively as shown in later sections.

The position of Q with respect to O is given by

$$Z_{Q/O} = R_{CS} \cdot cos(\theta)$$

$$Y_{Q/O} = -R_{CS} \cdot sin(\theta)$$

Then the acceleration of Q is given by

$$a_{Qz} = \ddot{Z}_{Q/O} = -\omega^2 \cdot R_{CS} \cdot cos\theta$$

$$a_{Qy} = \ddot{Y}_{Q/O} = \omega^2 \cdot R_{CS} \cdot sin\theta$$

Table 2.1: Nomenclature

Symbol	Description
X-axis	The wrist pin axis.
Y-axis	The thrust axis, with positive y axis pointing to thrust side.
Z-axis	The cylinder axis, with positive z axis pointing upward.
Point O	Center of the crankshaft bearing.
Point Q	Center of the connecting-rod large end bearing.
Point P	Center of the wrist pin bearing.
R_{CS}	Crankshaft radius, the length of OQ.
L_{CR}	Connecting-rod length, the length of PQ.
R_{cb}	Nominal radius of cylinder bore.
R_{ps}	Nominal radius of piston skirt.
p_{com}	Combustion pressure.
y_{pin}	Pin offset.
m_{ps},m_{wp},m_{cr}	mass of piston, wrist pin and connecting-rod.
I_{ps},I_{wp},I_{cr}	moment of inertia of piston, wrist pin and connecting-rod with respect to their centers of gravity.
θ	Crankshaft angle, measure from positive Z-axis to OQ.
β	Connecting-rod angle, it is positive when $Y_{Q/O}$ is positive.
ϕ	Angular position of piston, also called piston tilt. The tilt angle is positive when the top of piston is tilt toward anti-thrust side.
$\dot{\beta}$, $\ddot{\beta}$	Angular velocity and acceleration of β.
$\dot{\phi}$, $\ddot{\phi}$	Angular velocity and acceleration of ϕ.
ω	Engine speed, $\dot{\theta}$.
$Y_{Q/O}$,$Z_{Q/O}$	Position of Q in Y direction and Z direction, relative to point O.
$Z_{P/O}$	Position of P in Z direction, relative to point O.
a_{Qz},a_{Qy}	Accelerations of point Q in Z direction and Y direction.
V_{pz}	Piston speed, it is positive when piston is moving toward top dead center.
a_{pz},a_{py}	Acceleration of point P in Z direction and Y direction.
Y_{crcg0},Z_{crcg0}	The original position of connecting-rod center of gravity with respect to point Q.
$Y_{crcg/Q}$,$Z_{crcg/Q}$	The position of connecting-rod center of gravity with respect to point Q when β is nonzero.
$Y_{crcg/O}$,$Z_{crcg/O}$	The position of connecting-rod center of gravity with respect to point O when β is nonzero.
a_{crcgz},a_{crcgy}	Accelerations of connecting-rod center of gravity in Z direction and Y direction.
Y_{pscg0},Z_{pscg0}	The original position of piston center of gravity with respect to point P.
$Y_{pscg/P}$,$Z_{pscg/P}$	The position of piston center of gravity with respect to point P when ϕ is nonzero.
$Y_{pscg/O}$,$Z_{pscg/O}$	The position of piston center of gravity with respect to point O when ϕ is nonzero.

The connecting-rod angle is given by

$$\beta = arcsin(\frac{Y_{Q/O}}{L_{CR}})$$

The connecting-rod angular velocity and angular acceleration are

$$\dot{\beta} = -\frac{\omega \cdot R_{CS} \cdot cos\theta}{L_{CR} \cdot cos\beta}$$

$$\ddot{\beta} = tan\beta \cdot (\dot{\beta})^2 + \frac{\omega^2 \cdot R_{CS} \cdot sin\theta}{L_{CR} \cdot cos\beta}$$

The vertical position of P with respect to O is

$$Z_{P/O} = Z_{Q/O} + L_{CR} \cdot cos\beta$$

The sliding speed and acceleration of piston primary motion are

$$V_{pz} = \dot{Z}_{P/O} = -\omega \cdot R_{CS} \cdot sin\theta - \dot{\beta} \cdot L_{CR} \cdot sin\beta$$

$$a_{pz} = \ddot{Z}_{P/O} = -\omega^2 \cdot R_{CS} \cdot cos\theta - \ddot{\beta} \cdot L_{CR} \cdot sin\beta - (\dot{\beta})^2 \cdot L_{CR} \cdot cos\beta$$

Figure 2-2 shows the connecting-rod geometry and position of its center of gravity. When there is nonzero connecting-rod angle β, the position of connecting-rod center of gravity with respect to point Q can be given by

$$Y_{crcg/Q} = Y_{crcg0} \cdot cos\beta - Z_{crcg0} \cdot sin\beta$$

$$Z_{crcg/Q} = Y_{crcg0} \cdot sin\beta + Z_{crcg0} \cdot cos\beta$$

And the position of connecting-rod center of gravity with respect to point O can be given by

$$Y_{crcg/O} = Y_{crcg/Q} + Y_{Q/O}$$

$$Z_{crcg/O} = Z_{crcg/Q} + Z_{Q/O}$$

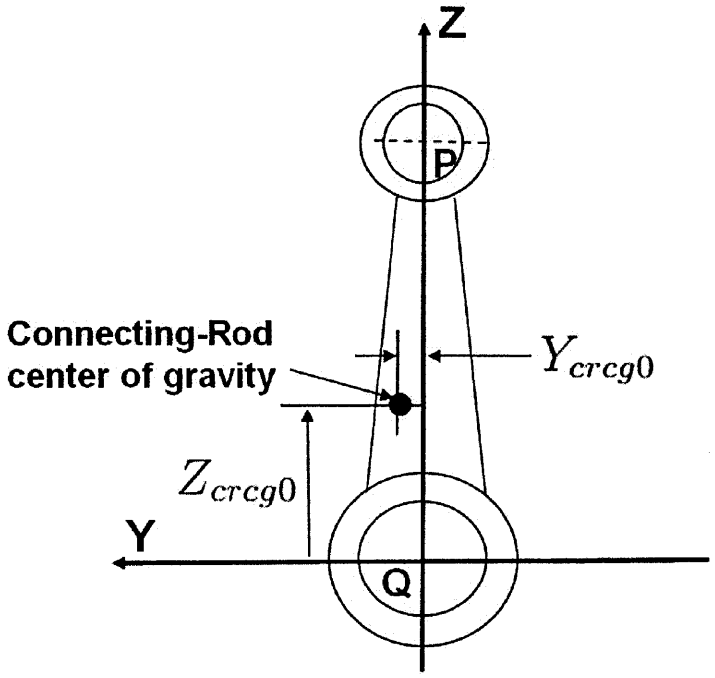

Figure 2-2: Connecting-rod geometry

Since the connecting-rod mass is quite large compared with piston mass, the inertia of connecting-rod cannot be neglected. The acceleration of connecting rod center of gravity (CG) is given here

$$a_{crcgy} = \ddot{Y}_{crcg/O} = a_{Qy} - \ddot{\beta} \cdot Z_{crcg/Q} - (\dot{\beta})^2 \cdot Y_{crcg/Q}$$

$$a_{crcgz} = \ddot{Z}_{crcg/O} = a_{Qz} + \ddot{\beta} \cdot Y_{crcg/Q} - (\dot{\beta})^2 \cdot Z_{crcg/Q}$$

Figure 2-3 shows the piston geometry and position of its center of gravity. When there is nonzero piston tilt angle ϕ, the position of piston center of gravity with respect to point P is given by

$$Y_{pscg/P} = Y_{pscg0} \cdot cos\phi - Z_{pscg0} \cdot sin\phi$$

$$Z_{pscg/P} = Y_{pscg0} \cdot sin\phi + Z_{pscg0} \cdot cos\phi$$

And the position of piston center of gravity with respect to point O is given by

$$Y_{pscg/O} = Y_{pscg/P} + Y_{P/O}$$

$$Z_{pscg/O} = Z_{pscg/P} + Z_{P/O}$$

Then the acceleration of piston center of gravity (CG) is given by

$$a_{pscgy} = \ddot{Y}_{pscg/O} = a_{py} - \ddot{\phi} \cdot Z_{pscg/P} - (\dot{\phi})^2 \cdot Y_{pscg/P}$$

$$a_{pscgz} = \ddot{Z}_{pscg/O} = a_{pz} + \ddot{\phi} \cdot Y_{pscg/P} - (\dot{\phi})^2 \cdot Z_{pscg/P}$$

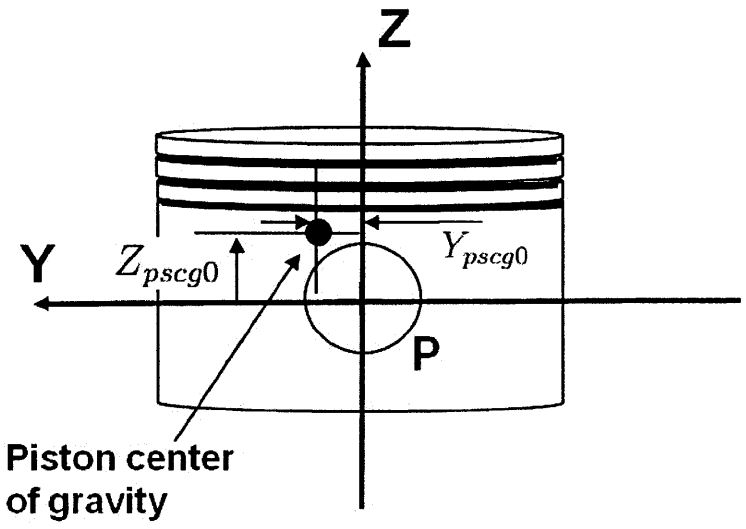

Figure 2-3: Piston geometry

2.3 System Kinematics

Based on the dynamics of each component, this section introduces the force balance and moment balance for each component.

First, the forces acting on the piston along Z direction are analyzed. Along Z direction, the piston is subject to the combustion chamfer pressure force on top of the piston, the force from the wrist pin and the frictional force generated between the

skirt-liner interface. Neglecting the frictional force since it is small compared with the other two, applying Newton's second law along Z direction to piston gives

$$Fz_{wp2ps} = -Fz_p + m_{ps} \cdot a_{pz}$$

Where Fz_{wp2ps} is the force acting on wrist pin from piston along Z direction. Fz_p is the force acting on piston along Z direction due to combustion chamber pressure. Note the these forces, positive value means the force is pointing to positive Z direction.

and the combustion chamfer pressure force Fz_p is given by

$$Fz_p = -p_{com} \cdot \pi r_{cb}^2$$

Then the forces acting on the wrist pin along Z direction are analyzed, which gives

$$Fz_{cr2wp} + Fz_{ps2wp} = m_{wp} \cdot a_{pz}$$

Where Fz_{cr2wp} is the force acting on wrist pin from the connecting rod along Z direction. Fz_{ps2wp} the force acting on wrist pin from piston along Z direction.

Note that

$$Fz_{ps2wp} = -Fz_{wp2ps}$$

Now we have

$$Fz_{wp2cr} = -Fz_{wp2ps} - m_{wp} \cdot a_{pz}$$

Then for the connecting-rod, apply the moment balance with respect to point Q. The lateral force acting on the connecting-rod from the pin can be solved to be:

$$Fy_{wp2cr} = \frac{-L_{CR} \cdot sin\beta \cdot Fz_{wp2cr} - Y_{crcg/Q} \cdot m_{cr} \cdot a_{crcgz} + Z_{crcg/Q} \cdot m_{cr} \cdot a_{crcgy} - I_{cr}\ddot{\beta}}{L_{CR} \cdot cos\beta}$$

Where Fy_{wp2cr} is the force acting on the connecting rod from wrist pin along Y

direction.

Then force balance of wrist pin along Y direction gives

$$Fy_{ps2wp} + Fy_{cr2wp} = m_{wp} \cdot a_{py}$$

Where Fy_{ps2wp} is the force acting on the pin from piston along Y direction. that is

$$Fy_{wp2ps} = -Fy_{wp2cr} - m_{wp} \cdot a_{py}$$

This lateral force Fy_{wp2ps} acting on piston is the main part of the driving force for piston lateral motion.

Due to piston tile angle, the combustion chamber pressure force also have a lateral component Fy_p acting on the piston, which is given by

$$Fy_p = -Fz_p \cdot tan\phi$$

Next, the forces acting on the wrist pin along Y direction are analyzed. Along Y direction, the piston is subject to the force generated between the skirt-liner interface Fy_{cb}, the lateral force from the pin Fy_{wp2ps} and Fy_p. According to Newton's second law, the forces should satisfy

$$Fy_{cb} + Fy_{wp2ps} + Fy_p = m_{ps} \cdot a_{py}$$

The equation above is essentially very complex. It involves the following unknown parameters:

- a_{py} and ϕ. They are related to the piston secondary motion.
- Fy_{cb}. The force generated between the skirt-liner interface, and need to be obtained by solving the hydrodynamic lubrication between the skirt and the liner.

Now we formulate the moment balance for the piston. Relative to the center of

gravity of the piston, the net moment T_{ps} acting on the piston includes the following parts.

- The moment from the pin, due to Fy_{wp2ps} and Fz_{wp2ps}.
- The moment T_{pcom} from combustion chamber pressure force. Usually when there is pin offset, this term can be significant around top dead center of expansion stroke. Due to piston tilt angle, the later force component may also contribute to T_{pcom}.

$$T_{pcom} = -Fz_p \cdot (y_{pin} + Y_{pscg/P})$$

- The moment T_{cb} from the skirt-liner interface.

$$T_{ps} = Fy_{wp2ps} \cdot Z_{pscg/P} - Fz_{wp2ps} \cdot Y_{pscg/P} + T_{pcom} + T_{cb}$$

Then Newton's Law states:

$$T_{ps} = I_{ps} \cdot \ddot{\phi}$$

Similarly to the force balance equation, the moment balance equation above also involves the piston secondary motion term (the tilt ϕ) and the detailed interaction between the skirt-liner interface.

2.4 Numerical Solution Method

2.4.1 The Unknowns

We have discussed the variables that will be needed in the model. In order to define the system dynamics with given engine operational parameters and crank angle, the unknowns can be simplified to be:

- The piston lateral displacement y_p and lateral velocity V_{py}. In the model, first order difference of velocity is used to calculate the lateral acceleration.

$$a_{py} = \frac{V_{py}^{i} - V_{py}^{i-1}}{\Delta t}$$

where V_{py}^{i} and V_{py}^{i-1} are the lateral velocity of point P of current time step and previous time step, respectively.

- The piston tilt angle ϕ and angular velocity $\dot{\phi}$. In the model, the angular acceleration is also calculated by first order difference:

$$\ddot{\phi} = \frac{\dot{\phi}^{i} - \dot{\phi}^{i-1}}{\Delta t}$$

where $\dot{\phi}^{i}$ and $\dot{\phi}^{i-1}$ are the angular velocity of piston of current time step and previous time step, respectively.

- The structural deformation of piston skirt and liner. Currently in the model, the deformation is related to the force field acting on the surface by the compliance matrix provided by model users.

Notice that while the clearance profile h is used to calculate the pressure distribution between the skirt and liner interface, the deformation d instead of h is chosen as the unknown. This is because the clearance is determined once the deformation and piston secondary motion ϕ, x_{py} is determined. In the model, two sets of grid are used. A coarse grid is used for structural deformation on which deformation d is defined. And a fine grid is used for hydrodynamic lubrication on which h is defined. So the clearance h on the fine grid is obtained by combining the piston secondary motion and the interpolated deformation on the fine grid.

Also notice that the oil transport does not show up here. In the model, a oil transport model is used to track the oil mass within the whole system and define the oil boundary condition for the skirt lubrication region. However, to simply the

calculation, explicit scheme is used for oil transport which decouples the oil transport model from the main model.

2.4.2 Globally Convergent Newton's Method

With the unknowns defined in previous section, we can state the governing equations that need to be satisfied by a feasible solution.

- Force balance for piston.
- Moment balance for piston.
- The relationship between deformation profile and calculated force field should satisfy the structural compliance.

This chapter describes in detail the algorithm for calculating the forces and moments. The calculation of force field between skirt liner interface is described in chapter 6.

In order to solve for these highly nonlinear equations, a globally convergent Newton's method is applied, which is a method for finding successively better approximations to the true solution. The fundamental idea is very simple. First choose proper initial guess of the unknowns vector X, which includes:

- Piston secondary motion.
- Skirt and liner deformation.

Use $FVEC(X)$ to denote the function vector which represents the governing equations. It includes the force balance, moment balance and deformation convergence:

- Force balance of piston along lateral direction.

$$FVEC(1) = Fy_{cb} + Fy_{wp2ps} + Fy_p - m_{ps} \cdot a_{py}$$

- Piston lateral velocity equation.

$$FVEC(2) = V_{py}^{i} - \frac{x_{py}^{i} - x_{py}^{i-1}}{\Delta t}$$

- Angular moment balance for piston.

$$FVEC(3) = Fy_{wp2ps} \cdot Z_{pscg/P} - Fz_{wp2ps} \cdot Y_{pscg/P} + T_{pcom} + T_{cb} - I_{ps} \cdot \ddot{\phi}$$

- Piston angular velocity equation.

$$FVEC(4) = \dot{\phi}^{i} - \frac{\phi^{i} - \phi^{i-1}}{\Delta t}$$

- The error in deformation. Assume the guessed deformation is d_0, the force field calculated accordingly is F_0, the compliance matrix is C, then the error in deformation for each node is given by

$$FVEC(5 : end) = CF_0 - d_0$$

With this guessed unknowns X, the initial clearance profile can be obtained and the lubrication between skirt liner interface can be calculated which gives the force generated there. Then the net force and net moment acting on piston can be calculated. Ideally, we should have

$$FVEC(X) = 0$$

That is, force and moment balance should be satisfied, and the deformation under the calculated force field should equal the initial guess of deformation, if the initial guess is the true solution. If this is not the case, the initial guess is not correct and need to be modified.

Now the problem becomes finding out the proper change ΔX in X such that $X + \Delta X$ is the true solution, and

$$FVEC(X + \Delta X) = 0$$

To get ΔX, which is called the Newton step, the Jacobean J of the equation system is calculated. That is, we try to relate the change in $FVEC(X)$ to the change in X:

$$FVEC(x + \Delta X) = FVEC(X) + J\Delta X = 0$$

Then ΔX can be solved from the linear system

$$J\Delta X = -FVEC(X)$$

When the function vector $FVEC(X)$ is sufficiently close to zero, as specified by some predefined stopping criterion, a solution is assumed to be obtained for the current time step and the model will move to next time step. Otherwise, the model will keep iterating until either a solution is obtained or failed if too many time steps have passes.

The Jacobean relates to the force and moment balance can be derived analytically from previous sections of this chapter. The Jacobean relates to the lubrication between skirt liner interface is derived in chapter 6.

One important point is the choosing of the stopping criterion. Sometimes the stopping criterion might be too strict and a convergent solution may not be possible with the resolution of the model.

Another point is the choosing of the Newton step, ΔX, sometimes the full step ΔX may be too big and may lead to divergence, particularly if the function vector is very nonlinear around X. So in the model, the full step will be tried first and the result will be checked to see whether stopping criterion becomes "smaller". If not, the Newton' step will be scaled by a small number and try again. Also note that the function vector is a vector, so a proper definition of "smaller" deserves careful

thinking. The elements of the function vector include the error in force, moment and deformation, with different unit and scale.

As Newton's method, the choice of initial guess deserves some consideration. Generally, the closer the initial guess is to the true solution, the faster the convergent result can be achieved. In the model, while time step is small enough and the differences between successive time steps are hopefully small as well, we can choose proper projection from previous time step results as the initial guess. Generally, convergent results can be obtained very quickly.

Chapter 3

Major Factors of Modeling Consideration

This chapter illustrates the major factors influencing the performance of skirt lubrication we are going to model. From the dynamics and kinematics of each component, the driving force of piston lateral motion can be calculated, as shown in chapter 2. The piston is pushed by this force to move laterally while being constrained by the cylinder liner. And this force will generally be balanced by the reacting force from the liner. For a typical engine, this force can achieve several thousand Newton during expansion stroke and will cause high friction force if the skirt liner interface is not well lubricated. The skirt is one of the major sources of engine friction. This emphasizes the need to build a physically based model for the skirt lubrication.

A lubrication problem includes the load being carried, the two surfaces in relative motion, and the lubricant in between. The load has already been discussed in detail in chapter 2. This chapter will start with an introduction to the geometry of the skirt liner interface. The geometry not only depends on the nominal profile, but also depends on the deformations of the surfaces. Then the lubrication between the skirt and the liner will be introduced. In order to properly define the oil boundary condition for the skirt lubrication region, the oil exchange between the skirt region and its surroundings is also analyzed.

3.1 The Geometry of the Interface

For a lubrication problem, the geometry is very important. The macro shape largely affects the ability of hydrodynamic pressure generation. At near contact area, micro geometric features can also be important, affecting both the hydrodynamic part and the asperity contact part.

The geometry we are talking about here includes four parts:

- Original skirt profile. This is the profile of the piston skirt when structural deformation due to carried force is not considered. This profile may include both the piston cold profile and the thermal expansion.
- Original liner profile. This is the profile of the cylinder liner when structural deformation due to carried force is not considered. This profile may include both the liner cold profile and the thermal expansion.
- Piston skirt structural deformation due to carried force.
- Cylinder liner structural deformation due to carried force.

Fig3-1 illustrates the general geometry for the piston skirt-liner interface. During engine operation, the skirt surface slides over the liner surface with a thin film of oil between them to lubricate the interface. This figure only shows the sliding direction (Z-axis) and the lateral direction (Y-axis), the third dimension is along the circumferential direction.

The length scales in the sliding direction (Z-axis) and circumferential direction are in the order of 10-100 mm while the length scale in the Y direction (the clearance between the skirt and liner) is in the order of 1-100um. The oil film thickness is usually very small compared with the length scales along the other two dimensions, even assuming there is full of oil between the skirt and liner. So the inertia terms in the Navier-Stokes equation can be neglected and the Navier-Stokes equation can be simplified to the Reynolds equation.

The lubrication performance of the skirt-liner interface depends heavily on the oil film thickness and the load (side force). Intuitively, when the oil film thickness is

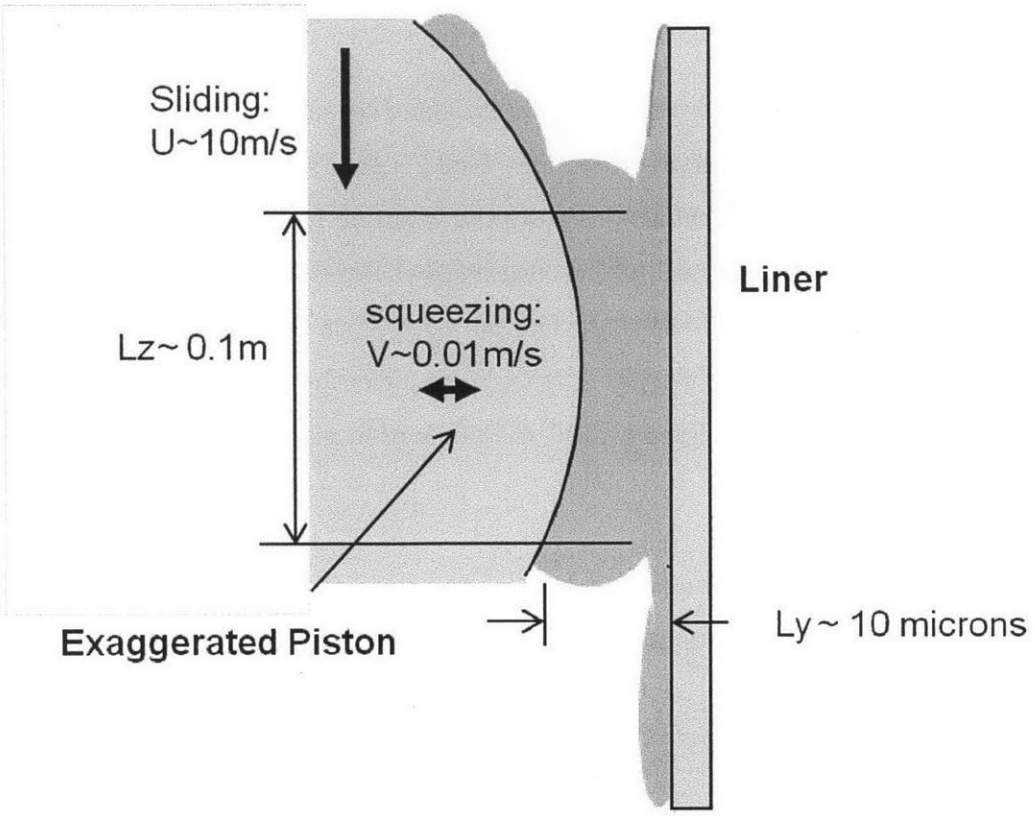

Figure 3-1: Piston skirt-liner interface

large relative to the wave height of surface texture (e.g. skirt tooling mark) and the side force is not too high, the skirt and liner are totally separated by oil film and the lubrication regime is hydrodynamic lubrication regime. On the other hand, when the oil film thickness is small relative to the wave height of surface texture and the side force is relatively high, the peaks of the tooling mark may penetrate the oil film and solid-solid contact may occur. The complexity comes from that the oil film thickness varies with both time and space, depending on the oil supply, surface profiles of the interface and engine operating conditions. In this section, the surface profiles of the skirt and liner will be illustrated. The detailed oil transport will be described later in this chapter.

3.1.1 Piston Skirt Geometry

The piston skirt profile is characterized by ovality along the circumferential direction and a barrel shape along the sliding direction. Fig3-2 shows a simplified piston skirt profile (top view) with ovality, which describes the variation in skirt radius along circumferential direction. Due to ovality, the clearance between skirt and liner is smaller around thrust side (and anti-thrust side) than pin side. Since the side force acting on piston mainly happens along the Y axis, it is most efficiently supported around the thrust and anti-thrust. With piston ovality, the lubrication mostly happens at thrust side and anti-thrust side.

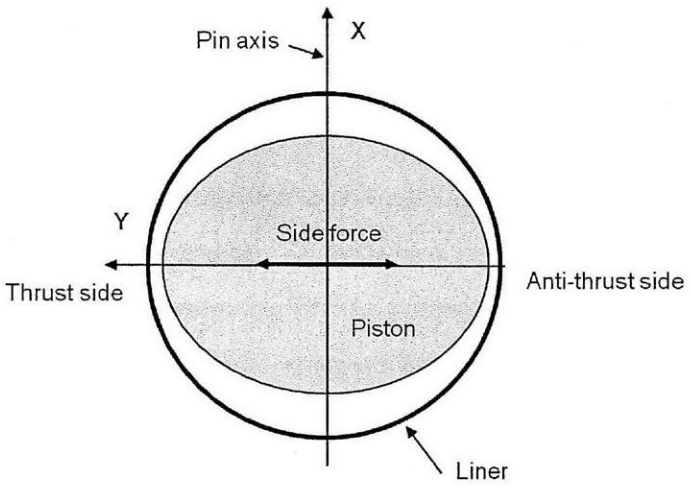

Figure 3-2: Piston skirt profile: ovality

The skirt barrel shape can be seen from fig3-1. Instead of being flat, the skirt has a curved macro shape which can reduce contact near the piston top and bottom lines. As the skirt moves over liner, the convergent profile will help generate hydrodynamic pressure and help support the side force.

Besides the macro geometric features including ovality and barrel shape, the micro geometric features such as surface texture also play a very important role. Fig3-3 shows the exaggerated skirt profile with triangular tooling marks machined on the surface along the circumferential direction. The wavelength can be around several hundred microns and the wave height can be around 10 to 20 microns, measured

from peak to valley. Since the oil film thickness is also at this order of magnitude, the effect of the surface texture cannot be neglected.

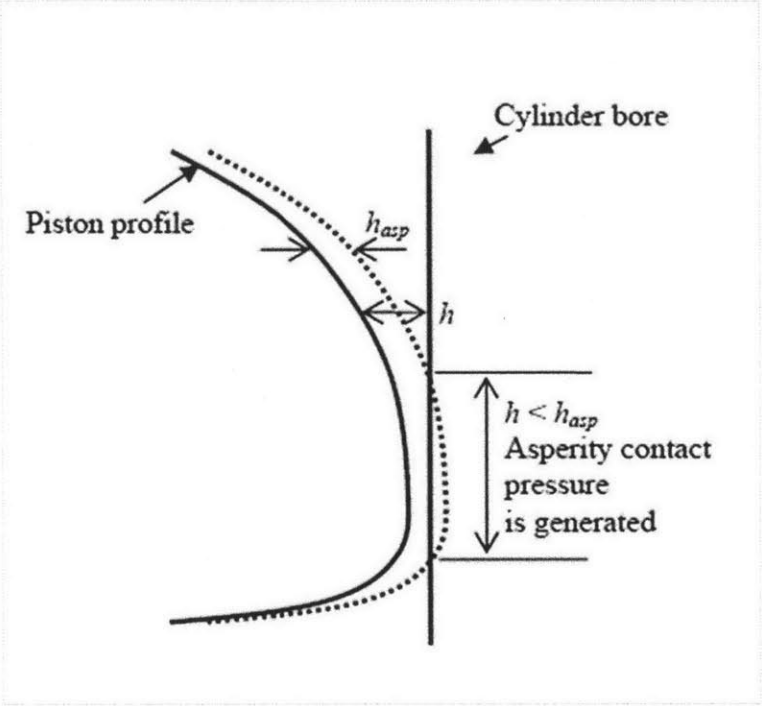

Figure 3-3: Piston skirt tooling marks

During engine operation, there will be temperature rise and the skirt will expand accordingly. Depending on the material of the skirt and the temperature distribution, the thermal expansion can reach 100um or even bigger around top of skirt. Since the temperature around the top of skirt is generally higher than the temperature around the bottom of skirt, upper skirt region generally expands more than lower skirt region.

3.1.2 Liner Geometry

As the other component of the skirt-liner interface, the overall shape of the liner is quite flat. However, due to the mechanical stress (e.g. the clamping forces that result from the installation of cylinder heads) and the dynamic stress (e.g. heat and pressure), the variations in cylinder bore radius can be comparable to the oil film thickness; hence can change the lubrication significantly. Due to the variations in

liner geometry, the height distribution (clearance between the skirt and liner) varies as piston moves over liner even assuming there is no piston lateral motion and tilt. The liner geometry, generally called bore distortion, is required as an input for the model and should be supplied by the model user.

3.1.3 Structural Compliance

The previous two sections have described the original profiles of the skirt and liner. However, since both the skirt and the liner are flexible, they will deform under the load field acting on them. When combustion pressure is high or engine speed is high, the piston skirt deformation due to combustion pressure and axial inertia can also reach the size of oil film thickness and thus need to be considered in the model. The resulting profile of each surface includes both the original profile (free of load) and the corresponding deformation. Typically, the surface deformation can reach 60 microns or even larger during expansion stroke and can significantly change the clearance distribution. The solution of the hydrodynamic and contact pressures and oil film thickness are very sensitive to the structural deformation of the two surfaces.

The current model does not directly work on the structure part. Instead, it is expected that the user will generate such information using their own finite element model. Then a preprocessing program is used to transform such information into proper format that is easy to use by the model.

Currently, the structure compliance information of the skirt and the liner are supplied by the so called compliance matrix. The details can be found in Fiona's thesis. Here only a simple introduction will be given.

In the model, a uniform grid is used and the deformations of the surfaces are defined on this grid. Denote the deformation of the nodes as d, which is a vector. Then clearly, the distribution of deformation d depends on the force distribution acting on the surfaces. Denote the force acting on the nodes as F, which is also a vector.

The compliance matrix C is such a matrix that relates the deformation to the force:

$$d = CF$$

That is, the compliance matrix C is a square matrix with entry $C_{i,j}$ representing the deformation at node i due to unit force applied at node j.

Since both skirt and line may deform, denote the compliance matrix of the skirt as C_s and the compliance matrix of the liner as C_l. Currently in the model, a 17 by 17 grid is used for skirt structural deformation. For liner, which is much larger than the skirt, another grid is used.

Although the whole liner may deform under the load generated between the skirt liner interface, only the part contained in the skirt liner interface is needed. Since in the end, it is the clearance h between the skirt and liner that is used in hydrodynamic pressure calculation, we can combine the skirt deformation and liner deformation. That is, at a given crank angle, the vertical position of the skirt is known, and the portion of liner that corresponds to the skirt is also known. Since only the deformation of this portion of liner is necessary to formulate the h, we can interpolate the liner compliance matrix C_l on the skirt grid and obtain the compliance matrix C_{ls} only for the portion of liner contained in the skirt-liner interface. In the model, in order to simply the calculation, C_{ls} and C_s are defined on the same grid. Then the total deformation of the skirt and liner can be given by

$$d_{total} = d_s + d_l = C_s F + C_{ls} F = (C_s + C_{ls}) F = C_{tot} F$$

Then in formulating the Jacobean, we can also use C_{tot}, which simplifies the calculation.

The skirt compliance matrix is a dense matrix. Typically, the central lower region of the piston skirt is softer than the sides and the upper region of the skirt. Notice that the central lower region is also usually where skirt will initially impact the liner. Thus this feature allows the contact region to deform and results in a larger area of hydrodynamic pressure generation. Therefore the peak pressure will decrease as the side force remains constant. For the liner, the compliance may depend on where the

liner is supported.

3.2 Contact Model

Between the skirt liner interface, not only hydrodynamic lubrication may happen, asperity contact may also occur. A proper sub-model dealing with the asperity contact pressure generation is needed. The asperity contact sub-model describes the way in which asperity pressure is generated by solid-solid contact as two surfaces approach each other. Clearly, this will depends on the material and the geometry. In the current model, we assume that there is horizontal triangular surface tooling marks on the skirt, as shown in Figure3-3. Nowadays, these coating is applied for adaptive break in to obtain better conformability.

With the presence of surface tooling marks, the contact pressure generation can be simplified as blunt wedge against flat plane by assuming flat liner locally, as shown in Figure3-4. Typically, the wavelength λ is much bigger than the wave height Ω, so it is justified to use the analytical solution for a blunt wedge against a plane given by Johnson (1985) to calculate the contact pressure based on given wavy contact deformation

$$\delta = \frac{\Omega}{2} - h$$

The details can be found in McClure's Thesis[13].

3.3 Skirt Liner Lubrication

This section introduces the oil film and hydrodynamic generation between the skirt and liner.

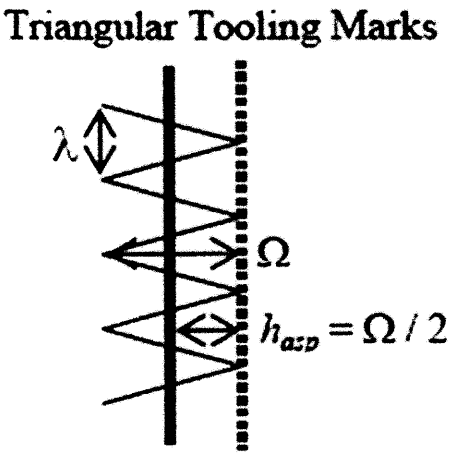

Figure 3-4: Triangular tooling marks

3.3.1 Reynolds' Equation at full film region

In the so called full film region where there is sufficient oil to fill the gap between the piston skirt and cylinder liner, the hydrodynamic lubrication between the two surfaces is governed by the Reynolds' Equation. It is derived from the Navier-Strokes equation under the Reynolds' assumptions of Newtonian lubricant, incompressible flow, thin film geometry, no slip between the lubricant and the solid surfaces, and negligible inertia and body forces. Here the geometry is a key assumption. Based on the observation that the length scale along the film thickness direction is much smaller than the length scale along the sliding and circumferential directions, the pressure gradient across the oil film can be neglected and the Navier-Strokes equation can be simplied to Reynolds' equation.

$$\frac{\partial}{\partial x}\left(\frac{h^3}{12\mu}\frac{\partial p}{\partial x}\right) + \frac{\partial}{\partial z}\left(\frac{h^3}{12\mu}\frac{\partial p}{\partial z}\right) = \frac{U}{2}\frac{\partial h}{\partial z} + \frac{\partial h}{\partial t}$$

In this equation, X refers to the circumferential direction, and Z refers to the

sliding direction, as described in chapter 1. U is the piston sliding speed which is in the range of 0-10m/s. h is the clearance (called height in the thesis) between the skirt and the liner. p is the hydrodynamic pressure generated. t refers to time and μ is the dynamic viscosity of the lubricant.

The Reynolds' Equation is essentially a statement of conservation principles. Intuitively, there are two mechanisms of oil transport at the skirt-liner interface, Couette flow and Poiseuille flow. Couette flow or shear flow is driven by the viscous drag force acting on the fluid due to the relative movement of the surfaces. Poiseuille flow or pressure flow is driven by the pressure gradient. The two terms at the left hand side of Reynolds' equation can be understood as the mass transported due to pressure gradients along X direction and Z direction. The term $\frac{h^3}{12\mu}$ can be called the interface conductivity and represents how easy the oil mass can be transported due to pressure gradient. It can be seen that with given pressure gradient, larger $\frac{h^3}{12\mu}$ allows more oil mass to across the interface. The term $\frac{U}{2}\frac{\partial h}{\partial z}$ represents the mass transported due to Couette flow along the piston sliding direction. And the $\frac{\partial h}{\partial t}$ term is the unsteady term which is the rate of change of mass. So Reynolds' Equation describes the mass conservation law.

3.3.2 Mechanisms of Pressure Generation

Since the main thesis project is based on the hydrodynamic pressure generation behavior of the skirt-liner interface which is described by Reynolds' Equation and some of its generalized forms, the mechanisms of pressure generation at the interface will be described here. From the pressure generation perspective, the right hand side of Reynolds' Equation represents the causes of pressure generation. The two terms at the left hand side are the reacting pressure distribution generated to satisfy the mass conservation principle. The term $\frac{U}{2}\frac{\partial h}{\partial z}$ represents the macro shape effect: pressure generation when lubricant oil is driven from shear drag force along a converging shape. The $\frac{\partial h}{\partial t}$ term represents the squeeze effect: pressure generation as the two surfaces moves toward each other. As described before, the two-dimensional profile of the height is characterized by the piston ovality along circumferential direction

and the barrel shape along the piston sliding direction. Because of piston secondary motion, the skirt will move toward or away from the liner. Also, since the cylinder liner is not ideally flat due to bore distortion and thermal expansion, as piston skirt slides over the liner, the height profile will change over time even when there is no piston secondary motion. The barrel shape of piston skirt and piston secondary motion contributes to the $\frac{\partial h}{\partial z}$ term, and can help generate hydrodynamic pressure, especially during mid-stroke when piston sliding speed U is high. The piston ovality contributes to the $\frac{h^3}{12\mu}$ term and generally allows the Poiseuille flow along circumferential direction to push oil to the left and right sides where height is large. The piston secondary motion, especially around top dead center of expansion stroke when piston slap happens (that is piston moves toward the liner laterally with very small piston sliding speed), can contribute to the $\frac{\partial h}{\partial t}$ term and help generate hydrodynamic pressure.

3.3.3 Cavitation and Partial Film

Cavitation and partial film are important phenomenon between skirt-liner interface. Cavitation may occur when the local pressure in the oil film reaches a level below the cavitation pressure of the oil for that temperature. Since lubricant oil can not exist at pressures below its cavitation pressure, once the local pressure drops to the cavitation pressure, the oil will start to cavitate and a void filled by oil vapor and dissolved gas will occur. This may happen when the skirt is leaving the liner due to piston secondary motion. This may also happen for sufficiently diverging macro shape. In the cavitation region, fluid pressure is assumed to be maintained at cavitation pressure, which is close to ambient pressure. The cavitation region is called partial film region in this thesis because the gap is only partially filled by oil.

The Jakobson-Floberg-Olsson (JFO) theory, as described by Elrod, proposes that the fluid field can be divided into two different regions, the full film region and the partial film region. The pressure generation in the full film region is still governed by the Reynolds' Equation. In the cavitation region, there is no pressure gradient and hence no Poiseuille flow.

3.3.4 Universal Reynolds Equation

The presence of cavitation makes the fluid field harder to solve since there are now two distinct regions with different governing equations. The first difficulty comes from how to decide the full film region and partial film region. Physically, cavitation will occur at locations where local hydrodynamic pressure drops to cavitation pressure, which requires knowledge of the hydrodynamic pressure distribution. However, the hydrodynamic pressure distribution is actually the unknowns we are trying to solve. Second, the unknowns at different regions are different. At full film region, the hydrodynamic pressure p is the unknown. At partial film region, the local pressure equals cavitation pressure which is known, while the local oil density ρ is unknown. So the location of full film (partial film) region and the pressure (density) distribution must be solved simultaneously and this makes the problem nonlinear.

Elrod proposed a Universal Reynolds Equation to solve this problem. The key point is to define a set of new variables that have different meanings in full film region and partial film region. Then the two different governing equations at partial film region and full film region can be combined to a single equation.

Instead of solving pressure and density directly, a indicator variable F is introduced. It will take value one at full film region and take value zero at partial film region. This indicator variable defines the flow region (partial or full). Then another global variable Φ is defined as follow. Now notice that the unknowns variables now are two global variables F and Φ that are valid at both full film region and partial film region, while the original unknown variable p and ρ are local variables that are only valid at their corresponding region.

$$p = F\Phi P_{ref}$$

$$\rho = [1 + (1 - F)\Phi]\rho_{ref}$$

Here P_{ref} is the scaling factor for pressure and is chosen to be 1bar. ρ_{ref} is the lubricant density.

In the full film region, $F = 1$ and Φ represents pressure. In the partial film region, $F = 1$ and $1 + \Phi$ represents the local oil filling ratio. In the full film region, $\rho = \rho_{ref}$ since the gap is full of oil. In the partial film region, $\rho = (1 + \Phi)\rho_{ref}$

The resulting Universal Reynolds Equation is given by:

$$\frac{\partial}{\partial x}\left(\frac{h^3}{12\mu}\frac{\partial(F\Phi)}{\partial x}\right)+\frac{\partial}{\partial z}\left(\frac{h^3}{12\mu}\frac{\partial(F\Phi)}{\partial z}\right) = \frac{U}{2}\frac{\partial}{\partial z}\{[1+(1-F)\Phi]h\}+\frac{\partial}{\partial t}\{[1+(1-F)\Phi]h\}$$

One key assumptions made in the Universal Reynolds Equation is the full attachment assumption. It's assumed that in the partial film region the lubricant attaches both the skirt and the liner. Then the velocity profile across the oil film has a linear form with minimum value zero at the liner surface and maximum value U at the skirt surface. It is under this assumption that the Couette flow term has its current form:

$$\frac{U}{2}\frac{\partial}{\partial z}\{[1+(1-F)\Phi]h\}$$

This full attachment assumption may be unrealistic. Imagine the case when the two surfaces are far away from each other and between them there is only relatively thin oil film. This situation is quite possible to happen due to piston secondary motion. Under this circumstance, the oil film on the skirt will be separated from the oil film on the liner and full attachment assumption will be incorrect and will lead to unrealistic redistribution of oil between the skirt-liner interface.

3.3.5 Average Reynolds Equation

From the Reynolds Equation, it can be seen that the height distribution h is one of the key parameters determining hydrodynamic pressure generation. While the macro profiles of the piston skirt and the liner are usually quite smooth, thus moderate amount of grid (about 50 to 100 both for sliding direction and circumferential direction) is enough to capture the macro shape. The micro geometrical feature such as skirt tooling marks does require much finer grid to accurately capture the local geometry. For example, the 2D LIF engine used partly as experimental supporting

to the thesis project has a skirt length of 30mm along sliding direction, and the skirt tooling marks wavelength is 0.25mm. If 16 grids are used for each wavelength, about 2000 grids is necessary along the sliding direction. Then even only use 20 grids along the circumferential direction, totally 40,000 grids are needed to discretize the calculation domain. Such a dense grid will require very long calculation time and will make the model not very useful as a design tool. Patir and Cheng developed an average Reynolds Equation to handle this problem. The main idea is using the averaged macro smooth profile for hydrodynamic pressure calculation. And use a set of flow factors to correct for the local micro geometric features. For the details, please refer to Dong Zhu.

For the thesis project, a deterministic model which uses fine grid to capture micro geometry is built to solve for the detailed hydrodynamic pressure generation. An average model is also built which uses the flow factor method. Choosing between the two reflects the trade-off between accuracy and calculation time.

3.4 Oil Transport

The oil boundary condition plays a predominant role in determining the lubrication condition of the skirt region. This section will introduce the oil transport between the skirt lubrication region and its surroundings.

3.4.1 Oil Transport Overview

In order to describe the oil transport between the skirt and its surroundings, the system is divided into three regions as shown in Figure3-5. Right below the oil control ring, there is a deep piston chamfer where the clearance between the skirt and the liner is usually quite big. Typical clearance at chamfer region can be several hundred microns. This is a big room that can hold lubricant oil and act as a oil reservoir. Because the large clearance, there is no direct pressure generation within chamfer region. Below the chamfer is the piston skirt region. The skirt region is where hydrodynamic pressure is generated. It is also where asperity contact may occur when

load is high and oil film is relatively thin. Below the skirt is the liner region where possible splash may happen and add oil onto the liner surface. Notice that the skirt region relevant here is defined by the piston positions at top dead center and bottom dead center. From TDC to BDC, the length that the piston travels is the stroke of the engine. For the whole system consisting of these three regions, the exchange of oil with its surroundings includes possible splash of oil to the liner below skirt, possible oil scraped down by the piston during down stroke and oil release through the oil control ring groove or drain holes (if there is any). While previous works generally only consider the skirt region and asks users to supply the boundary condition for the skirt region, the framework laid out here extends the system boundary and now the boundary condition of skirt region is integrated into the model.

In the current model, the splash of oil is taken as input. Generally splash is quite engine specific. For example, depending on whether there is oil jet and its flow rate as well as its orientation, the oil addition to the liner can be very different.

Here, it is also important to notice that in the system there are both full film region and partial film region, with different oil transport mechanisms for each region. At regions with oil attaching both the skirt and the liner, Couette flow and Poiseuille flow move oil around. At regions where oil film separates, there is zero pressure gradient and zero shear force, and thus the oil film on the liner will stay on the liner stationary while the oil film on the skirt will go with the skirt. If attach the coordinate with the skirt, it can be seen that two active oil transport mechanisms are oil dragged by the moving liner and the oil flow on the skirt surface driven by inertia. Details will be discussed in following sections.

3.4.2 Overall Oil Transport During Down Stroke

Clearly, the system is not symmetric and the oil transport processes of up stroke and down stroke are different. This section will give a big picture of the oil transport during down stroke, that is, when piston is moving downward from top dead center to bottom dead center, as shown in Figure3-6. Now the inlet boundary for the skirt

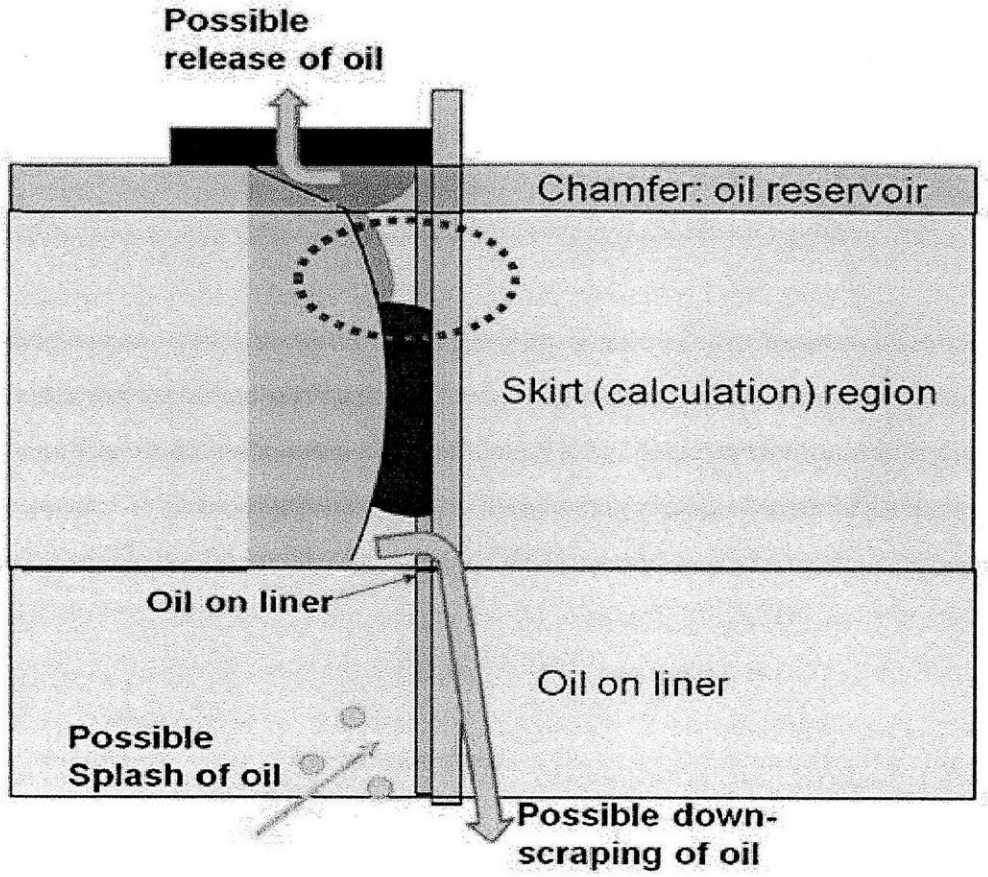

Figure 3-5: Oil transport overview

region is the bottom of skirt, and the oil supply to the skirt-liner interaction region is the oil on the liner below the skirt. At the outlet boundary for the skirt region, some oil will be dragged out of the skirt region with the liner. Because of the oil control ring scraping, most of the oil on the liner leaving the outlet boundary will be collected when it reaches the oil control ring. The scraped oil will accumulate in the piston chamfer during down stroke.

Fixing the coordinate with the piston skirt, the governing equation for the liner region below skirt is trivially rigid translation of the oil with the same speed of the liner. The governing equation of the skirt region is a form of Universal Reynolds' Equation with separation considered. For the inlet boundary, at least two scenarios

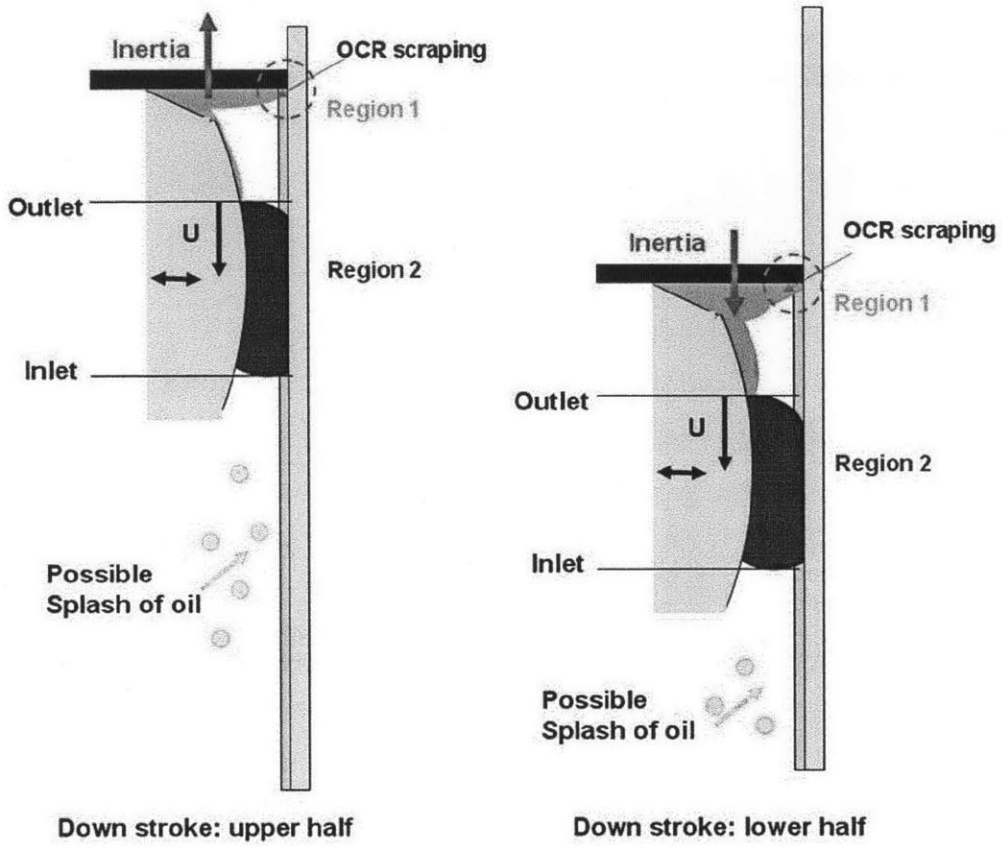

Figure 3-6: Oil transport during down stroke

may happen. Consider the case when the clearance between the skirt and liner is small and the oil film thickness on the liner below the skirt is very thick, then the situation is similar to fully-flooded inlet boundary condition, as shown in Figure3-7. On the other hand, when the clearance is relatively large, there may even not be sufficient oil to form full film region.

In the chamfer region, the movement of the accumulated oil depends on the inertia. When the piston is moving from top dead center to mid-stroke, it is accelerating. Relative to the piston, inertia will drive oil to move upward. On the other hand, when the piston is moving from mid-stroke to bottom dead center, it is decelerating and inertia will drive oil to move downward relative to the piston. So in this period, the oil may be driven out of the chamfer and move down to the skirt region. Nevertheless, it has been observed from the 2D LIF experiment that oil recirculation sometime may

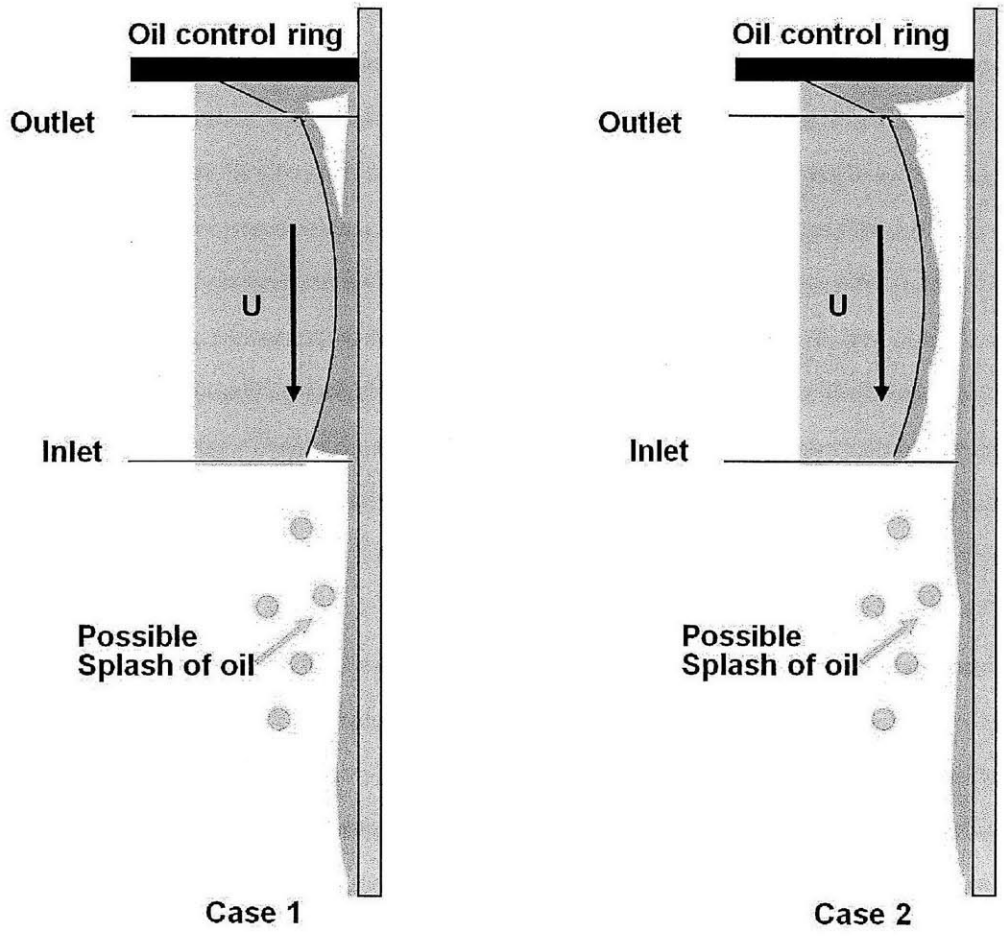

Figure 3-7: Two cases of oil transport during down stroke

occur. When the oil film is thick relative to the clearance at the neck region, the downward moving oil flow driven by inertia may touch the liner. Since now the liner moves up relative to the piston, it will drag the oil back to the chamfer region. So although inertia tends to drive oil out from chamfer, the liner may drag it back when the oil touches the liner. Generally, in this range, the oil film in chamfer is quite thick after having accumulating oil for half stroke, so oil recirculation is quite possible to happen. Also since inertia effect is strong only when the oil film is thick, while thick oil means recirculation is more likely to occur, so approximately the inertia effect is offset by the oil recirculation. This is intuitively true when the clearance is not so big which is generally the case.

3.4.3 Overall Oil Transport During Up Stroke

When piston is moving upward from bottom dead center to top dead center, the skirt follows the control ring. Typically, the oil control ring is designed to properly control the amount of oil that can pass it and reach the top two rings, which affects the oil consumption. To control oil consumption, the oil film thickness on the liner after the oil control ring is very thin, at the order of 0.5um. Now the inlet boundary for the skirt region is the top of skirt, and the oil supply to the skirt-liner interface is the oil from the chamfer.

Figure3-8 shows the oil transport during up stroke. When piston is moving upward from bottom dead center to mid-stroke, piston is accelerating and inertia will drive oil to flow downward relative to the piston. During this period, generally the oil supply to the skirt region is sufficient. There are several reasons. Firstly, the amount of oil accumulated within the chamfer reaches maximum near bottom dead center. So from bottom dead center moving up, there is large amount of oil available in the chamfer. Secondly, inertia is strong near bottom dead center. Thirdly, now the liner moves downward relative to the skirt. So if the oil film can touch the liner, the liner will also drag the oil with it and bring it to the skirt region.

However, the situation changes after mid-stroke. Firstly, a large portion of the oil in the chamfer has already been released, so there is much less oil in the chamfer. Secondly, inertia changes direction. Now piston is decelerating, and inertia will drive the oil to move up relative to the skirt, flowing back into the chamfer. Notice now the north boundary of the skirt is the inlet boundary, thus the skirt region has no boundary oil supply along skirt. However, sometimes it has been observed from 2D LIF results that the so called bridge effect may occur. That is, within the chamfer the oil flow driven by inertia shoot the liner and then spread out along the bottom of the oil control ring, and some of the oil may eventually reach the liner and may be dragged to the skirt region later on by the liner.

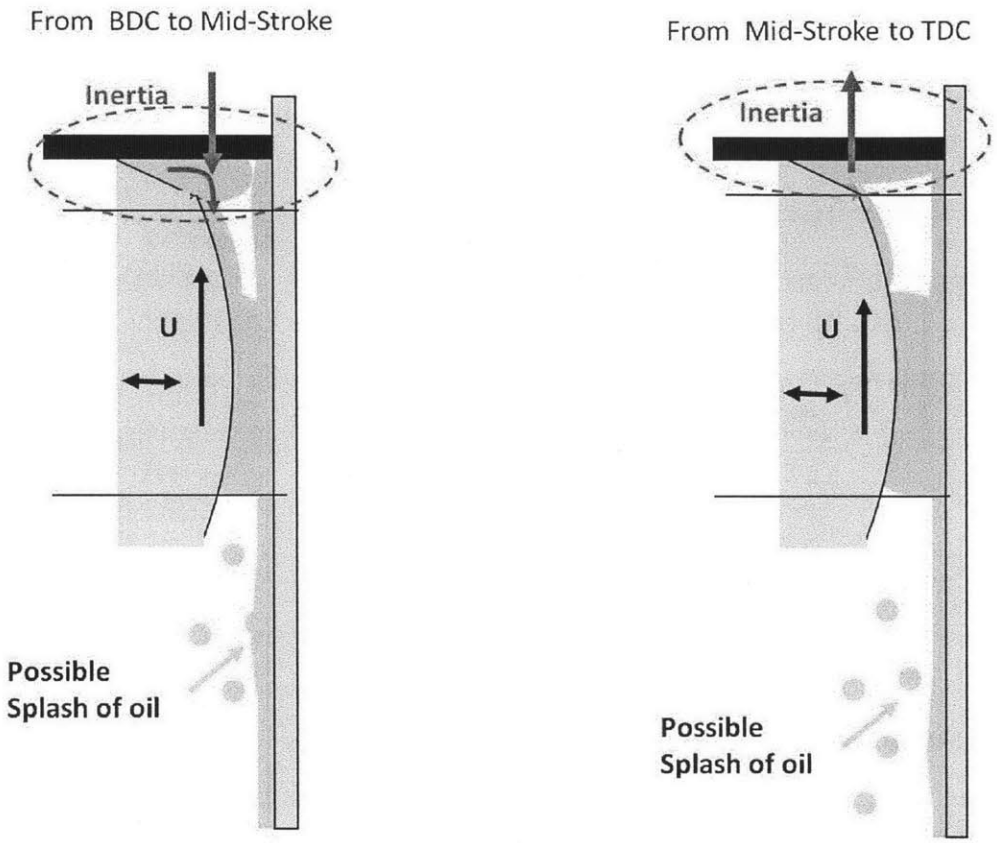

Figure 3-8: Oil transport during up stroke

3.4.4 Oil Release From Chamfer

This section will take a closer view at the oil release from the chamfer region. The skirt region is generally where direct skirt-liner interaction happens, while the chamfer serves as a reservoir of lubricant. Because of the barrel shape of the skirt along piston sliding direction, the clearance at the chamfer region is usually much bigger compared with the central skirt region. While the nominal clearance at the central skirt region is at the order of 10um, the nominal clearance at the chamfer region is at the order of 100um. During engine operation, although piston tilt may make the clearance at chamfer region smaller, usually the clearance at chamfer region is still quite large. So generally, both hydrodynamic lubrication and possible asperity contact will only happen at the skirt region. In the model, the skirt region is where both Reynolds Equation (in its proper form) and asperity contact are solved and is also where is

side force from the pin is mainly balanced. Although having no pressure generation, the chamfer region is very important as it defines the oil boundary condition for the skirt region. When piston is moving from bottom dead center to top dead center, the upper boundary of the skirt is the inlet boundary, and the only oil supply for the whole skirt lubrication region can only be the chamfer reservoir.

Now two important questions arise. The first question is totally how much oil is contained in the chamfer. If there is only very limited oil contained in the chamfer, it will not be able to supply sufficient oil to the skirt region. The second question is how the oil contained in the chamfer is released to the skirt region. What are the driving mechanisms that drive the oil to flow from chamfer region to skirt region, if there is any.The answer to the first question depends on the oil control ring scraping during downstroke. The answer to the second question will be analyzed here.

To understand the oil supply process from piston chamfer to skirt region, two-dimensional LIF experiment results are analyzed. Then the oil transport mechanisms identified from experiment observations are modeled. The two-dimensional LIF experiments, which are conducted by a couple of students including Eric, Ralf and dallwoo, help a lot in gaining better understanding of the oil transport. The experiment observations show the inertia driven flow at upper skirt region right below the chamfer.

Figure3-9 illustrates the inertia driven oil flow on the piston skirt. It is assumed that the oil film thickness on the skirt is less than the clearance between the piston skirt surface and the cylinder liner surface such that the oil film does not touch the liner and the upper surface of the oil flow is free surface. Notice that the inertia force only acts along the piston sliding direction (Z-axis), so the oil flow driven by the inertia force can be simplified to be one-dimensional. Please refer to Benoist Thirouard's thesis[35] and McGrogan's thesis[37] for more detail about the modeling of inertia driven flow.

The Navier-Stokes Equation is given by:

$$\frac{\partial w}{\partial t} + v\frac{\partial w}{\partial y} + w\frac{\partial w}{\partial z} = \nu\frac{\partial^2 w}{\partial y^2} + a_p$$

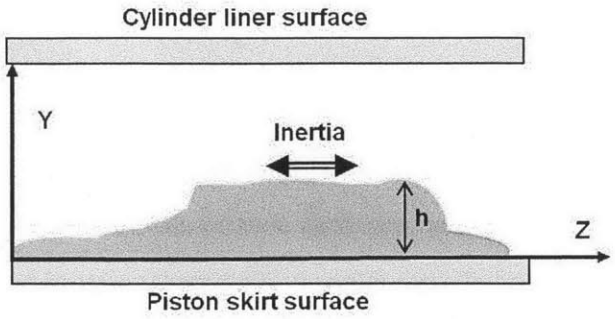

Figure 3-9: Inertia driven flow along piston skirt

Here w is the speed along the Z axis, v is the oil velocity along the Y axis, a_p is the piston acceleration and v is the kinematic viscosity of the oil.

The ratio of the convection terms at the left hand side to the viscous term is given by

$$\frac{w \cdot h}{\nu} \cdot \frac{h}{L}$$

Here h is the oil film thickness and L is the characteristic length along the Z direction. From the solution of the fully developed viscous flow developed below, the maximum velocity along Z axis for that flow is

$$w_{max} = \frac{a_p \cdot h^2}{2\nu}$$

and use this velocity as an estimate, the ratio of the convection terms at the left hand side to the viscous term is given by

$$\frac{a_p \cdot h^3}{2\nu^2} \cdot \frac{h}{L}$$

When oil film is thin, plug in $\nu = 7 \times 10^{-6} m^2/s$, $L = 1mm$, $h = 20um$, $a_p = 4000m^2/s$, then the ratio is hen the ratio is 0.0065 and the left hand terms can be neglected. When oil film is thick, plug in $\nu = 7 \times 10^{-6} m^2/s$, $L = 1mm$, $h = 100um$, $a_p = 4000m^2/s$, then the ratio is 4 and the left hand terms are at the same order as the viscous term and thus can not be neglected. Notice that the dependence on

clearance h has a power 4.

Generally the oil film thickness within the chamfer can be above 100um when the piston is near bottom dead center, so within the chamfer the error of neglecting the convection terms can be high. As oil flows out of the chamfer, the oil film thickness is relatively small, around 20um to 40um, and the convection terms can be neglected.

Now assuming the oil film thickness is small, the left hand terms can be neglected and the equation above can be further simplified to be

$$\nu \frac{\partial^2 w}{\partial y^2} + a_p = 0$$

And the boundary conditions are the no-slip boundary condition at the fluid-solid interface

$$w\big|_{y=0} = 0$$

and the zero shear force boundary condition at the fluid-gas interface

$$\frac{\partial w}{\partial y}\Big|_{y=h} = 0$$

The velocity profile of w can be solved by integration to be:

$$w = \frac{a_p}{\nu}(h - \frac{y}{2})y$$

From mass conservation, we have

$$\frac{dh}{dt} + \frac{dq}{dz} = 0$$

where q is the mass flux. Ingrating the velocity profile of w across oil film thickness gives

$$q = \frac{a_p \cdot h^3}{3\nu}$$

Then the governing equation for the inertia driven flow along the piston skirt surface

is given by

$$\frac{\partial h}{\partial t} + \frac{\partial}{\partial z}\left(\frac{a_p \cdot h^3}{3\nu}\right) = 0$$

This is a one-dimensional wave equation. The wave speed depends linearly on the piston acceleration. This point agrees with the LIF observations which show faster wave speed with higher engine speed(and thus higher piston acceleration). The wave speed also depends on the square of the oil film thickness. This means the wave moves faster where oil film is thick and moves slower where oil film is thin. Eventually, discontinuity of the oil film thickness will develop and a steep wave front will occur.

Chapter 4

Solving Method

4.1 Introduction

This section will introduce the numerical model for the unsteady hydrodynamic lubrication between piston skirt and cylinder liner. This model starts from the classical Reynolds' Equation. In order to track the oil transport more accurately, the model has considered the phenomena of oil separation and reattachment, and the corresponding inertia driven oil transport on the piston skirt surface. By doing so, the model can provide more realistic boundary condition for the skirt lubrication region. Furthermore, by keeping track of the oil mass on piston skirt and skirt liner separately, the model avoids the artificial oil mass transfer introduced by Reynolds' Equation when separation happens.

4.2 The Universal Lubrication Algorithm

This section introduces the lubrication model for the skirt region. As described before, this region is where hydrodynamic pressure is generated and the side force is mainly supported.

While the classical Reynolds' Equation for thin film lubrication is linear and straightforward to solve numerically, it cannot directly be applied in partial film region. Due to piston lateral movement and tilt, if the local clearance between the

skirt and liner cannot be filled by oil, partial film will occur. So the total modeling region can be divided into full film region and partial film region. In the full film region, the oil film fills the gap and attaches both surfaces, and Reynolds' Equation governs the oil transport. If we fix the coordinate with the piston skirt surface, as is in the model, the Reynolds' Equation is in the form of

$$\frac{\partial(\rho h)}{\partial t} + \frac{\partial}{\partial z}\left[\frac{\rho h U}{2}\right] = \frac{\partial}{\partial z}\left[\frac{\rho h^3}{12\mu}\frac{\partial p}{\partial z}\right] + \frac{\partial}{\partial x}\left[\frac{\rho h^3}{12\mu}\frac{\partial p}{\partial x}\right]$$

To solve the equation numerically, we use finite volume method to discretize it into a system of algebraic equations. The procedure is shown below. First, the computational domain is divided into a number of small cells called control volumes. Then instead of solving directly the partial differential equation, the integral form is solved so that the conservation law is enforced for each small control volume. Figure4-1 shows a control volume with its neighboring nodes and the interfaces between the control volumes. The field variables such as pressure, oil filling ratio are located at the center of each control volume. The flux variables such as the mass influx and out flux for each cell are located at the interfaces between control volumes. Later on a mass conservation equation will be formulated for the central control volume P, which is the grid point of interest. In the figure, N, S, W, E denote the north, south, west and east nodal points, respectively; and n,s,w,e denote the north, south, west and east boundary surface of the control volume P.

For each control volume P, the mass flux into and out of it across its four control surfaces can be represented using the local information (such as clearance, pressure and oil density) of P and its four neighbors. Then for each node an algebraic equation based on mass conservation can be formulated.

Since the fundamental idea of how to solving the hydrodynamic lubrication problem is based on the mass conservation characteristic of Reynolds' Equation, it will be derived here.

For thin film lubrication such as the case here, the inertia terms in the Navier-Stokes equation can be neglected, giving the following simplified governing equations:

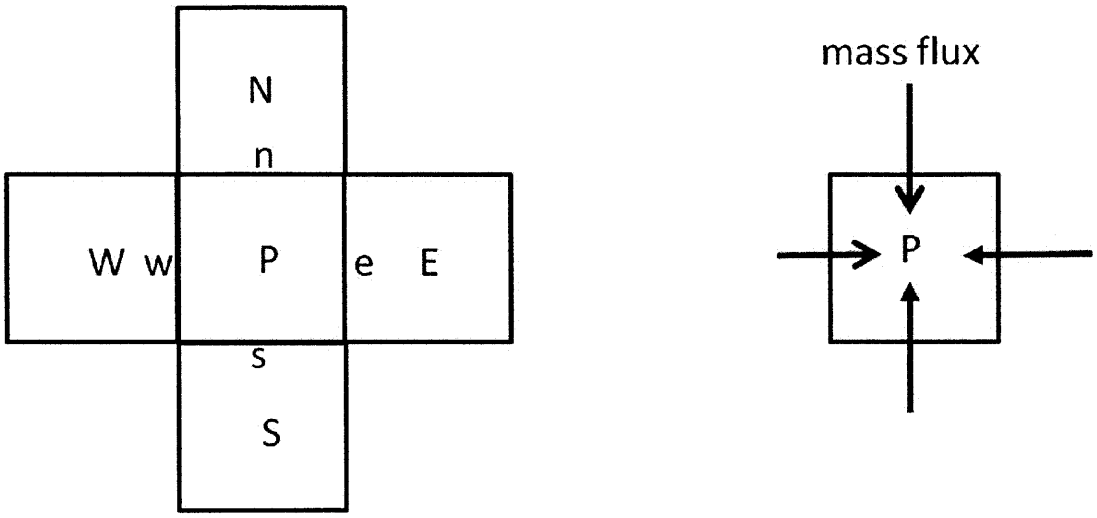

Figure 4-1: Control volume: relative locations of nodes and control surfaces

$$0 = -\frac{\partial p}{\partial x} + \mu \frac{\partial^2 u}{\partial y^2}$$

$$0 = -\frac{\partial p}{\partial y}$$

$$0 = -\frac{\partial p}{\partial z} + \mu \frac{\partial^2 w}{\partial y^2}$$

Apply the no-slip boundary conditions of

$$u(y = 0) = 0$$

$$u(y = h) = 0$$

$$w(y = 0) = 0$$

$$w(y = h) = U$$

Notice that in the model the coordinate is fixed on the piston skirt.

The resulting velocity profile in X- and Z- directions are given by

$$w = \frac{1}{2\mu} \frac{\partial p}{\partial z} \cdot y(y - h)$$

$$u = \frac{1}{2\mu}\frac{\partial p}{\partial x} \cdot y(y-h) + \frac{U}{h} \cdot y$$

The mass flow rate across the control surface of unit length is given by

$$q_z = \int_0^h \rho w dy = -\frac{\rho h^3}{12\mu}\frac{\partial p}{\partial z} + \frac{\rho U h}{2}$$

$$q_x = \int_0^h \rho u dy = -\frac{\rho h^3}{12\mu}\frac{\partial p}{\partial x}$$

Then the law of mass conservation for a fixed control volume gives

$$-\frac{\partial q_z}{\partial z} - \frac{\partial q_x}{\partial x} = \frac{\partial(\rho h)}{\partial t}$$

Substituting in the flow rate q_z and q_x, we can obtain the Reynolds' Equation.

4.2.1 Discretization of Reynolds' Equation

This section introduces the discretization of Reynolds' Equation, which applies in the full film region.

To obtain the algebraic discretized equations, for each control volume integrating the Reynolds' Equation over time from t to $t + dt$ and space. The resulting equation can be written in a mass conservation form shown below.

First, the coordinate system is the same as defined before, namely, the X axis points horizontally from node W to node E and the Z axis points vertically from node S to node N. In the model, a uniform Cartesian coordinate is used.

The original total mass in a control volume cell at time t is given by

$$M_t = \int_{x_w}^{x_e}\int_{z_s}^{z_n} \rho h dz dx$$

Here ρ and h are evaluated at time t, and x_w is the X coordinate of control surface w, x_e is the X coordinate of control surface e, z_s is the Z coordinate of control surface s, z_n is the Z coordinate of control surface n.

In the current model, assuming the density and clearance is uniform within each control volume (which is equivalent to use step function to approximate the variables),

the above result can be simplify to be:

$$M_t = \rho_t h_t \cdot \Delta x \Delta z$$

where ρ_t,h_t are the local oil density and clearance for control volume P at time t, and Δx,Δz are the grid size in X and Z directions, respectively.

Note that now the integration over each control volume can be replace by a multiplication of the grid size $\Delta x \Delta z$.

At the start of time step $t + \Delta t$, M_t is known.

After time increment Δt, the total mass in a control volume cell at time $t + \Delta t$ can be given by

$$M_{t+\Delta t} = \rho_{t+\Delta t} h_{t+\Delta t} \cdot \Delta x \Delta z$$

where $\rho_{t+\Delta t}$,$h_{t+\Delta t}$ are the local oil density and clearance of control volume P at time $t + \Delta t$.

Here, once the clearance profile $h_{t+\Delta t}$ is given, $\rho_{t+\Delta t}$ is the unknown to be solved.

Also note here the grid is fixed with the piston skirt and is time invariant.

Next we need to evaluate the mass flowing into the control volume P during this time period. Geometrically, the mass flow can come across each of the four control surfaces n, s, w and e. Physically, since the piston sliding direction is along the Z axis, the couette flow can only happen across control surfaces s and n. Pressure driven flow, on the other hand, can happen across each of the four control surfaces. For time step $t+\Delta t$, once the clearance profile $h_{t+\Delta t}$ is given, the hydrodynamic pressure generated $p_{t+\Delta t}$ is the unknown to be solved.

First, evaluate the mass flow into the control volume P driven by pressure across control surface w

$$Q_w = \int_t^{t+\Delta t} \int_{z-0.5\Delta z}^{z+0.5\Delta z} q_x\big|_w dz dt$$

where the flux $q_x\big|_w$ are evaluated at the west control surface w.

In space coordinate, we can assume the flux is uniform along the west control surface. Then the above equation can be simplified to be

$$Q_w = \int_t^{t+\Delta t} (q_x|_w \Delta z) dt$$

For the integral over time, implicit method is used in the model for convergence purpose. That is, in time dimension the flux term q_x is evaluated at time $t + \Delta t$ instead of at time t. This will simplify the above equation to

$$Q_w = q_x|_{w,t+\Delta t} \Delta z \Delta t$$

where $q_x|_{w,t+\Delta t}$ indicates the flux is evaluated at time $t + \Delta t$.

Plug in q_x, we get

$$Q_w = -\Delta z \Delta t \frac{\rho h^3}{12\mu} \frac{\partial p}{\partial x}\bigg|_{w,t+\Delta t}$$

Similarly, the mass flow into control volume P driven by pressure across control surface e during the time period t and $t + \Delta t$ can be given by

$$Q_e = -q_x|_{e,t+\Delta t} \Delta z \Delta t = \Delta z \Delta t \frac{\rho h^3}{12\mu} \frac{\partial p}{\partial x}\bigg|_{e,t+\Delta t}$$

Note that the variables are evaluated at control surface e and time $t + \Delta t$.

The mass flow into control volume P driven by pressure across control surface n and control surface s during the time period t and $t + \Delta t$ can be given by

$$Q_{n,p} = -q_z|_{n,t+\Delta t} \Delta x \Delta t = \Delta x \Delta t \frac{\rho h^3}{12\mu} \frac{\partial p}{\partial z}\bigg|_{n,t+\Delta t}$$

$$Q_{s,p} = q_z|_{s,t+\Delta t} \Delta x \Delta t = -\Delta x \Delta t \frac{\rho h^3}{12\mu} \frac{\partial p}{\partial z}\bigg|_{s,t+\Delta t}$$

The term $\frac{h^3}{12\mu}$ in the equations above has properties similar to heat conductivity. It represents how easy oil can flow through the control surfaces between neighboring control volumes. Following the method proposed by Patankar, we define the flow

conductivity K as

$$K = \frac{h^3}{12\mu}$$

The flow conductivity in the above equations is a property defined at the interfaces where mass exchange between control volumes happen. It can be represented by the arithmetic average or the harmonic average of the flow conductivity at the adjacent control volumes. Asymptotically the two representations will converge.

In the model, the unit um is used for the clearance h, so we scale it as

$$H = \frac{h}{h_{ref}}$$

with

$$h_{ref} = 1e-6$$

where H is the clearance with unit um.

Then

$$K = \frac{H^3 h_{ref}^3}{12\mu}$$

For each interface of control volume P, the conductivity is given by

$$K_w = \frac{h_{ref}^3}{12\mu} \cdot H_w^3 = \frac{h_{ref}^3}{12\mu} \cdot A_w$$

$$K_e = \frac{h_{ref}^3}{12\mu} \cdot H_e^3 = \frac{h_{ref}^3}{12\mu} \cdot A_e$$

$$K_n = \frac{h_{ref}^3}{12\mu} \cdot H_n^3 = \frac{h_{ref}^3}{12\mu} \cdot A_n$$

$$K_s = \frac{h_{ref}^3}{12\mu} \cdot H_s^3 = \frac{h_{ref}^3}{12\mu} \cdot A_s$$

The pressure gradient across each interface can also be represented by the pressure of adjacent control volumes.

$$\left.\frac{\partial p}{\partial z}\right|_n = \frac{p_N - p_P}{\Delta z}$$

$$\left.\frac{\partial p}{\partial z}\right|_s = \frac{p_P - p_S}{\Delta z}$$

$$\left.\frac{\partial p}{\partial z}\right|_w = \frac{p_P - p_W}{\Delta z}$$

$$\left.\frac{\partial p}{\partial z}\right|_e = \frac{p_E - p_P}{\Delta z}$$

Due to piston sliding in the Z direction, there are also mass flows into control volume P due to Couette flow across control surfaces n and s. For this term, explicit method is used to simplify the resulting system of equations, which gives

$$Q_{n,c} = -\int_t^{t+\Delta t}\int_{x-0.5\Delta x}^{x+0.5\Delta x} \frac{\rho U h}{2} dx dt = -\Delta x \Delta t \left.\frac{\rho U h}{2}\right|_{n,t}$$

$$Q_{s,c} = \int_t^{t+\Delta t}\int_{x-0.5\Delta x}^{x+0.5\Delta x} \frac{\rho U h}{2} dx dt = \Delta x \Delta t \left.\frac{\rho U h}{2}\right|_{s,t}$$

To evaluate the convection terms, upwind scheme is applied. For example, when piston is moving upward from bottom dead center to top dead center, then the liner is moving downward relative to the coordinate which is fixed on the piston. Now the oil flows downward and for control surface s, the amount of oil across it comes from its upwind cell or cells. If the time step Δt is controlled such that

$$|U|\Delta t < \Delta z$$

Then all the oil mass that flows across surface s between time t and $t + \Delta t$ comes from control volume P. So we can use the state of control volume P to approximate the properties (such as ρ) across surface s. This is essentially the idea of upwind scheme. And the Couette flow component across surface n can be formulated similarly.

So when piston is sliding upward

$$\rho_n = \rho_N$$

$$\rho_s = \rho_P$$

And when piston is sliding downward

$$\rho_n = \rho_P$$

$$\rho_s = \rho_S$$

The interface clearance can be given by the average of neighboring nodes

$$h_s = \frac{h_P + h_S}{2}$$

$$h_n = \frac{h_P + h_N}{2}$$

Now for control volume P, the algebraic equation is given by

$$Q_w + Q_e + Q_{n,p} + Q_{s,p} + Q_{n,c} + Q_{s,c} + M_t = M_{t+\Delta t}$$

4.2.2 Universal Discretization Scheme

The previous section only treats the full film region. Nevertheless, it provides the basic idea of formulating the algebraic equations. This section extends the idea to partial film region and introduces a universal scheme for the whole flow field.

The idea of universal scheme is developed by Elrod. In his scheme, Elrod introduces a set of new variables that are valid in both full and partial film regions. Payvar and Salant present an alternative universal method to avoid the numerical instability.

In this thesis, we introduce the same set of universal variables as Payvar and Salant. Instead of solving pressure and density directly, a indicator variable F is introduced. It will take value one at full film region and take value zero at partial film region. This indicator variable defines the flow region (partial or full). Then another global variable Φ is defined as follow. Now notice that the unknowns variables now are two global variables F and Φ that are valid at both full film region and partial film region, while the original unknown variable p and ρ are local variables that are

only valid at their corresponding region.

$$p = F\Phi P_{ref}$$

$$\rho = [1 + (1 - F)\Phi]\rho_{ref}$$

Here P_{ref} is the scaling factor for pressure and is chosen to be 1bar. ρ_{ref} is the density of liquid oil.

In the full film region, $F = 1$ and Φ represents pressure. In the partial film region, $F = 1$ and $1 + \Phi$ represents the local oil fraction. In the full film region, $\rho = \rho_{ref}$ since the gap is full of oil. In the partial film region, $\rho = (1 + \Phi)\rho_{ref}$

Replacing the pressure and density with the universal variable F and Φ, the corresponding terms for full film region from previous section can be rewritten as

$$Q_w = \frac{\rho_{ref}\Delta z\Delta t P_{ref} h_{ref}^3}{12\mu\Delta x} A_w(F_W\Phi_W - F_P\Phi_P)$$

$$Q_e = \frac{\rho_{ref}\Delta z\Delta t P_{ref} h_{ref}^3}{12\mu\Delta x} A_e(F_E\Phi_E - F_P\Phi_P)$$

$$Q_{n,p} = \frac{\rho_{ref}\Delta x\Delta t P_{ref} h_{ref}^3}{12\mu\Delta z} A_n(F_N\Phi_N - F_P\Phi_P)$$

$$Q_{s,p} = \frac{\rho_{ref}\Delta x\Delta t P_{ref} h_{ref}^3}{12\mu\Delta z} A_s(F_S\Phi_S - F_P\Phi_P)$$

The oil mass within control volume P at time $t + \Delta t$ is given by

$$M_{t+\Delta t} = \rho_{ref}\Delta x\Delta z \cdot h_{ref} \cdot [1 + (1 - F_P)\Phi_P] \cdot H_P$$

In the equations above, the variables are evaluated at time $t + \Delta t$. And the Fs and Φs are unknown variables.

At the start of time step $t + \Delta t$, the mass exchange due to Couette flow are known because explicit method is used for this term

when piston is moving upward

$$Q_{s,c} = -\rho_{ref}\Delta x\Delta t \cdot h_{ref} \cdot [1 + (1 - F_P^{i-1})\Phi_P^{i-1}]\frac{|U|H_s}{2}$$

$$Q_{n,c} = \rho_{ref}\Delta x\Delta t \cdot h_{ref} \cdot [1 + (1 - F_N^{i-1})\Phi_N^{i-1}]\frac{|U|H_n}{2}$$

when piston is moving downward

$$Q_{s,c} = \rho_{ref}\Delta x\Delta t \cdot h_{ref} \cdot [1 + (1 - F_S^{i-1})\Phi_S^{i-1}]\frac{|U|H_s}{2}$$

$$Q_{n,c} = -\rho_{ref}\Delta x\Delta t \cdot h_{ref} \cdot [1 + (1 - F_P^{i-1})\Phi_P^{i-1}]\frac{|U|H_n}{2}$$

The oil mass of time step t is also known

$$M_t = \rho_{ref}\Delta x\Delta z \cdot h_{ref} \cdot [1 + (1 - F_P^{i-1})\Phi_P^{i-1}] \cdot H_P^{i-1}$$

Where F_P^{i-1}, H_P^{i-1} and Φ_P^{i-1} denote the states of previous time step (time t) and are known.

We can divide each terms by $\rho_{ref}\Delta x\Delta z \cdot h_{ref}$ to scale the equation.

Then the original mass at previous time step can be represented by

$$M^{i-1} = [1 + (1 - F_P^{i-1})\Phi_P^{i-1}] \cdot H_P^{i-1}$$

The mass at current time step can be represented by

$$M^i = [1 + (1 - F_P)\Phi_P] \cdot H_P$$

The mass inflow across each control surface can be represented by

$$Q_w = \frac{\Delta t P_{ref} h_{ref}^2}{12\mu\Delta x^2} A_w(F_W\Phi_W - F_P\Phi_P) = K_X \cdot A_w(F_W\Phi_W - F_P\Phi_P)$$

$$Q_e = \frac{\Delta t P_{ref} h_{ref}^2}{12\mu\Delta x^2} A_e(F_E\Phi_E - F_P\Phi_P) = K_X \cdot A_e(F_E\Phi_E - F_P\Phi_P)$$

$$Q_{n,p} = \frac{\Delta t P_{ref} h_{ref}^2}{12\mu\Delta z^2} A_n(F_N\Phi_N - F_P\Phi_P) = K_Z \cdot A_n(F_N\Phi_N - F_P\Phi_P)$$

$$Q_{s,p} = \frac{\Delta t P_{ref} h_{ref}^2}{12\mu\Delta z^2} A_s(F_S\Phi_S - F_P\Phi_P) = K_Z \cdot A_s(F_S\Phi_S - F_P\Phi_P)$$

Where K_X and K_Z are constants defined in equations above.

when piston is moving upward

$$Q_{s,c} = -0.5 \cdot K_S \cdot [1 + (1 - F_P^{i-1})\Phi_P^{i-1}] \cdot H_s$$

where K_S is a constant defined as

$$K_S = \frac{|U|\Delta t}{\Delta z}$$

$$Q_{n,c} = 0.5 \cdot K_S \cdot [1 + (1 - F_N^{i-1})\Phi_N^{i-1}] \cdot H_n$$

when piston is moving downward

$$Q_{s,c} = 0.5 \cdot K_S \cdot [1 + (1 - F_S^{i-1})\Phi_S^{i-1}] \cdot H_s$$

$$Q_{n,c} = -0.5 \cdot K_S \cdot [1 + (1 - F_P^{i-1})\Phi_P^{i-1}] \cdot H_n$$

It is easy to check this set of equations reduces to Reynolds' Equation in full film region where $F = 1$ and reduces to full attachment assumption in partial film region. And it also automatically takes care of the inner boundary between full film region and partial film region.

4.2.3 Separation Model

The introduction of universal variables avoids tracking the partial film boundary and makes the lubrication easier to solve. However, they use full attachment assumption in the partial film region, which is not always a good assumption between the skirt and liner interface. In this thesis work, the idea of universal scheme is used while the full attachment assumption is modified to better capture the reality.

In the current model at each nodal location, instead of having one control volume between the skirt and liner, there are two control volumes, as illustrated in figure4-2 . One control volume is attached with the skirt, representing the amount of oil on

piston skirt. The other control volume is attached with the liner, representing the amount of oil on the liner. This way, the model can consider the oil separation and reattachment naturally. We introduce the following variables

ho_S: oil film thickness on skirt surface

ho_L: oil film thickness on liner surface

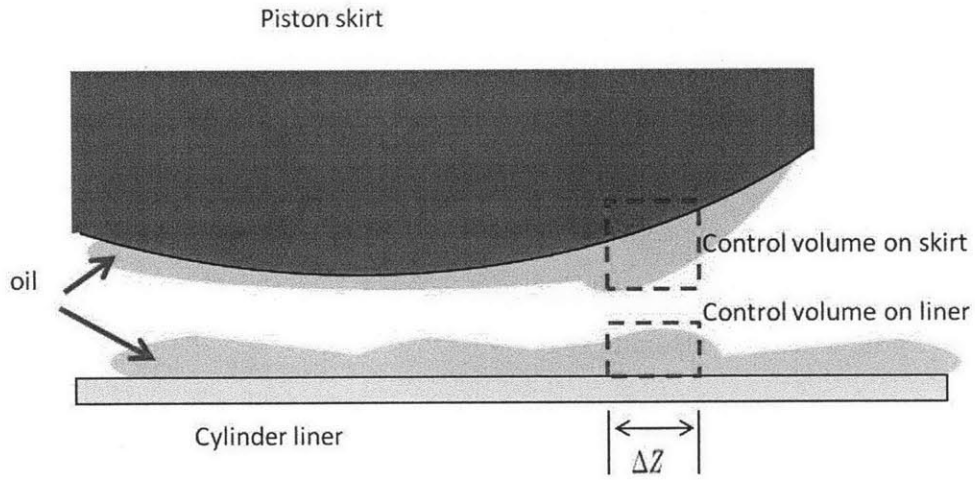

Figure 4-2: Control volumes between skirt and liner

In full film region, the gap is filled fully by oil and full attachment assumption applies and the two control volumes actually become one. The local density in full film region is the density of liquid oil at corresponding condition. And the local oil fraction is one. The local oil fraction can be represented by

$$\frac{ho_S + ho_L}{h}$$

where h is the local clearance between the two surfaces.

In partial film region, the local oil fraction is smaller than one. And the local density can be approximated by the product of oil fraction and the density of liquid oil, since gas density is much smaller than liquid oil density. Due to surface tension,

in partial film region, different scenario may occur. Firstly, totally separation may occur. That is, the oil film on skirt and the oil film on liner are totally separated by gas between them. Intuitively, separation is more likely to occur as the local oil fraction goes to zero. That is when the gap is relatively big while oil film is thin. On the other hand, full attachment is more likely to occur as the local oil fraction approaches one. That is, when gap is relatively small while oil film is thick. Between these two extreme cases, more complex model may be needed to relate the local status to local variables such as local clearance, oil fraction, surface properties, local surface geometry, sliding speed and so on.

In the thesis, as a starting point, we use some simple mapping functions to relate local status to local oil fraction. One example, which is currently used in the model, can be defining only one threshold number (e.g. 0.5 as in the model). For a given control volume, if local oil fraction ρ is larger than this threshold number ρ_s, full attachment is assumed to occur here. If local oil fraction is smaller than this threshold number, totally separation is assumed to occur.

$$\text{status}: \begin{cases} \text{separation} & \text{if } \rho < \rho_s \\ \text{full attachment} & \text{if } \rho \geq \rho_s \end{cases}$$

The solving procedure is described as follow.

At the start of each time step, we use explicit method to formulate the Couette flow term. That is, we check the oil fraction of each control volume at previous time step. Then we calculate the status(separated or attached) of each control volume based on this oil fraction. Once we have determined the status of each cell, upwind scheme is used to calculate the mass flow into each cell. For a control volume where the oil film on skirt is separated from the oil film on liner, the oil velocity profile within it is illustrated in figure4-3. Note that the coordinate is fixed on piston and the liner slides relative to the piston. For the node where separation occurs, the Couette flow term for the control volume attached to the skirt is zero while the Couette flow term (absolute value) for the control volume attached to the liner is

$$\rho_{ref}\Delta x|U|\Delta t \cdot ho_L$$

or $K_S \cdot Ho_L$ aftering scaling.

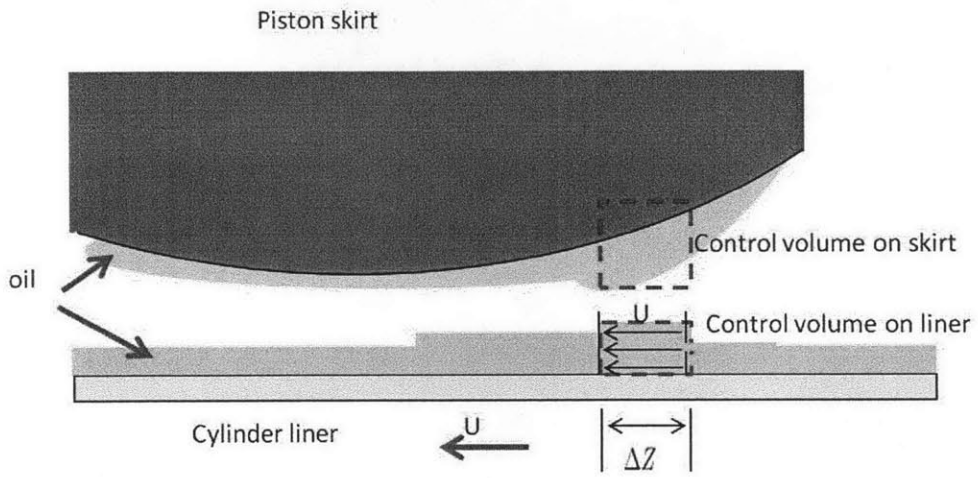

Figure 4-3: Oil velocity profile when separation occurs

On the other hand, for a control volume where full attachment (not necessarily full film) occurs, the oil velocity profile is shown in figure4-4. The mass transport due to Couette flow can be formulated according to the velocity profile as well.

While this treatment is still very rough, it does allow the consideration of separation phenomenon and is an improvement over the previous always full attachment assumption. Still, one drawback of the current mapping function is that it is a step function and there is a jump of cell status when local density ρ goes across the threshold number ρ_s. Physically, the transition from totally separation to full attachment may be smoother. So another mapping function can be when the local oil fraction at given location is smaller than certain threshold number, we assume totally separation occurs. When the local oil fraction at given location is larger than another threshold number, we assume full attachment occurs. In between, we use a smooth function to

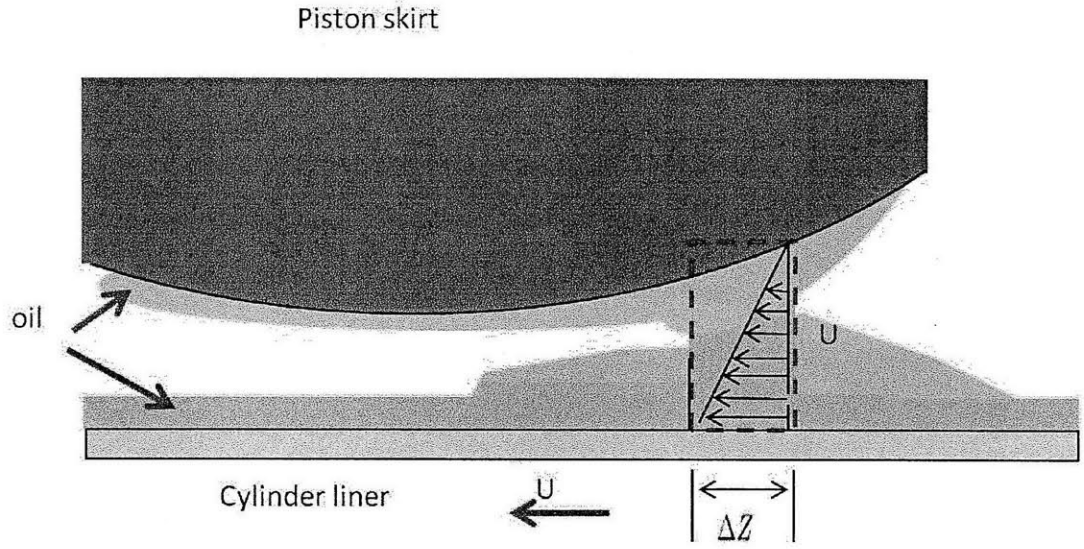

Figure 4-4: Oil velocity profile at full attachment cell

connect the two extreme cases. Here, we can see the benefit of using explicit method for the Couette flow term. Since the velocity profile as well as the local status depends only on the variables of previous time step, which are known, we can apply more complex mapping functions.

4.2.4 Inertia Driven Mass Transport

One term that has been neglected in Reynolds' Equation is the inertia term. This term happens because of piston primary acceleration and deceleration. For example, when piston is accelerating downward, as it is moving from top dead center to mid-stroke, the inertia will drive oil to move upward relative to the piston. This is usually fine when engine speed is not too high and oil film not too thick. However, when piston is moving upward from bottom dead center, it has been observed from 2D LIF experiment that there may be thick oil puddle release from chamfer. Also, within piston chamfer where oil film can be very thick, up to several hundred um. The

engine speed for racing cars can also reach more than 10,000rpm. To accommodate these conditions, this inertia term is added to Reynolds' Equation.

At regions where full attachment happens, inertia force acts as additional body force similar to pressure gradient. In the current model, the inertia force term is neglected when full attachment happens for simplicity. And as mentioned before, this is also generally the treatment adopted by other models and is a good approximation for a wide range of operating condition. However, there may still be cases when the inertia component can be important.

At regions where separation happens and thus there is free fluid surface, the oil flows can form a wave propagating along the piston skirt, due to the inertia force. The governing equation for this type of flow is given by

$$\frac{\partial h}{\partial t} + \frac{\partial}{\partial z}\left[\frac{a_p h^3}{3\nu}\right] = 0$$

here h denotes the thickness of the oil film on skirt surface. The details are shown in chapter 5. Here we will focus on how to discretize the the equation. First notice that this is a one dimensional conservation law, describing the wave moving along the Z-direction. In the equation, a_p is the acceleration or deceleration of the piston, which is a variable depends on crank angle and operational parameters such as engine speed. But at a given crank angle with specified engine condition, it can be easily calculated and is known.

From chapter 5, we know the velocity profile with the oil film is given by

$$w = \frac{a_p}{\nu}(h - \frac{y}{2})y$$

The mass enters a given cell from its upwind cell due to this term is

$$Q_I = \Delta x \int_t^{t+\Delta t} \int_0^h \rho_{ref} w dy dt = \rho_{ref} \frac{\rho \cdot a_p \cdot h^3}{3\nu} \cdot \Delta t \Delta x = \frac{a_p \cdot H^3 \Delta t}{3\nu \Delta z} \cdot h_{ref}^2 \cdot \rho_{ref} \Delta x \Delta z h_{ref}$$

Similarly, scaling it by dividing $\rho_{ref}\Delta x\Delta z \cdot h_{ref}$, we get

$$Q_I = \frac{a_p \cdot \Delta t \cdot h_{ref}^2}{3\nu\Delta z} \cdot H^3$$

where H is the oil film thickness on the skirt surface with unit um.

In the current model, the finite volume method with upwind scheme is used to treat the inertia term. Generally speaking, this method satisfies mass conservation and can handle the situation of shock formation. Nevertheless, this method is first order in space and hence not very accurate.

After adding the inertia term, now for control volume P, the algebraic equation is given by

$$Q_w + Q_e + Q_{n,p} + Q_{s,p} + Q_{n,c} + Q_{s,c} + Q_I + M_t = M_{t+\Delta t}$$

4.2.5 Assemble the Linear Equation System

From previous sections, for each control volume, the mass flowing into and out of it is represented by the variables listed below

1. F, universal indicator variable for the current time step, which is the unknown to be solved.

2. Φ, universal variable for the current time step, which is the unknown to be solved.

3. F^{i-1}, universal indicator variable of previous time step, which is known at the start of the current time step.

4. Φ^{i-1}, universal variable of previous time step, which is known at the start of the current time step.

5. h, current clearance profile. Note that the interface conductivities can be represented by h.

6. h^{i-1}, the clearance profile of previous time step.

7. ho_S, ho_L, the oil film thickness on skirt and liner, for current time step. They are unknowns at partial film region. On full film region, they sum up to the clearance h and the gap is totally filled.

8. ho_S^{i-1}, ho_L^{i-1}, the oil film thickness on skirt and liner, of previous time step. They are known at the start of the current time step.

For each control volume, the governing equation is

$$Q_w + Q_e + Q_{n,p} + Q_{s,p} + Q_{n,c} + Q_{s,c} + Q_I + M_t = M_{t+\Delta t}$$

First, recognize that when using explicit method for the Couette flow term and inertia term, all the following terms of the above equation only depend on the results of previous time step and thus are known $Q_{n,c}$, $Q_{s,c}$, Q_I,M_t

The discretized governing equation can be seen as of the following form

$$M(F,h)\vec{\Phi} = b(F,h)$$

where $M(F,h)$ is a matrix whose entries are functions of F and h. And $b(F,h)$ is a vector whos entries are functions of F and h. and $\vec{\Phi}$ denotes the unknown, a vector of the universal variable Φ.

Easy to see, the first thing we would like to know is the indicator variable. Since once we can define the full film region and partial film region, we can formulate the corresponding mass flow. And at different flow region, the mass flows have different forms. In the model, the process of solving the universal variables is an iterative process of tuning the universal variables to change oil mass flux until mass balance is reached for each control volume.

The model starts with an initial guess of the distribution of F. When the clearance profile h is given, $M(F,h)$ and $b(F,h)$ become known and Φ can be solved. Then, F is updated with the calculated Φ. At cell with value of Φ indicating partial film, F is updated to be zero. At cell with value of Φ indicating full film, F is updated to be

one. This process is repeated until consistent result are achieved, or stopped as failed when the times of iterations exceeds predefined maximum allowed iteration. Since the equation is essentially nonlinear, how fast convergent result can be achieved depends on the choice of the initial guess of F. In the model, the great thing is when time step is controlled properly, the difference in terms of flow regions between successive time steps can be small. So using the previous time step result F^{i-1} as the initial guess is usually a feasible choice. In the model, after properly choosing the time step, usually the iterative process of solving F and Φ can be done successfully within 20 iterations.

Once the F and Φ are solved, both the full film region and the partial film region are defined. Also, the information of pressure distribution at full film region and local oil fraction at partial film region can be extracted. For full film region, the only unknown variable is the pressure, so the problem is solved completely. For partial film region, since there are oil on the skirt and oil on the liner, we have two unknowns ho_S and ho_L at each node. At partial film region, Φ only gives the total oil film thickness by

$$h \cdot (1 + \Phi) = ho_S + ho_L$$

So we still need to solve ho_S and ho_L at partial film nodes. This can be done by solving mass conservation for the skirt control volume and liner control volume, respectively. Since for partial film region, there is no pressure driven flow, so the mass conservation equation is simply

$$Q_{n,c} + Q_{s,c} + Q_I + M_t = M_{t+\Delta t}$$

The only unknown is the $M_{t+\Delta t}$ which is directly related to ho_S for skirt control volume and ho_L for liner control volume. The calculation is then straightforward.

4.2.6 Assemble the Jacobean Matrix

In the previous sections, the clearance profile h is assumed to be known. Then the calculation of the fluid field is calculated based on it. However, due to piston secondary motion and the structural deformation of both surfaces, h is not a constant.

We can decompose h into several components. First, both the cylinder liner and the piston skirt have cold profiles. For the liner, the main feature is the bore distortion. For the skirt, the main features include ovality along circumferential direction and barrel shape along sliding direction. The cold profiles can be measured and viewed as fixed for different engine running conditions. On top of the cold profiles, both the skirt and the liner have thermal expansions, which depend on the temperature field of the specific engine condition. Even for the same engine, the temperature field can be quite different depends on operational parameters such as load, oil cooling jet rates. In theory, the temperature field may be time varying, giving time varying thermal expansion. However, if the engine is operated under steady state, it can be assumed to be time-invariant. The model currently uses this assumption to simplify the calculations. Specially, the model assumes the thermal expansions for both the skirt and the liner are known, which can come from either measurement or estimations from other packages. Generally, the user may have easy access to finite element packages which can output the expansion information, as least for the piston. This way, the model does not need to have a heat transfer model within it and can focus on the lubrication and oil transport. So currently in the model, both the cold profile and the thermal expansion are supplied by the model users. With these profiles, the so called nominal profile h_0 can be directly calculated by combining the profile of the skirt and the profile of the liner. h_0 is defined as the clearance between the skirt and liner when the piston is positioned in the center of the bore with zero tilt angle.

Due to piston secondary motion, the generally non-zero piston lateral displacement and tilt angle will also contribute to the clearance profile h. For example, if the piston is pushed toward the thrust side with no tilt, the clearance between the skirt and liner at thrust side will decrease and the clearance between the skirt and the liner at anti-

thrust side will increase.

Another important component is the structural deformation for both surfaces. Depends on the structure and the material of the piston and liner, the deformation for the surface can be around 20um to 40um during expansion stroke when side force is high. Considering that the nominal clearance is in the range of 10um to 100um, and more importantly, the clearance of the region where lubrication happens is around 10um to 20um, the deformation is able to change the lubrication situation significantly. The structural deformation makes the problem harder to solve by coupling the fluid field calculation with the structural compliance.

In the model, the problem is solved iteratively. For each time step, first make an initial guess of the deformation profile as well as the piston lateral displacement and tilt angle, then the initial guess of the clearance profile h can be constructed by combining these terms with the nominal clearance profile. With this h, the lubrication sub model is applied to calculate the hydrodynamic pressure and possibly asperity contact pressure. The calculated pressure field gives the load distribution applying on the skirt and liner surfaces. Using the compliance matrix, each surface's deformation under the load can be calculated. Ideally, this calculated deformation profile should be the same as the initial guessed deformation profile. In the model, this problem is solved iteratively using Newton's method. When the difference between the two deformation profiles are less than some small threshold number, convergent result can be assumed to be achieved. The detailed equations are introduced as below.

As described before, the discretized governing equation for hydrodynamic lubrication can be seen as of the following form

$$M(F,h)\vec{\Phi} = b(F,h)$$

For each time step, with given h, Φ can be solved from the equation above. To obtain the Jacobean matrix, applying the chain rule to relate the change in Φ to the change in h, the result in matrix form is shown below

$$M\Delta\vec{\Phi} + N\Delta\vec{H} = 0$$

Where matrix M and N depend on the clearance profile h and the calculated universal variable Φ.

It should be mentioned that in the model, different grids are used for the structural deformation and the lubrication calculation. The deformation is defined on the coarse grid while lubrication calculation is on the fine grid. The main reason is because the size of the compliance matrix is proportional to the square of the number of points for this grid, and will become prohibitively large both in terms of memory usage and calculation time as the grid points get large. Also, since the structural deformation is generally quite smooth, using a coarse grid generally will not lose too much accuracy. On the other hand, a fine grid is necessary in order to get accurate pressure distribution, especially for direct numerical simulation of piston skirt tooling marks. For example typical wavelength of surface tooling marks may be 250um, and then there will be around 100 waves on the skirt. In order to capture the local geometry, around 10 grids are needed for each wavelength, requiring about 1000 grids along that direction. Therefore it is natural to use two grids in the model. The structural deformation of the surfaces is defined over the coarse grid, and interpolation is used to define the deformation over the fine grid. The lubrication calculation, including the pressure distribution, oil transport and shear stress, is performed on the fine grid. The normal force and frictional force on the coarse grid are then obtained by integration over coarse grid. In the current model, to simplify the situation, the fine grid is constructed as follow. Firstly the coarse grid is specified. Then the find grid is obtained by dividing each cell of the coarse grid into several smaller cells along both directions.

Chapter 5

Model Results

This chapter aims to:

- Provide an overview of the piston secondary motion.
- Introduce the driving mechanism of piston lateral movement and tilt.
- Compare model predictions of piston secondary motion with experiment observations.
- Describe the oil transport between skirt and its surroundings.
- Study the main parameters affecting piston secondary motion and skirt lubrication.

5.1 Piston Dynamics and Skirt Lubrication

This section will give an overview of the piston secondary motion as well as the skirt lubrication. Piston secondary motion may affect where the load is supported, the clearance between the skirt and liner and eventually the skirt lubrication performance. The overall thesis project studies skirt lubrication, and requires accurate modeling of piston secondary motion. In this section, the driving mechanism of piston secondary motion will be introduced first. Then, the experiment observations from two-dimensional LIF engine will be used to extract information about piston

secondary motion. The information will be compared with model prediction. We will show how the experiment and the model give consistent results. Finally, we will discuss the areas where the model can be improved. Like any model, this model only captures part of the reality. The underlying assumptions and potential drawbacks will be discussed.

5.1.1 Piston Lateral Motion

Piston secondary motion tells at each given crank angle, the piston is on which side, and the relative position of the piston skirt. It includes both piston lateral displacement and the piston tilt. Piston lateral displacement is defined as the lateral position (along Y direction) of pin center P, and captures the parallel movement of the piston. Piston tilt captures the rotation angle of the piston. In the model, positive lateral displacement means the piston is on the thrust side, and positive tilt angle means the top of the piston tilts toward the anti-thrust side.

Figure 5-1 shows a predicted piston lateral displacement. Zero crank angle is the start of intake stroke. The result is for the two-dimensional LIF engine, with the key parameters as specified in Table5.1. Note that the value of the tooling mark wave height is not specified. It is because the wave height may change due to wear. Generally, the tooling marks are made of some soft material to allow breaking in. For this example, The speed is 1500rpm and the load is 700mbar, the nominal clearance is 10um in radius, and the tooling mark wave height is 2um. Note that the minimum nominal clearance in radius is 22um($0.5\times$Cylinder Bore$-0.5\times$Piston skirt diameter). However, to study the effect of minimum nominal clearance, the model allows user to specify the minimum nominal clearance, and in this example, 10um is used. In this example, the liner is also assumed to be rigid and only the deformation of piston skirt is considered.

To illustrate the driving mechanism of the piston secondary motion, the side force acting on piston from the wrist pin is shown in Figure 5-2. Comparing the piston

Table 5.1: Model Parameters of the LIF Engine

Parameter	value
Cylinder Bore	86.609 mm
Piston skirt diameter	85.565 mm
Connecting rod length	158 mm
Crankshaft radius	43 mm
Pin offset	0.5 mm to thrust side
Crankshaft offset	0 mm
Skirt height	32.4 mm
Pin height	20 mm above bottom of skirt
Piston mass	0.393 kg
Piston moment of inertia	$274.9\times10^{-6}kgm^2$
Wrist pin mass	0.12 kg
Wrist pin moment of inertia	$9.8\times10^{-6}kgm^2$
Connecting rod mass	0.758 kg
Connecting rod moment of inertia	$2750.5\times10^{-6}kgm^2$
Skirt tooling mark wavelength	250 um

lateral displacement with the side force on piston from the pin, we can see a clear relationship between the two. The piston lateral movement follows the driving force, with a little bit lag which is due to piston inertia. This is reasonable since the piston is pushed to move laterally by the side force from the pin. We can see clearly that the direction of the side force determines the direction of piston lateral motion. When the side force is positive, which means the piston is pushed toward thrust side, the piston lateral displacement also shows the piston moves toward thrust side.

On the other hand, the relationship between piston lateral displacement and the side force is not linear. For example, although the side force at early expansion stroke is much larger than the side force at early intake stroke, the piston lateral displacement is only twice as big. This is because the piston lateral displacement essentially includes two components. Consider the case when piston is initially in the middle of the cylinder and is now pushed to the liner. If there is some clearance between the skirt and the liner, the piston will first travel this distance. During this period, the piston is purely driven by the force from the pin. Then the piston will encounter the liner and the force generated between the skirt-liner interface will tend to decelerate the piston. Since the surfaces can deform, the pin center will not stop

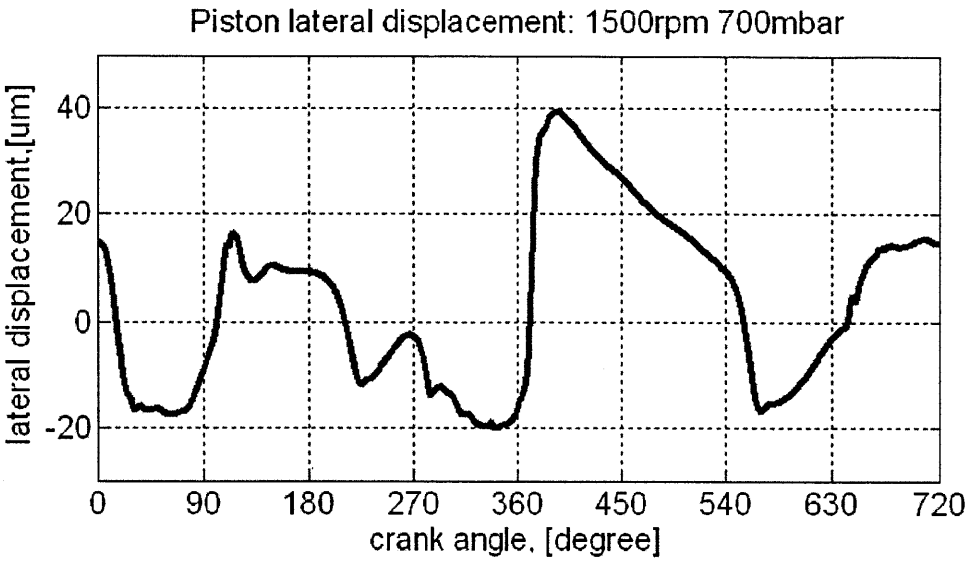

Figure 5-1: Piston lateral displacement: 1500rpm 700mbar

immediately. Instead, the pin center will move further until the piston lateral speed becomes zero. From this point of view, the structure deformations of the surfaces act as spring.

Another feature easy to see is that the curve of the side force is smoother than the curve of the lateral displacement. One reason is that the lateral displacement is defined as of the pin center. Since the piston also tilts and the tilt angle affects the location where the skirt impacts the liner, so the lateral displacement of pin center is also affected by the piston rotation.

Since the piston secondary displacement follows the side force from the pin, the components of the side force will analyzed here to gain better understanding of the system. In concept, the motion of the power cylinder system is driven the combustion pressure force. That is, during early expansion stroke, the high combustion pressure force on top of the piston is the driving force, pushing piston to accelerate. During other strokes when combustion pressure force is small, the piston motion is driven by inertia. So along the vertical direction, the main forces acting on piston are the combustion pressure force and the inertia force. Similarly, along the lateral direction, the side force acting on piston from the wrist pin can also be decomposed mainly to

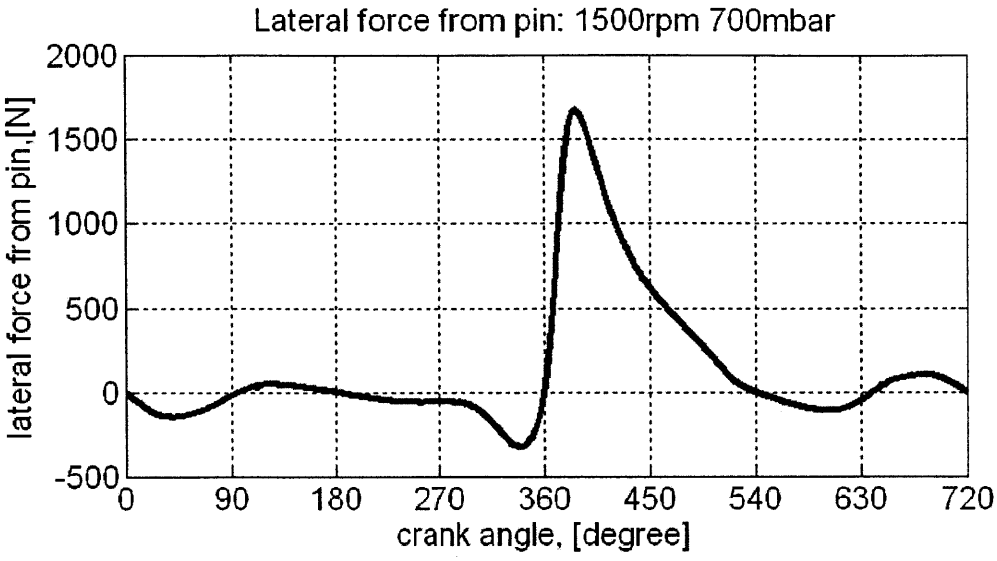

Figure 5-2: Lateral force from pin: 1500rpm 700mbar

the inertia component and the pressure component.

Figure 5-3 shows the inertia component of the side force. In the figure, the left side of the cylinder is the thrust side and the right side of the cylinder is the anti-thrust side. Four scenarios can be seen from the figure:

- During first half of intake stroke, piston is moving from top dead center toward mid-stroke and is accelerating. The connecting rod pulls the piston. Due to the connecting angle shown in the figure, there is a lateral force component due to inertia pulling the piston toward the anti-thrust side. The same situation occurs during the first half of expansion stroke, as shown in the figure.

- During second half of intake stroke, piston is moving from mid-stroke toward bottom dead center and is decelerating. The connecting rod pushes the piston to decelerate it. Due to the connecting angle shown in the figure, there is a lateral force component due to inertia pushing the piston toward the thrust side. The same situation occurs during the second half of expansion stroke, as shown in the figure.

- During first half of compression stroke, piston is moving from bottom dead

center toward mid-stroke and is accelerating. The connecting rod pulls the piston to accelerate it. Due to the connecting angle shown in the figure, there is a lateral force component due to inertia pushing the piston toward the anti-thrust side. The same situation occurs during the first half of exhaust stroke, as shown in the figure.

- During second half of compression stroke, piston is moving from mid-stroke toward top dead center and is decelerating. The connecting rod pulls the piston to decelerate it. Due to the connecting angle shown in the figure, there is a lateral force component due to inertia pulling the piston toward the thrust side. The same situation occurs during the second half of exhaust stroke, as shown in the figure.

To summarize, the inertia force component acting on piston along lateral direction changes direction at mid-stroke, top dead center and bottom dead center.

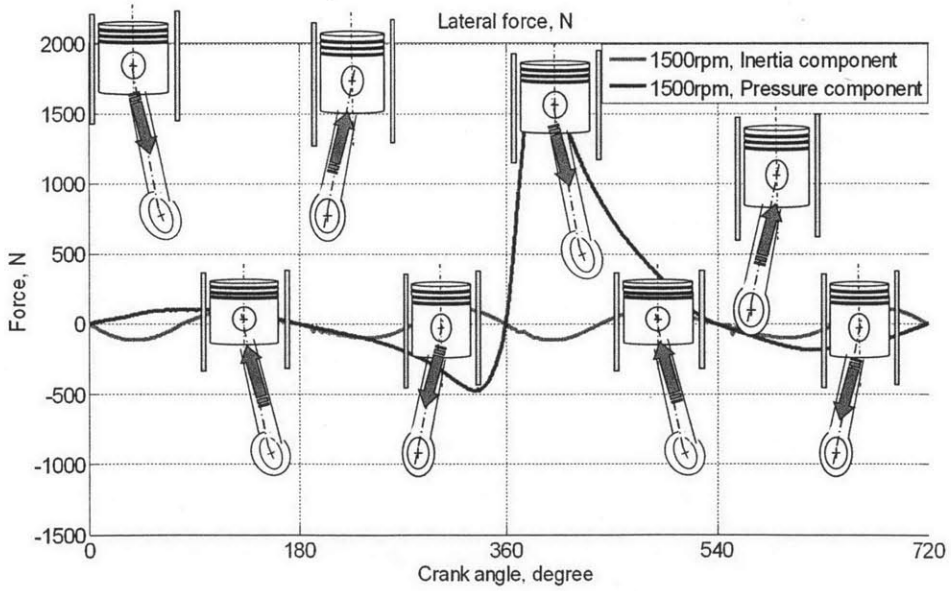

Figure 5-3: Inertia component of the side force: 1500rpm 700mbar

Besides the inertia force component, the piston is also subject to pressure force component. Figure 5-4 shows the pressure component of the side force. The combus-

tion pressure force is only significant during upper compression stroke and expansion stroke:

- During the second half of compression stroke, the combustion pressure force on top of piston tries to push piston downward. Due to the connecting rod angle shown in the figure, it will give a lateral force component pointing to anti-thrust side.
- During expansion stroke, due to the connecting rod angle shown in the figure, the combustion pressure force will give a lateral force component pointing to thrust side.

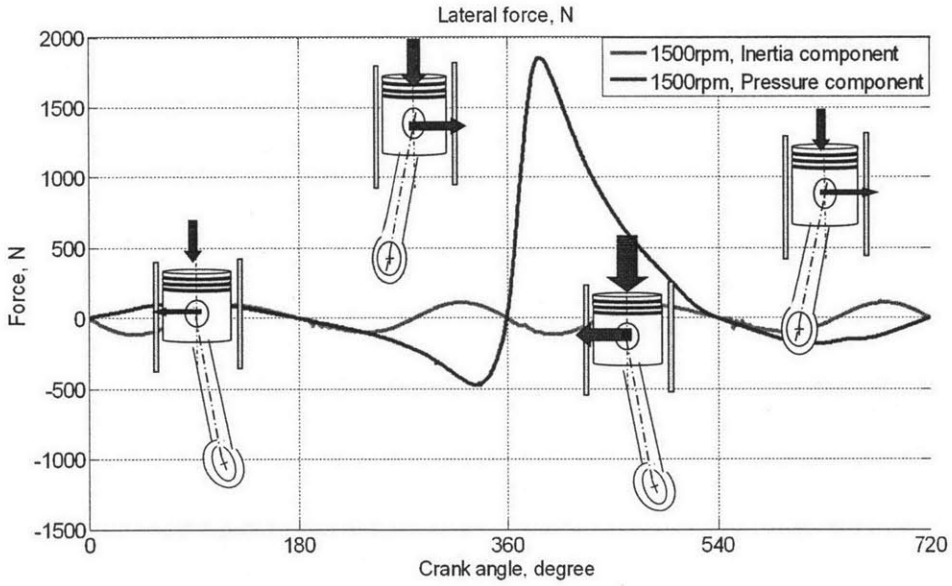

Figure 5-4: Pressure component of the side force: 1500rpm 700mbar

The lateral force on piston from wrist pin is the combination of the pressure force component and the inertia force component. It is interesting to note that:

- During intake stroke, lower compression stroke and exhaust stroke, generally inertia component is more significant and dominates.
- During expansion stroke, generally combustion pressure component is more significant and dominates.

- During upper compression stroke, inertia component and combustion pressure component competes and either one may be significant depends on operational conditions.

Piston tilt gives the rotation of the piston. While the piston lateral displacement is driven by the side force from the wrist pin and is relatively easy to interpret. The tilt is more complex. The direction of lateral displacement generally agrees with the direction of side force, with some lag caused by inertia. And the side force acting on piston can be decomposed to the inertia component and the pressure component, both components have clear physical meanings. For tilt angle, the dynamics of the piston becomes more important in interpreting the result.

In this section, an example will be analyzed to build the intuition. The result is also the LIF engine. Operational parameters: 1500rpm 700mbar. Minimum nominal clearance is 10um. The oil boundary condition is 2um uniform splash onto the liner below skirt. Figure 5-5 shows the predicted tilt angle. As said before, positive tilt means the top of the piston tilts toward anti-thrust side.

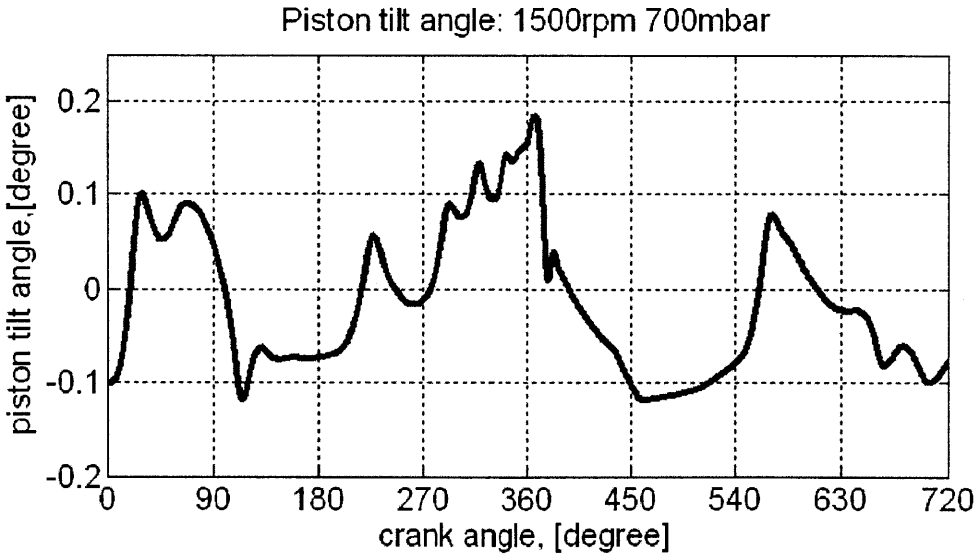

Figure 5-5: Piston tilt angle: 1500rpm 700mbar

One important feature of the piston affecting tilt is that the center of gravity is located above the pin center, as shown in figure 5-6. Due to this geometry, easy to

see that when the piston is only subject to side force from the wrist pin, the bottom of the skirt will move first.

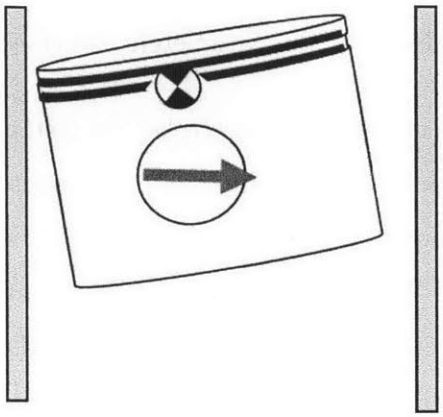

Figure 5-6: Piston center of gravity

Another parameter affecting piston tilt is the pin offset. For the two-dimensional LIF engine, the pin center is offset to the thrust side by 0.5mm. During late compression stroke and expansion stroke when the combustion force is significant, the piston will be pushed to tilt clockwise, giving positive tilt angle, as shown in figure 5-7.

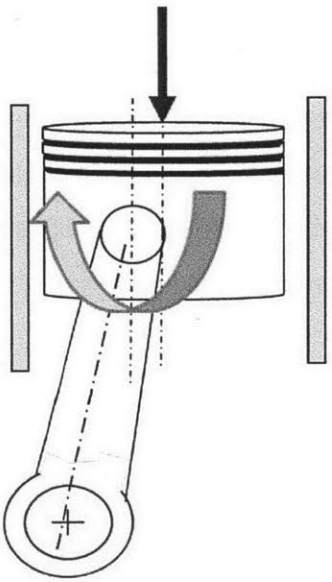

Figure 5-7: Piston pin offset

5.1.2 Piston Dynamics and Pressure Generation

A detailed description of the piston lateral dynamics is shown in this section. The results are for the LIF engine with the parameters described before.

- Right after top dead center of intake stroke, the piston is moving to anti-thrust side driven by the inertia force component. As mentioned before, during this transition, the bottom of the skirt moves first, giving negative tilt angle, as shown in figure 5-8. The left panel shows the piston secondary motion, with crank angle and the side force from the wrist pin indicated. The blue lines are the cylinder liner and the red lines are the piston skirt. The figure is distorted by using different scale along vertical direction and lateral direction to show the detailed shape of the skirt and liner. Along vertical direction, the unit is mm and along lateral direction the unit is um. The right panel shows the corresponding pressure generation between the skirt-liner interface, with the peak pressure indicated. From the figure, we can clearly see the transition process. Initially at zero crank angle, the size force is zero. Then the inertia force component contributes to the side force and pushes the piston to anti-thrust side. This side force tilts the piston anti-clockwise and gives negative tilt angle. At around 5 degree crank angle, the bottom of the skirt interact with the liner first and there is a reacting force from the liner trying to tilt the piston clockwise. As the piston moves further, there are large areas of interaction with the anti-thrust liner and the tilt angle keeps increasing.

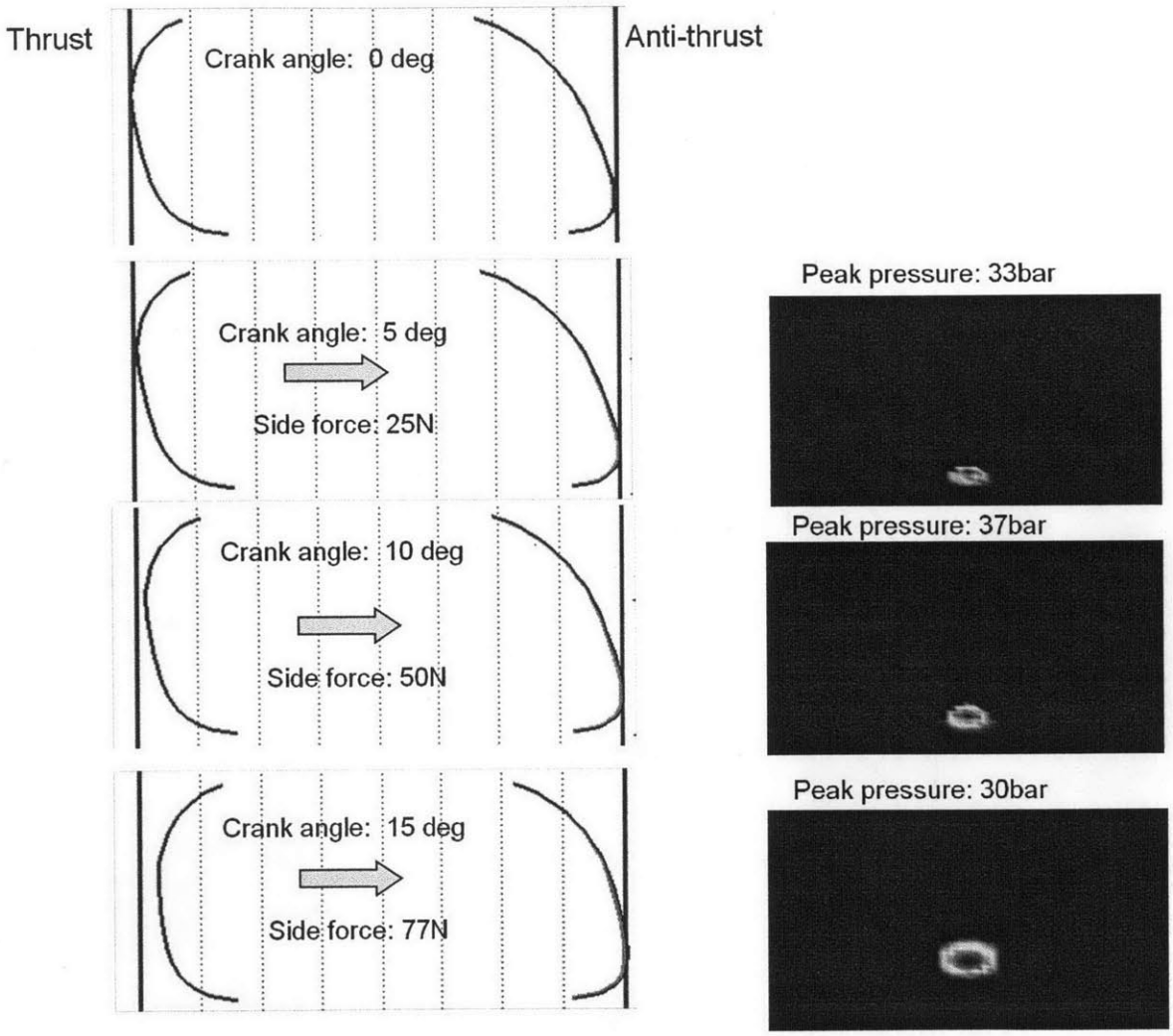

Figure 5-8: Piston secondary motion: CA 0 to CA 20

- For this case, after about 20 degree crank angle, the piston has already arrived the anti-thrust side. Figure 5-9 illustrates the scenarios between 20 degree crank angle and 80 degree crank angle. During this period, the piston is on the anti-thrust side. For the example described here, the amount of oil is quite sufficient. Hence due to the damping effect of the oil film, the piston does not have too much dynamics and is relatively easy to find a stable position. Due to the barrel shape of the piston skirt along the sliding direction, the piston will have positive tilt angle when the oil supply is sufficient, as for this case.

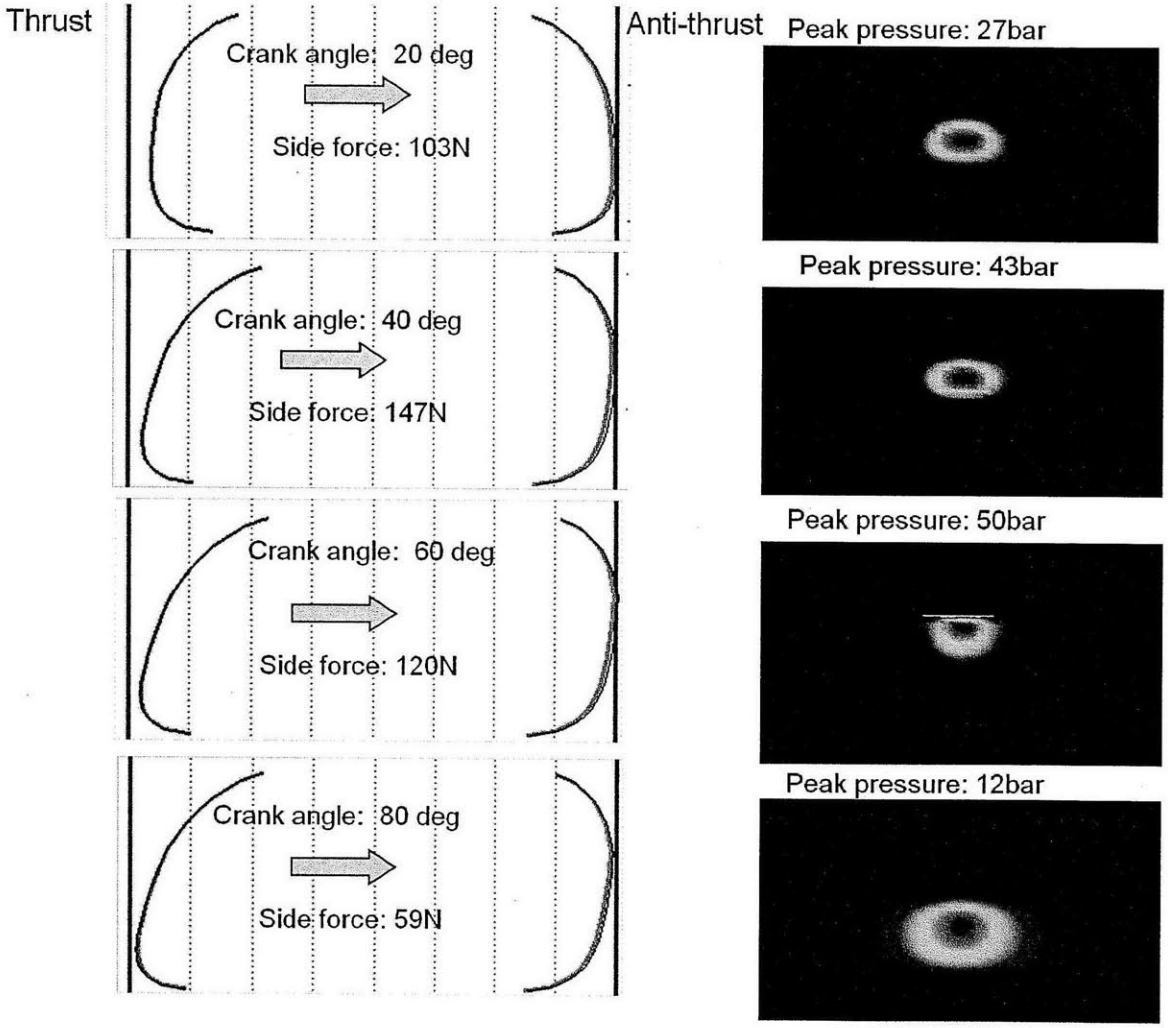

Figure 5-9: Piston secondary motion: CA 20 to CA 80

- Around mid-stroke, inertia component changes direction and will push the pis-

ton back to thrust side. Figure 5-10 illustrates this transition process. During this period, the tilt angle changes from positive to negative.

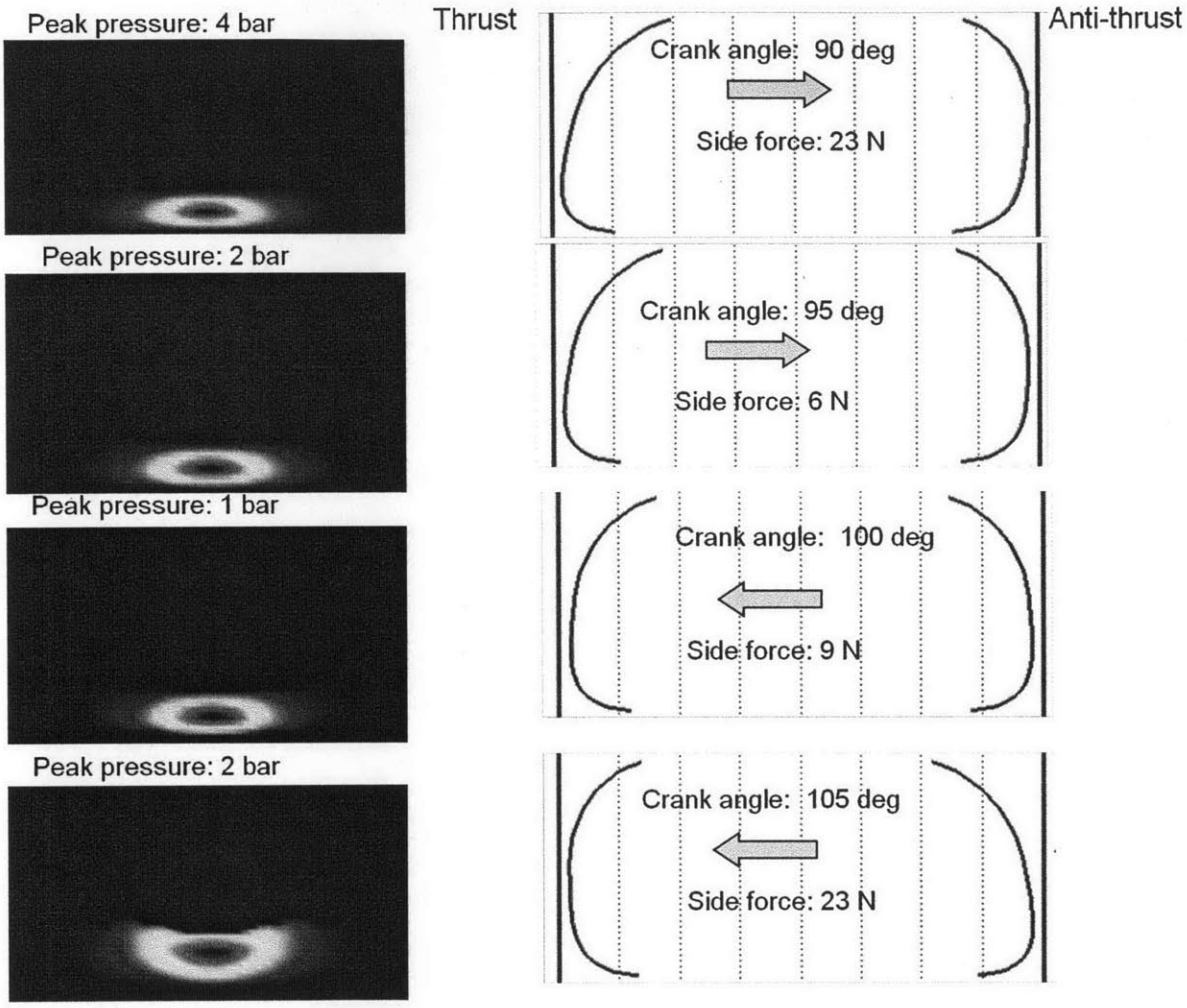

Figure 5-10: Piston secondary motion: CA 90 to CA 105

- From mid-stroke to bottom dead center of intake stroke, the piston is on thrust side. Since there is sufficient oil in this example, the piston slides over the liner steadily with a negative tilt angle. The results are shown in figure 5-11.

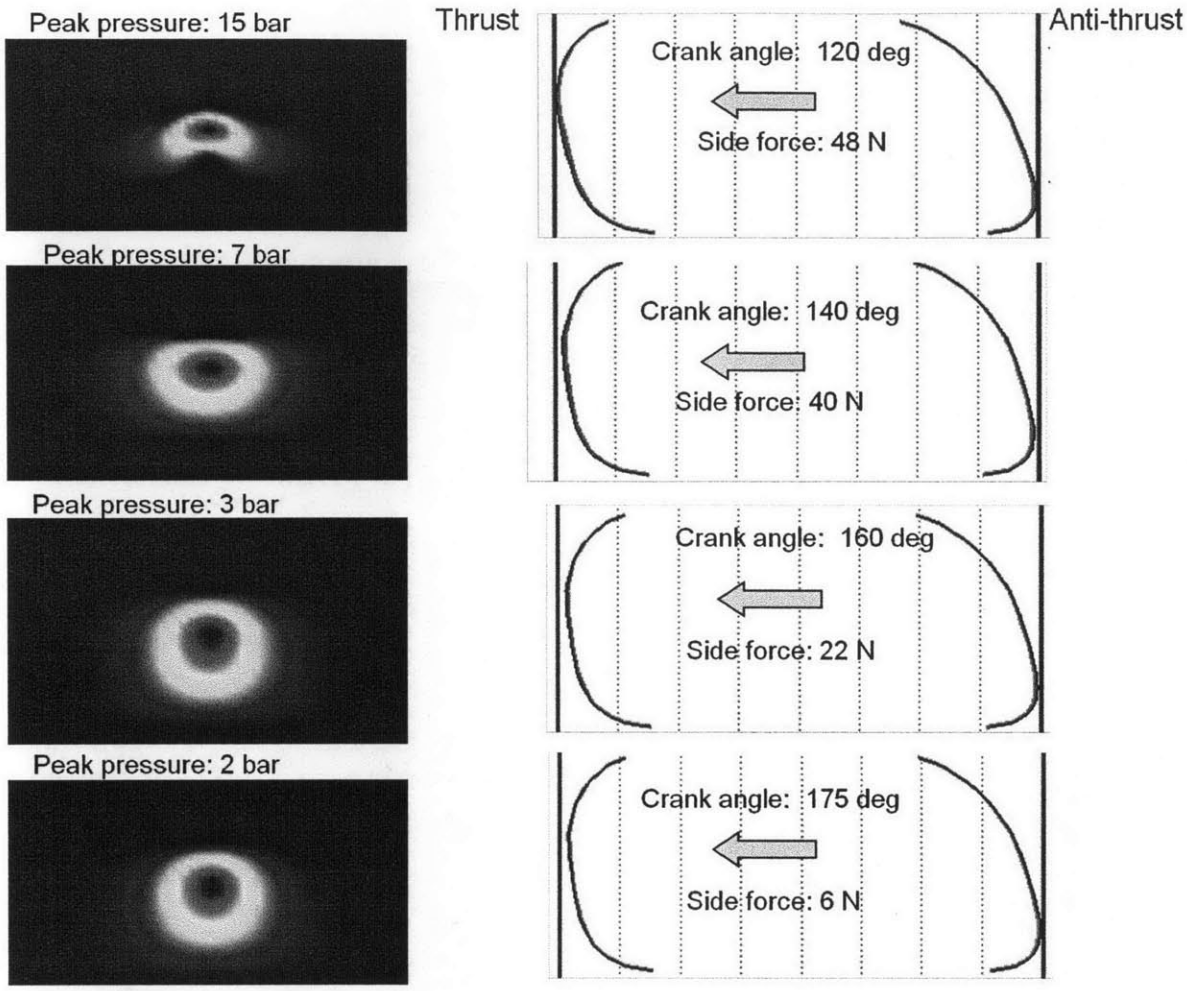

Figure 5-11: Piston secondary motion: lower intake stroke

- During lower compression stroke, the piston first moves to anti-thrust side at around bottom dead center due to the inertia component. Then during the lower compression stroke, the skirt is on anti-thrust side.

- During upper compression stroke, while the inertia force component pushes piston to thrust side, the combustion pressure component pushes the piston to anti-thrust side. For this case with low speed high load, the pressure component dominates. The results are shown in figure 5-12.

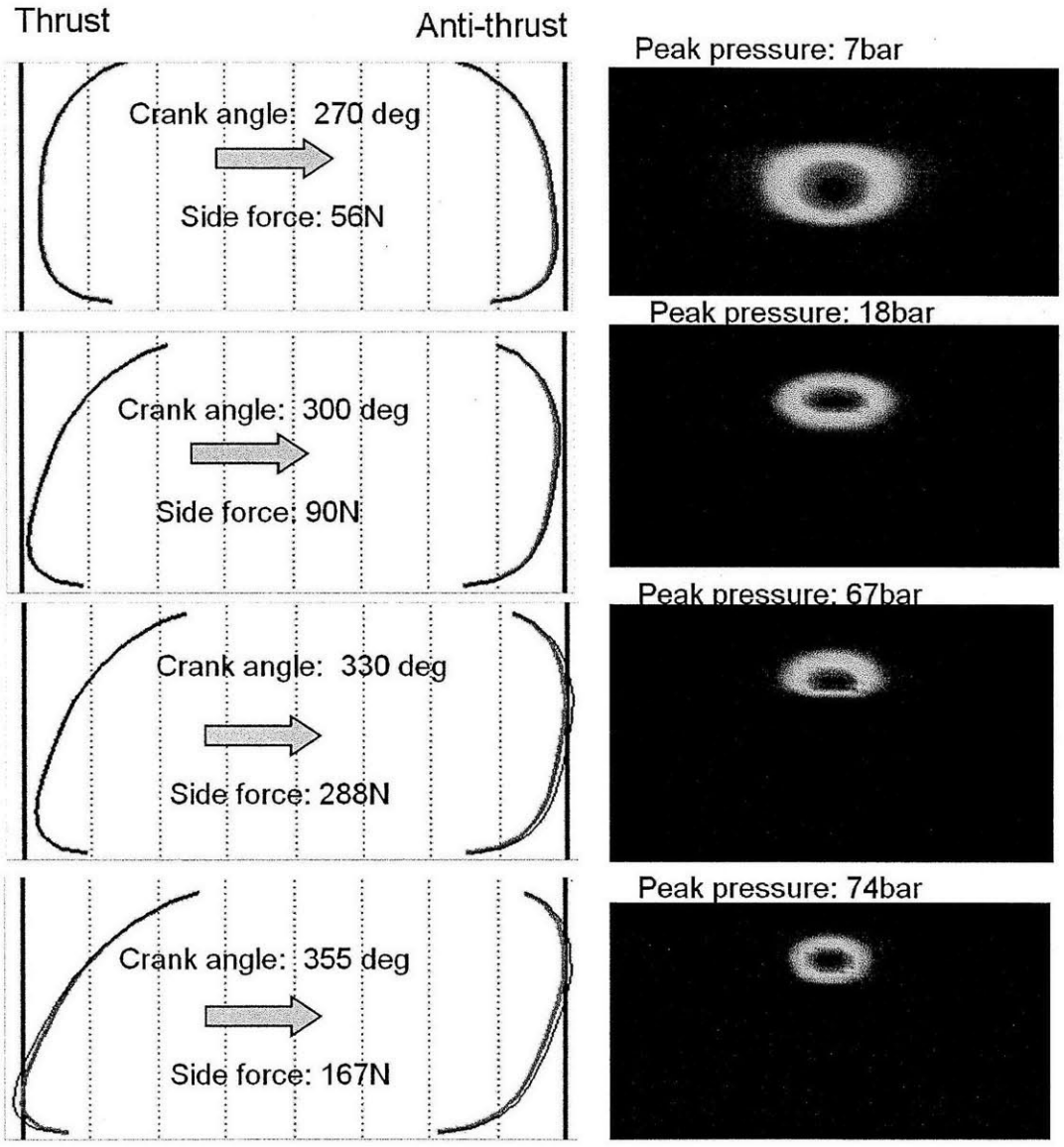

Figure 5-12: Piston secondary motion: upper compression stroke

- Around top dead center of expansion stroke, due to the positive pin offset, we can see clearly the piston slap process, as shown in figure 5-13. That is, the bottom area of the skirt first impacts the thrust side liner, then the piston rotates around the contact point anti-clockwisely. During this process, the speed of the skirt is low since it's around the top dead center. The hydrodynamic pressure between the skirt and liner at thrust side is mainly generated by the squeezing effect.

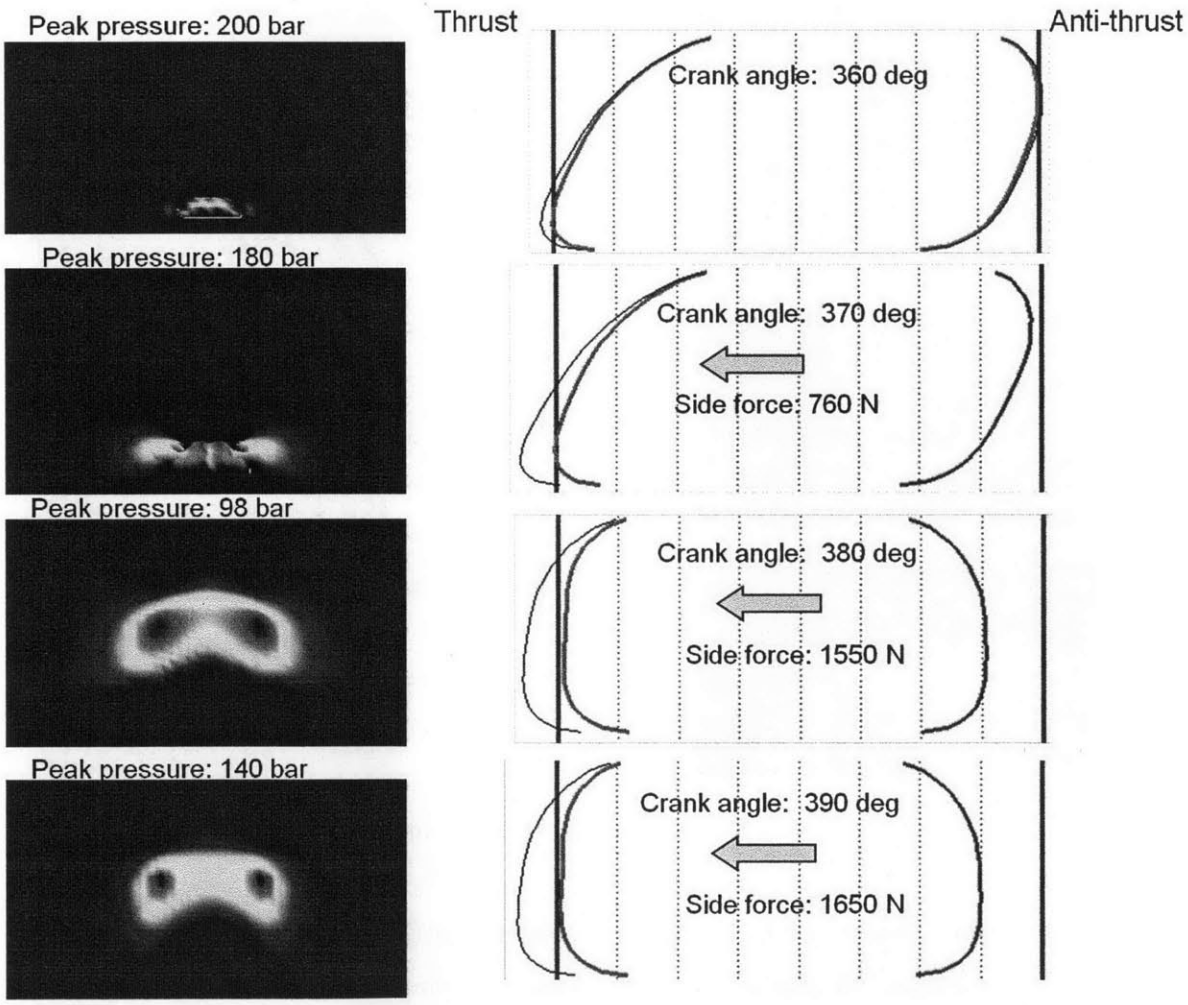

Figure 5-13: Piston secondary motion: piston slap around TDC of expansion stroke

- After about 400 degree crank angle, the piston has already find a stable position on the thrust side. Now the sliding velocity is high and the hydrodynamic

pressure is mainly generated by the sliding effect. Figure 5-14 shows the results. In this case with sufficient oil, the tilt angle is negative as the skirt slides over the liner steadily.

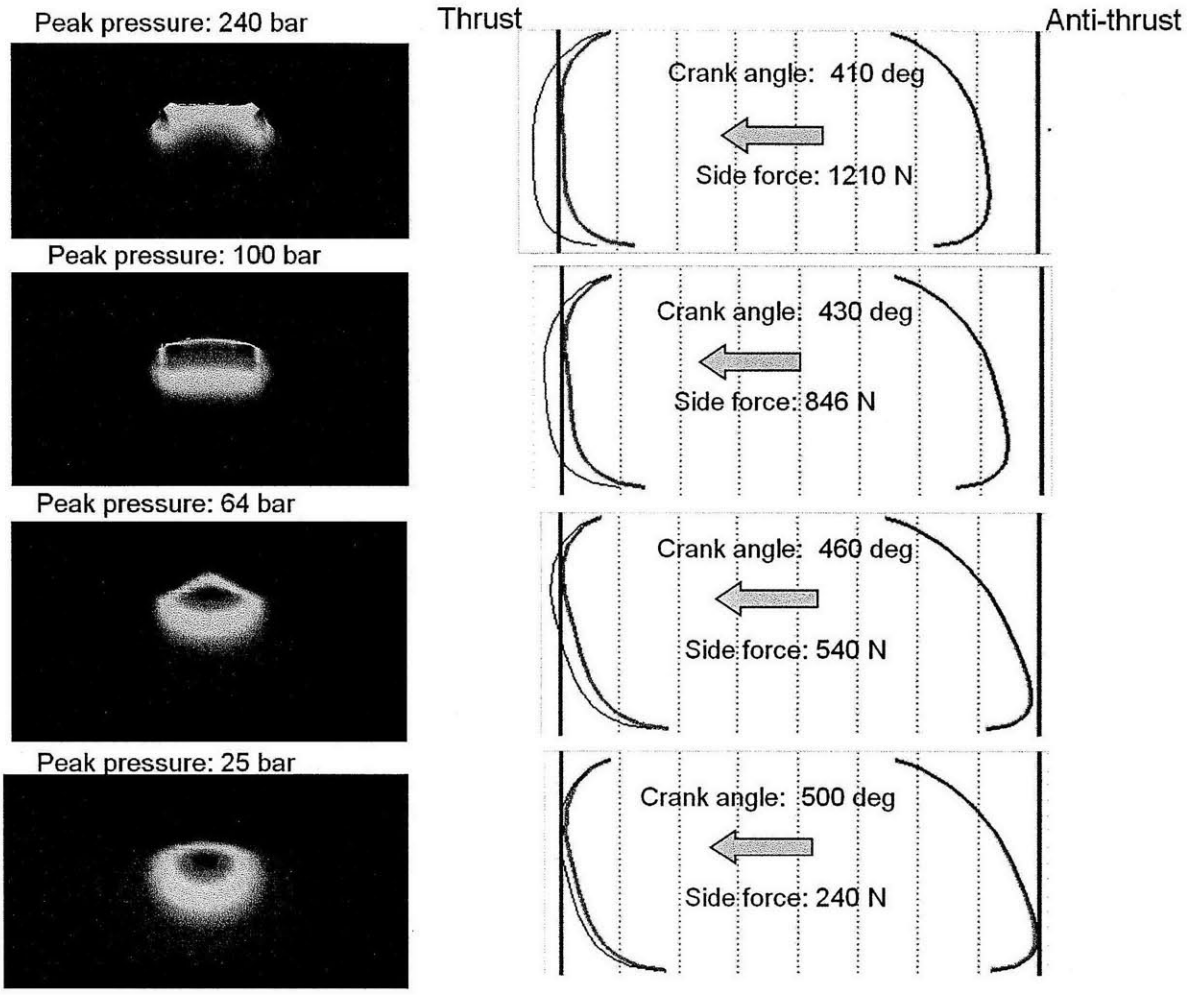

Figure 5-14: Piston secondary motion: expansion stroke after slap

- Lower exhaust stroke is similar to lower compression stroke. The skirt is on anti-thrust side due to the inertia force component.
- During upper exhaust stroke, the skirt is on thrust side due to the inertia force component.

5.1.3 LIF Observation

In this section, some of the model results are compared with the two-dimensional LIF observations. In the comparisons below, the overall trend will be compared instead of the exact numbers. One reason is the LIF observations only give the relative oil film thickness between the skirt-liner interface. The piston secondary motion information needs to be extract from the LIF results. Another reason is that some parameters for the model can not be directly measured. For example, the model requires the oil splash rate as input while physically it is hard to measure it for the LIF engine.

As described before, the inertia force component and the combustion pressure force component push piston to different direction during upper compression stroke. Note that the inertia component increases as engine speed increases and is approximately proportional to the square of engine speed. The pressure component depends on the engine load. Hence we can change the relative significance by changing engine speed and engine load, which are easy to adjust. In this section, we will focus on the upper compression stroke.

Figure 5-15 shows the thrust side two-dimensional LIF observation for the case of 1500 rpm 700mbar. Note that the bright color indicates the oil. From 290 degree crank angle to 340 degree crank angle, we can see the cloudy shape of the oil film which indicates that the oil on skirt and oil on liner are separated from each other and there is no full film region. This is consistent with the model prediction that the piston is on the other side(anti-thrust side). At 350 degree crank angle and 360 degree crank angle, we can see while the upper area of the skirt is still separated from the liner, the lower area of the skirt interacts with the liner, as indicated by the dark area in the figure. This is also consistent with the model prediction.

To further illustrate the competition between inertia component and combustion pressure component, the thrust side two-dimensional LIF observation for the case of 3500 rpm 700mbar is shown in figure 5-16. By maintaining the engine load while increasing the engine speed, the inertia component becomes more important.

Figure 5-17 shows the model predicted side force acting piston from the wrist pin.

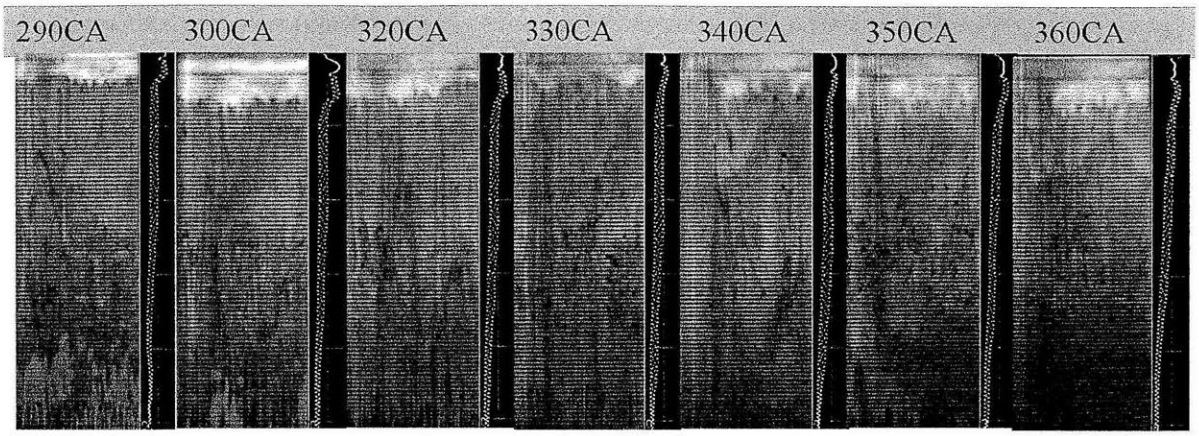

Figure 5-15: Thrust side 2D LIF observation: 1500 rpm 700 mbar

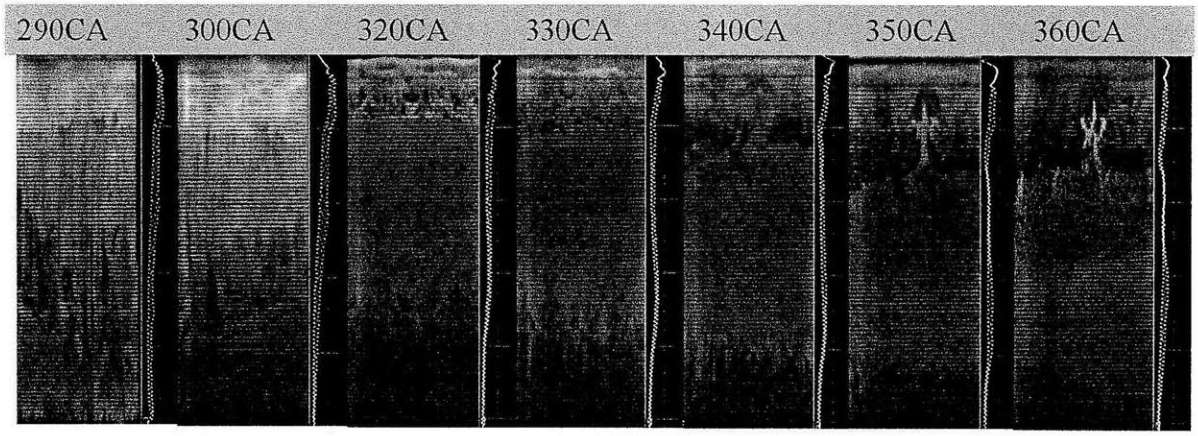

Figure 5-16: Thrust side 2D LIF observation: 3500 rpm 700 mbar

For the low speed case, the piston is always on the anti-thrust side during the upper compression stroke. For the high speed case, the inertia force component is actually strong enough to push the piston to thrust side for a while.

Figure 5-18 shows the model predicted piston position within the cylinder. The model prediction and the two-dimensional LIF observation match quite well.

- Originally during lower compression stroke until 290 degree crank angle, the model shows that the piston is on anti-thrust side. The cloudy 2D LIF figure also indicates that the piston is on the other side(anti-thrust side).

- At 300 degree crank angle, the model shows that the piston is pushed to thrust side, due to the high inertia. Also as described before, the bottom of the skirt

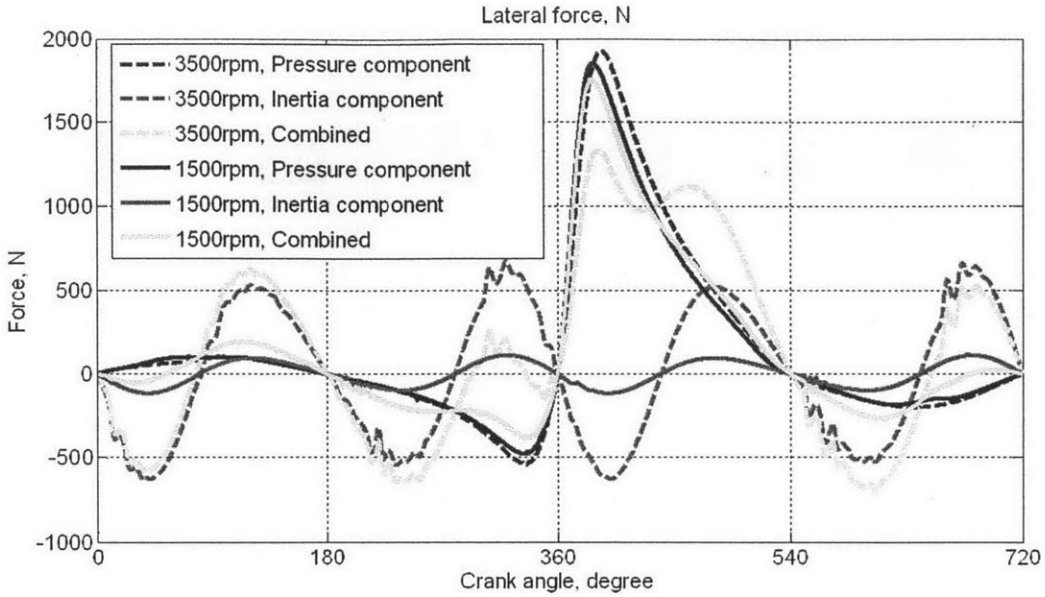

Figure 5-17: Side force acting on piston from wrist pin

moves first and interacts with the liner first. The dark area at the lower portion of the skirt in the 2D LIF figure tells the same thing.

- From 300 degree crank angle to 320 degree crank angle, the model shows that the piston is on thrust side and is trying to find a stable position. The skirt-liner interaction region extends from the lower skirt region to the upper skirt region. The clear horizontal streaks in the LIF figure also show that the upper skirt region touches the liner.

- As the piston approaches the top dead center, the model shows that the combustion pressure component becomes more important and the piston is pushed to the anti-thrust side. And as discussed before, the top of the piston tilts toward the anti-thrust side due to the positive pin offset. From the 2D LIF figures, the cavitation pattern on the upper skirt region shows clearly the same story.

For the results shown before, the minimal nominal clearance is 10um. That is, there is some room between the skirt and liner. In this case, when the skirt is on one

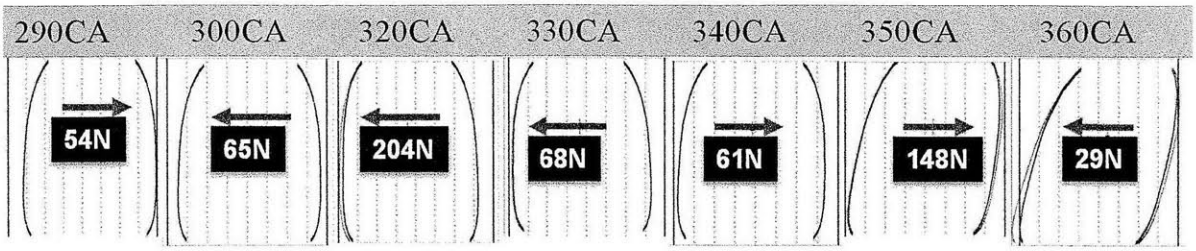

Figure 5-18: Model predicted piston position: 3500 rpm 700 mbar

side, there may be no contact on the other side. When the clearance between the skirt and liner is very tight, the results might be different. Imagine the case when there is overlap between the skirt and liner, then there might be contact on both sides. And the piston might not have too much dynamics since it is firmly held within the cylinder and there is not much room for it to move.

5.2 Oil Transport

This section will illustrate the oil transport between piston skirt and its surroundings, using some results of the 2D LIF engine as an example. The engine parameters are shown as before, the engine speed for this example is 3500rpm and the load is 700mbar. Since the surface tooling mark mainly affects the oil transport locally, and in this section the focus is the overall oil transport patterns, so the tooling mark wave height is chosen to be very small (0.1um) to make the result simpler.

The oil transport within the system can be viewed from the following point of view. Firstly, there is an initial condition, specifying the initial oil distribution within the system including the piston chamfer, the skirt and the liner area below skirt. Then as engine runs, there is also a set of boundary conditions. The top boundary defines the oil exchange between the piston chamfer and the oil ring groove, and there might be oil going to upper ring pack through oil ring groove and/or oil release from the drain holes, if there are any. The bottom boundary defines the oil addition to the liner area below skirt, with the oil being picked up by the skirt as the skirt moves over the liner later on. Of course there are also possible oil release from the system, including the oil release from the top boundary as described, the oil down scraping due to bottom of skirt and oil squeezed out from the sides. In the current model, the top boundary is generally assumed to be closed with no oil exchange with the oil ring groove and it will be interesting to build a sub model for this process. However, the current model does have a release scheme, draining the excess oil when the chamfer becomes full. The oil splash to the liner is also not fully analyzed in the current thesis work and may deserve further study. In the current model, the oil splash is asked as user input and requires the model user to have a good feeling about this oil addition. Since it is the ultimate oil supply to the whole system and plays significant role, further study will be beneficial. Besides the oil exchange between chamfer and oil ring groove and splash, the oil squeezed out from sides and skirt down scraping are already included in the current model.

As we discussed before, the hydrodynamic lubrication mainly happens between

the skirt and liner. So the boundary conditions relevant are the boundary conditions for the skirt region, with the top boundary lies between skirt and the chamfer and the bottom boundary as the bottom line of the skirt. Actually this is the traditional treatment in previous studies. In the current model, realizing that the top boundary condition for skirt region depends on oil down flow from chamfer and the bottom boundary condition for skirt region depends on oil film on liner below skirt, we extend the system boundary and include the chamfer and the liner area below skirt into the system. Now the original boundary for the skirt region becomes inner boundary inside the system and we make one step further, but on the other hand we create a new set of boundaries.

In the current model, the boundary condition for the whole system is characterized by the oil splash to the liner. It takes the following format. Each time the piston reaches top dead center, the model specifies the added oil distribution on the liner below skirt. Notice that there is already some oil film left on the liner and then the total oil film on the liner is the sum of the original oil film and the splashed oil. To simplify the situation, in the following results, the splash is assume to be an uniform distribution on the liner, that is, adding the same oil film thickness to the liner area below skirt when piston is at TDC.

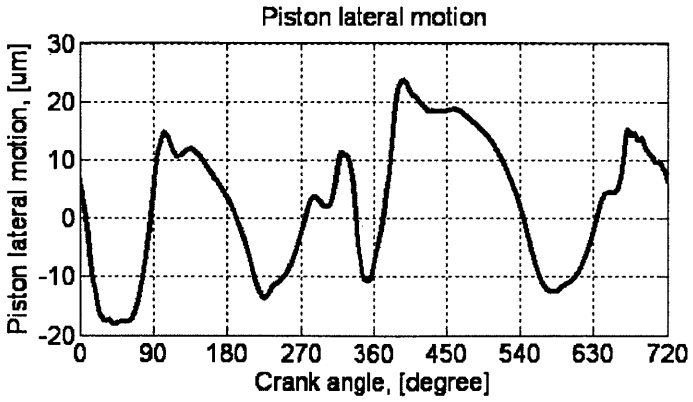

Figure 5-19: Predicted piston position: 3500 rpm 700 mbar

Next, the results with 1um uniform splash and 0um nominal clearance will be shown. Initially, assume the oil film thickness in piston chamfer and on the liner

below skirt is 20um. Between the skirt and liner, the oil film thickness is assumed to be full film where the local clearance is smaller than 20um and 20um otherwise. Since oil transport depends on piston motion, the piston secondary motion is shown first in Figure 5-19. As described before, piston generally shifts from one side to the other side around mid-stroke, TDC and BDC. Since the initial condition may affect the results of the first several cycles, the results shown in this figure are the results of the 6^{th} cycle.

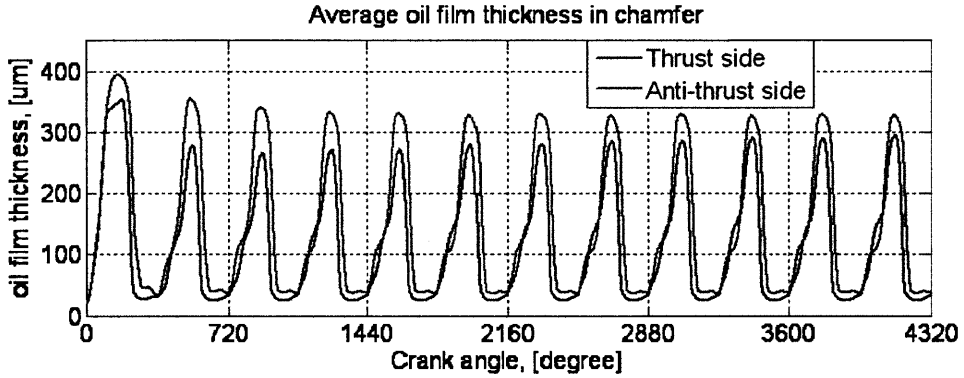

Figure 5-20: Average oil film thickness in chamfer: 3500 rpm 700 mbar

Figure 5-20 shows the average oil film thickness in piston chamfer for 6 cycles. Initially at crank angle 0, the average oil film thickness is the initial condition, 20um. For the first down stroke from crank angle 0 to crank angle 180, since initially the model assumes there is 20um oil on the liner area below skirt, the chamfer collects quite a lot of oil as it arrives BDC, 350um on average for thrust side and 400um on average for anti-thrust side in this case. From crank angle 180 to crank angle 360, the oil accumulated in the chamfer is released, leaving a sheet of oil on the liner. Generally, the oil film left on liner behind the skirt is quite thin (as will be shown later). As described before, to simulate the oil splash, the model adds 1um oil uniformly to the liner once the piston reaches TDC. Then from crank angle 360 to crank angle 540 which is the second down stroke, the oil on the liner is less than 20um, so the amount of oil accumulated is less than the first down stroke. From the figure, it can be seen that the initial condition becomes less important as time goes and after 3-4 cycles, the results seems to converge.

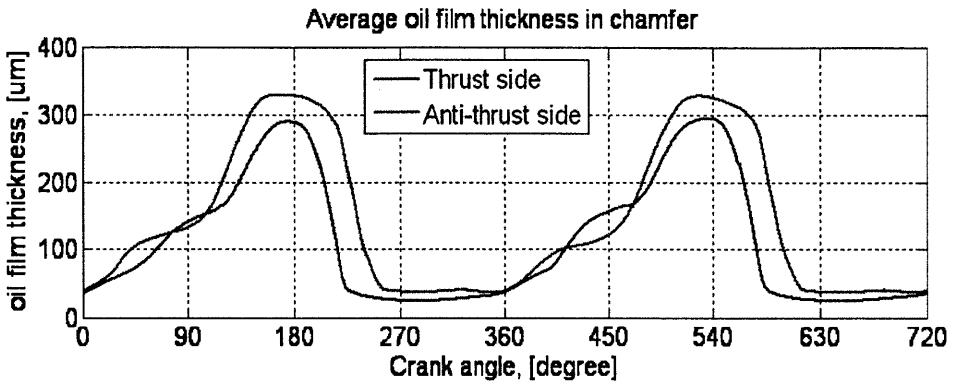

Figure 5-21: Average oil film thickness in chamfer for the 6th cycle: 3500 rpm 700 mbar

In order to examine the situation for a single cycle, Figure 5-21 shows the average oil film thickness for the 6^{th} cycle. The most noticeable pattern is the oil accumulation during down stroke and oil release during early up stroke. Firstly, we can see from TDC to BDC, the chamfer region can accumulate a big oil puddle. The following rough estimate can give some idea. For this engine with 86mm stroke and 2mm chamfer length, then 5um average oil being scraped will give 215um average oil film thickness in chamfer. Then as the piston move upward from BDC, this thick oil puddle will be released from chamfer to the lower skirt region. The result shows that the main oil release from chamfer occurs quite fast. Since the oil release schemes considered in the model are the inertia driven flow out of chamfer and the possible oil dragged by liner when the oil puddle touches the liner, this results is consistent with the model assumptions. The inertia effect is significant when the piston acceleration is large and the oil film is thick, both of which occur near BDC. As piston passes mid-stroke, inertia changes direction and will not drive oil to flow downward to skirt region. Also, the oil film thickness in chamfer during this period is small, hence not able to touch the liner and being dragged by the liner surface. So after mid-stroke during up stroke, the oil supply from chamfer to the skirt lubrication region is limited. From the figure we can see the amount of oil contained in the chamfer is almost constant after mid-stroke during up stroke. Nevertheless, the so called bridge effect can potentially provide some oil to the lower lubrication region, as observed

from the 2D LIF experiments. This process happens as the oil film in the chamfer is pushed toward the oil control ring by inertia, spread along the oil ring, and bridged to the liner. Once the oil can reach the liner, it can enter the skirt lubrication region later on as piston skirt comes. In the current model, the bridge effect is modeled very roughly. Namely, all the oil passing north boundary (the boundary between oil control ring and chamfer) driven by inertia is put on the liner below the oil ring. So while the total mass is maintained, the timing and rate may be not correct.

Another interesting point shown in the figure is the different oil release timing for thrust side and anti-thrust side. For example in this case during compression stroke, while at thrust side the oil release from chamfer happens between BDC and around 225 degree crank angle, the oil release from chamfer at anti-thrust side happens between BDC and around 260 degree crank angle, lasting a much longer period. This difference comes from the piston secondary motion. Around BDC, the piston shifts from thrust side to anti-thrust side, and it will stay on anti-thrust side moving upward until mid-stroke. Then clearly the clearance between the skirt and liner at thrust side is larger than that of anti-thrust side. As a result the oil puddle released from chamfer is harder to pass through the skirt region and can thus be held for longer time.

As described before, during down stroke, the piston slides over the liner below it and the oil film on the liner area below skirt defines the inlet oil boundary condition for skirt lubrication region. So it might be interesting to see how much oil is available there on the liner. One part of the oil on liner area below skirt comes from splash, which is assumed to be uniformly 1um everywhere in this example, although further study may be necessary in the future. The other part is the history left from previous up stroke, and this part may deserve detailed analysis. Figure 5-22 shows the average oil film thickness left on the liner below skirt for the central 40 degree along circumfenrential direction, when the piston arrives TDC at the start of the 6th cycle. This is the history left on liner from previous exhaust stroke. As shown in the figure 5-23, the vertical position of the liner measures from the top, with TDC indicates the location of skirt bottom line when piston is at TDC and BDC indicates the location of skirt bottom line when piston is at BDC.

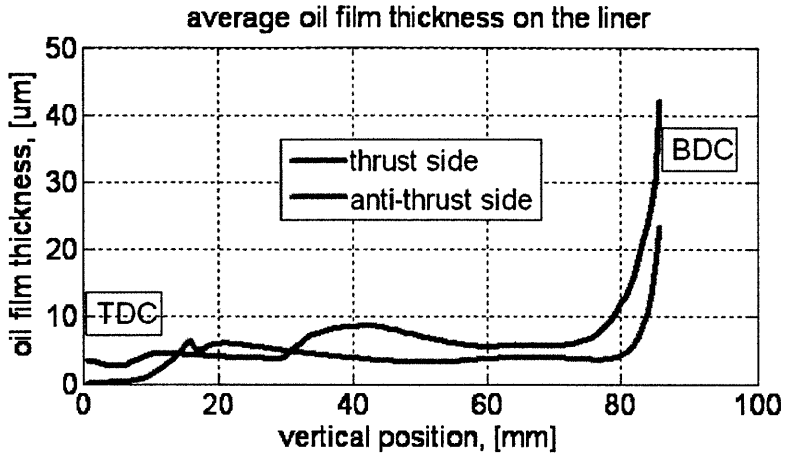

Figure 5-22: Average oil film thickness on liner area below skirt at TDC of intake

Generally, during the whole down stroke from TDC all the way to BDC, when the nominal clearance is small, not only the oil ring scrapes oil, the piston skirt in some sense can also scrape oil near its minimum clearance point. As the skirt slides down, hydrodynamic pressure generates around the minimum clearance point and will prevent oil to flow through. Then oil puddle may be accumulated before the minimum clearance point. Although due to piston lateral motion and tilt, the minimum clearance point may change location and makes the situation more complex, its still safe to say if oil film on liner below skirt is larger than the minimum clearance then some oil will accumulates on the lower portion of the skirt before the minimum clearance point. So near BDC, generally there is quite thick oil film (almost full film in this case) on the lower part of skirt both for thrust side and anti-thrust side, as can be observed from the 2D LID results. Then when piston moves up after BDC, the skirt may leave a thick oil film on the liner behind it. This explains the shape of figure 5-22 near BDC.

During early exhaust stroke, as the piston move upward from BDC, oil puddle in chamfer flows down to skirt region under inertia. Note that the oil control ring generally only leaves a very thin oil film (generally less than 0.5um, and assumed to be 0 here) on the liner, so unless there are full attachment region where the oil can be dragged by the liner, the liner will be quite dry. Around BDC the oil puddle in

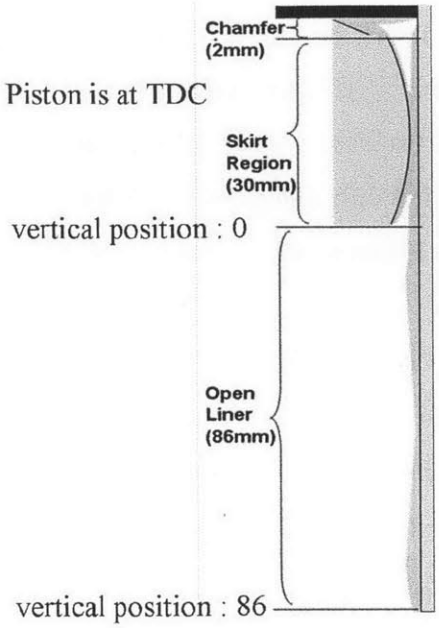

Figure 5-23: Liner area below skirt

chamfer is generally quite thick and oil film thickness can reach more than 200um. Due to piston secondary motion the piston is pushed onto anti-thrust side during early exhaust stroke, so the clearance of upper skirt area for anti-thrust side can be filled fully by the oil from chamfer, forming full film there. Then the oil puddle held on upper skirt region of anti-thrust side is gradually dragged away by the liner as the liner passes by, leaving a sheet of oil on the liner. As a result, in figure 5-22 we can see for anti-thrust side, as skirt passes over, it leaves an almost uniform oil film on liner until around 15mm below TDC position. The reason why the average oil film thickness on liner near TDC position is very small can be seen as follow. After mid-stroke the piston shifts to thrust side so the clearance between skirt and liner for anti-thrust side increases, also the oil puddle held on upper anti-thrust side skirt has already been released a lot, so in this case at around 15mm below TDC position it is no longer possible to form full film region between skirt and liner at anti-thrust side and hence the liner becomes quite dry.

The situation for thrust side is different. During lower exhaust stroke, the clearance at thrust side is relatively big. So it allows a thicker oil film to pass through

the skirt and will leave a thicker oil film on thrust side liner than anti-thrust side, as shown in figure 5-22. However, this also means the oil puddle on upper skirt region is consumed faster for thrust side. After mid-stroke, piston moves back to thrust side. Then for thrust side not only the oil left on liner is less, the minimum clearance through which oil can pass is also smaller, so the upper portion of the liner has thinner oil than the lower portion.

Figure 5-24 shows the average oil film thickness left on liner at the TDC of expansion stroke for the 6_{th} cycle. It represents the history of previous compression stroke. For this high speed case, the compression stroke is very much like the exhaust stroke and the two also have similar results.

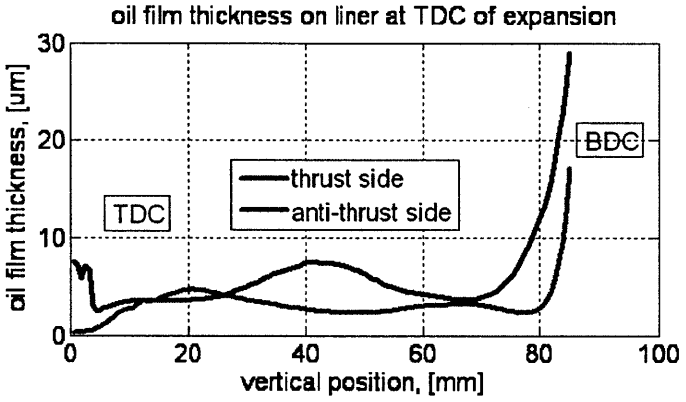

Figure 5-24: Average oil film thickness on liner area below skirt at TDC of expansion

The oil distribution within the system may be far from uniform, especially between the skirt liner interfaces. The anti-thrust side will be analyzed first. At BDC of intake stroke, due to skirt down scraping, the oil film thickness at the lower skirt area is generally very thick, or even fully flooded. On the other hand, the upper skirt area generally does not form full film region. The oil film distribution between skirt and liner for anti-thrust side at BDC of intake stroke is shown in figure 5-25. Then the oil puddle pours down from chamfer and gradually forms full film on upper skirt region. Figure 5-26 shows the oil distribution at 240 degree crank angle. Then as skirt moves up over the liner, at full film area half of the oil is dragged away by the liner as assumed in the model, a thick oil film is also left on the skirt surface. Figure 5-27

shows the process.

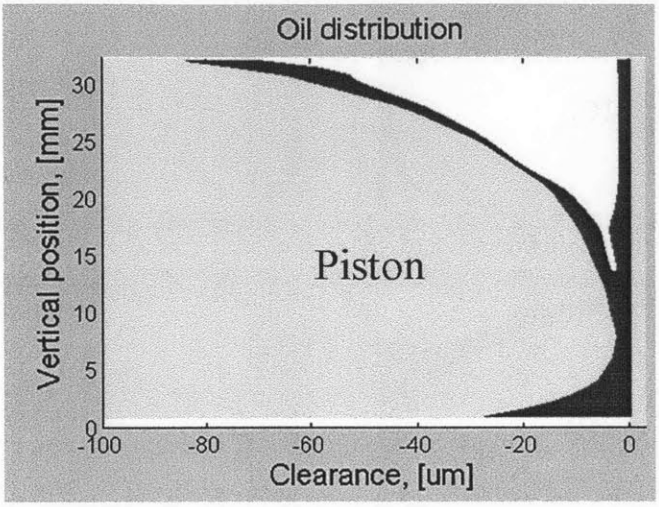

Figure 5-25: Oil film distribution for anti-thrust side at BDC of intake stroke

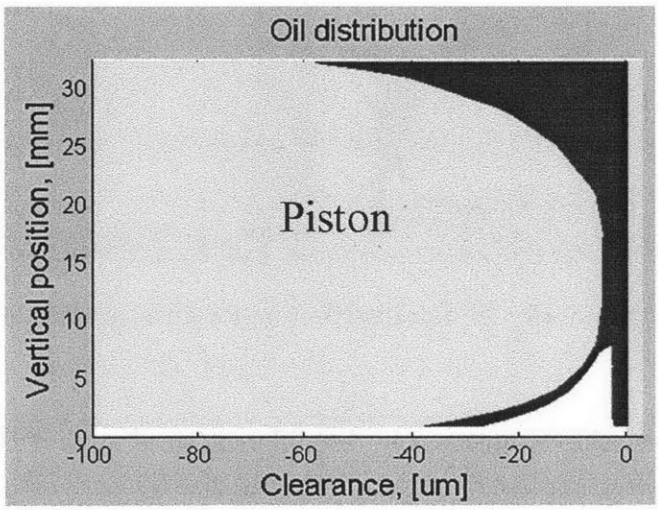

Figure 5-26: Oil film distribution for anti-thrust side at 240 degree CA

The situation for thrust side is more complex. Since during lower compression stroke, the clearance at thrust side can be much larger than anti-thrust side. It may or may not be able to form full film region at upper skirt area. Generally the story can be like this. Within the chamfer, the oil puddle is driven by inertia to flow down and may touch the liner surface. Then the liner surface will drag a big oil puddle with it. Unlike anti-thrust side where full film will be formed on upper skirt area

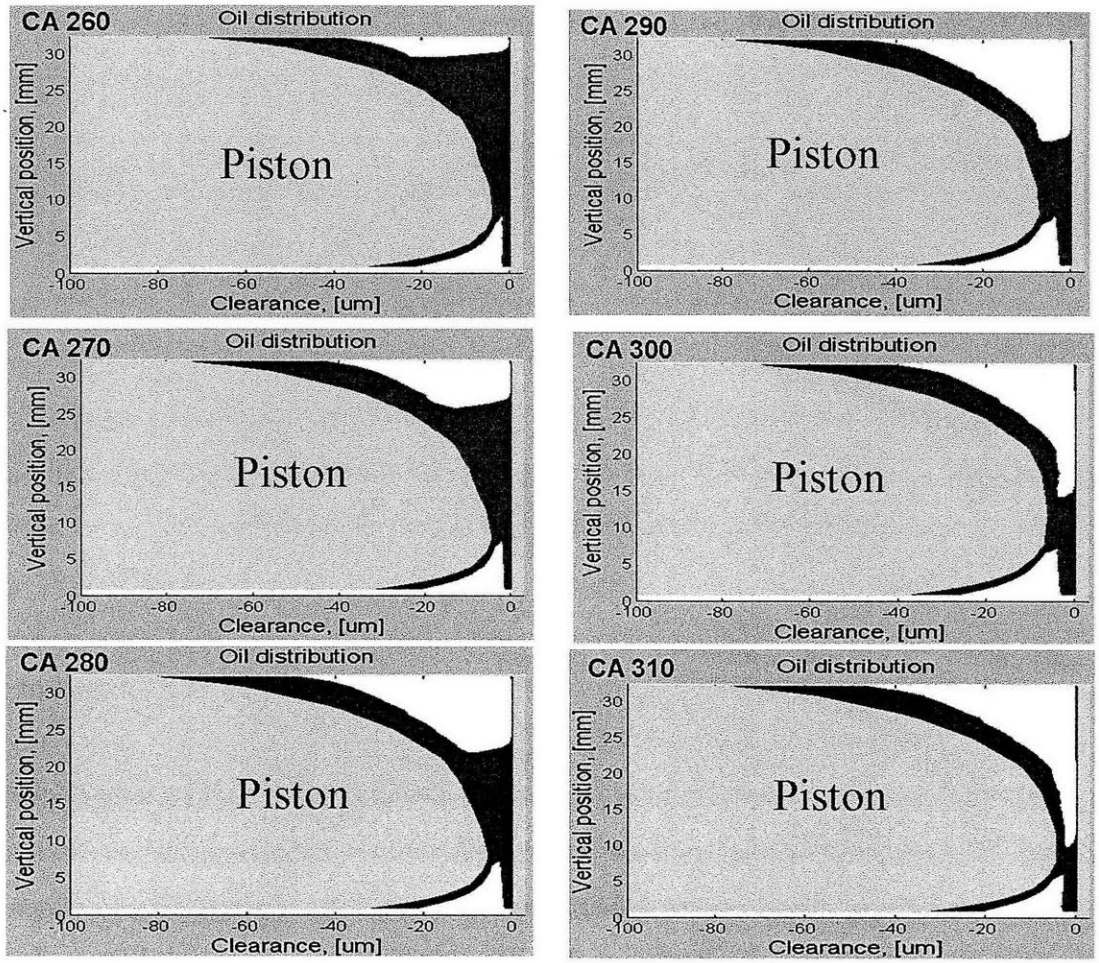

Figure 5-27: Oil film distribution for anti-thrust side

very quickly, thrust side situation may be different since around BDC the skirt is leaving the liner at thrust side. Figure 5-28 shows the oil distribution of thrust side at 220 degree crank angle. Notice the oil puddle dragged by the liner. If it can touch the skirt, it will transfer some oil to the skirt surface. Otherwise, it will move with the liner. In some sense it might be beneficial to transfer some oil from liner to upper skirt area since as the skirt moves upward there is a long distance to go before it reaches TDC. This figure also shows one important parameter that may deserve further study. As described in previous chapter, in the model even in partial film region, each local control volume can be divided into two types, either separated or fully attached, depending on local status such as oil fraction ratio. So by changing

the corresponding criterion we can change the location where full attachment between skirt and liner starts. This will in turn change the results of oil transfering from liner to skirt.

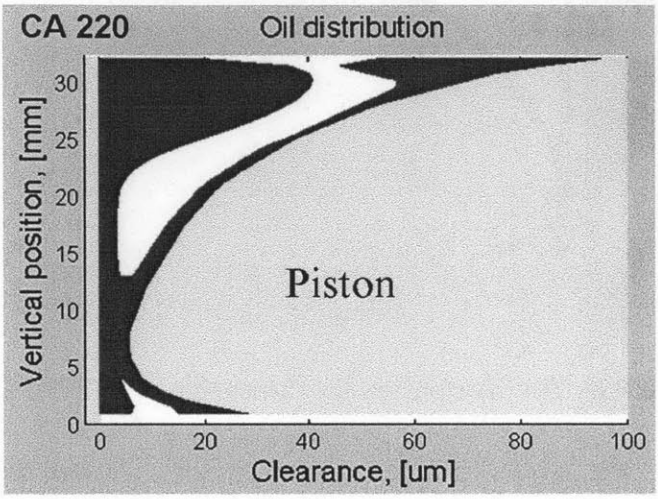

Figure 5-28: Oil film distribution for thrust side at 220 degree CA

From mid-stroke to TDC the lubrication situation can be tough. As dicussed before, there is no oil supply except for possible bridge effect during this period. For this high speed case, inertia component dominates and pushes piston onto thrust side. Then thrust side skirt will constantly losing oil to the liner as it passes by. When the skirt approaches TDC, the on film thickness on skirt can be limited. Figure 5-29 shows the oil distribution of thrust side at TDC of expansion stroke. And figure 5-30 shows the process in between. Also note that from the figure some unsmooth zigzag shape shows up. This is caused by the explicit method used in the model when determining the local status. Further treatment may be necessary in order to obtain smooth result. One drawback of the current treatment is it may cause jump in local status due to numerical scheme while real transition may be smooth.

Since friction may be a problem during expansion stroke. It may also be interesting to examine the oil distribution evolution during this period. Since throughout expansion stroke the skirt is pushed hard onto thrust side, we will focus on thrust side as well. The first part of expansion stroke is characterized by the "piston slap", ranging from TDC to around 390 degree crank angle. During this process, the skirt

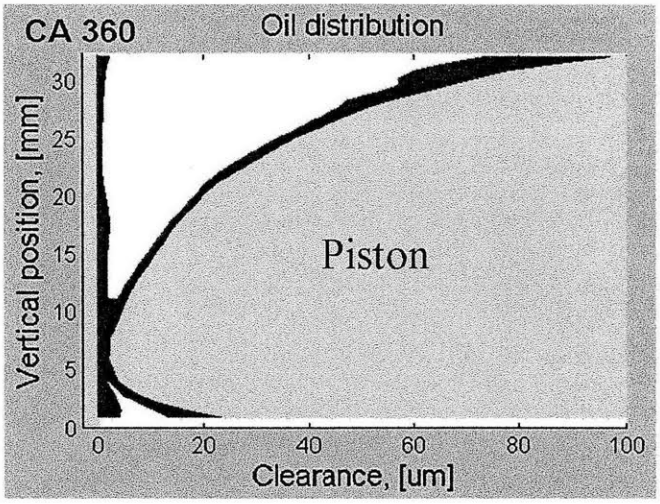

Figure 5-29: Oil film distribution for thrust side at TDC of expansion

rotates along its bottom and goes against the liner and eventually find a stable position along the liner. Figure 5-31 shows the oil distribution at thrust side during the slap process. Since the piston sliding speed is very small near TDC, the hydrodynamic pressure is mainly generated due to squeezing effect. Here we can see the effect of the surface waveheight. If the waveheight is large relative to the film thickness, it will be more likely to have solid-solid contact, giving larger frictional force. Another thing needs mentioning is the oil accumulation below the minimum clearance point. As the full film region below the minimum clearance point gets larger and piston speed becomes bigger, hydrodynamic pressure generated there also gets larger, helping lift the skirt. After around 390 degree crank angle, the piston finds a stable position on the liner and moves downward. During this period, the minimum clearance point is at upper skirt region and the oil accumulation below it is quite obvious, as shown in figure 5-32. The same results are observed from 2D LIF engine as well.

To sum up, the results show clear oil accumulation within chamfer during down stroke. During lower upstroke, the oil puddle in chamfer is released quickly to the skirt region. For thrust side which has large clearance between skirt and liner, the location where fully attached region starts may depend on the model specified criterion. Nevertheless, large clearance means thick oil film can pass through the skirt region and leave a relatively thick oil film on the lower portion of liner. As the piston moves

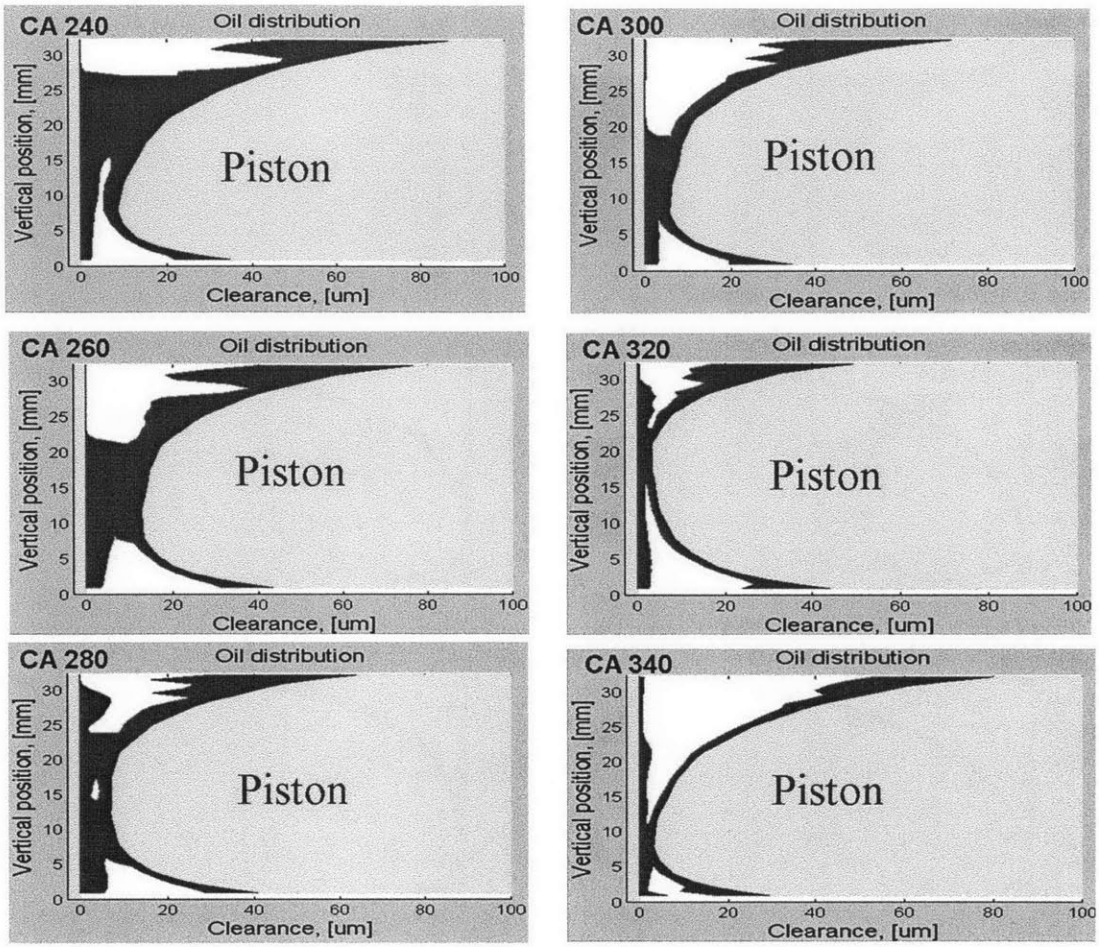

Figure 5-30: Oil film distribution for thrust side

upward and the oil puddle gets consumed along the way, the oil film thickness on thrust side skirt gradually gets smaller and the oil film left on liner also gets thinner. On the other hand for anti-thrust, since the clearance is small at lower up stroke, the oil pouring out from chamfer can flood the upper skirt area. The oil puddle held on upper skirt region is then gradually dragged away by the liner, leaving a sheet of oil film on the liner until the full attachment area disappears as piston approaches TDC.

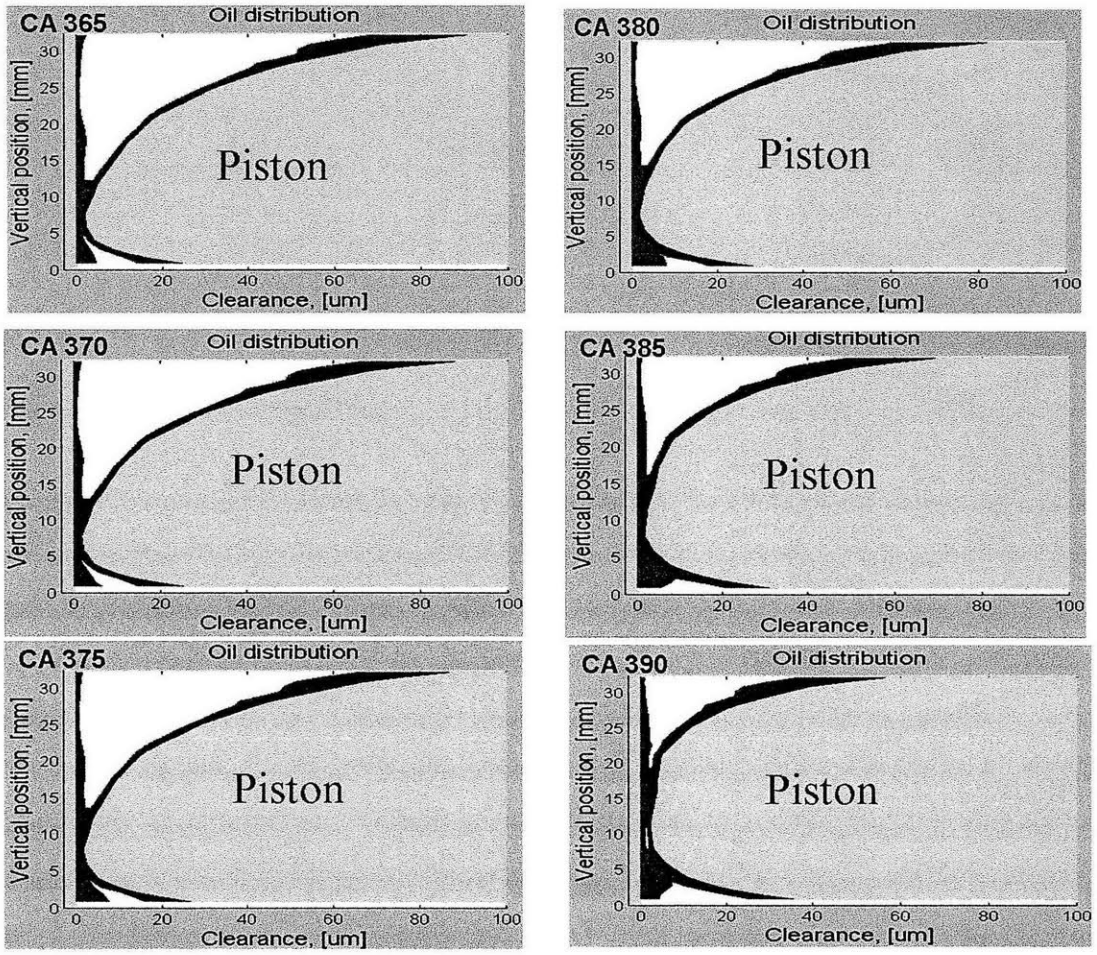

Figure 5-31: Oil film distribution for thrust side during piston slap

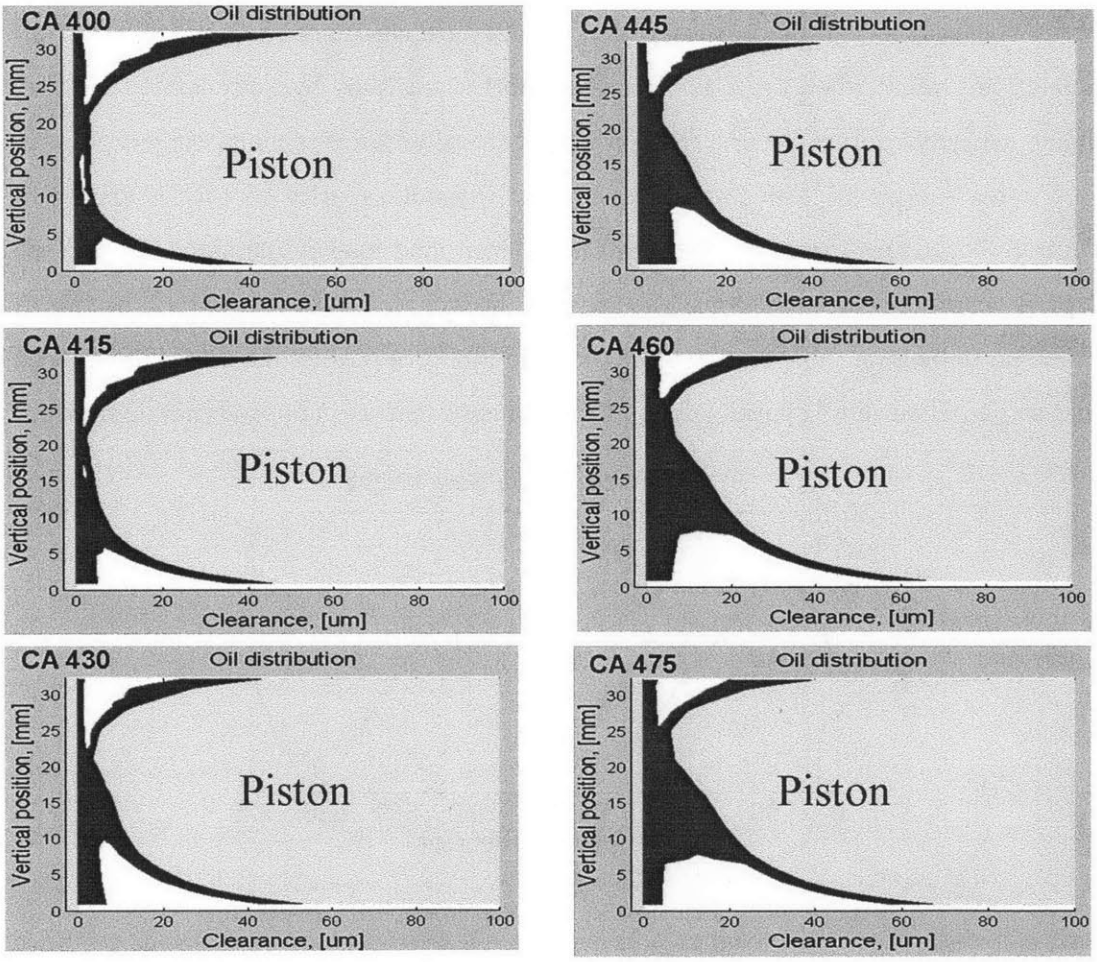

Figure 5-32: Oil film distribution for thrust side during expansion

5.3 Friction and Asperity Contact

The friction includes two components, the hydrodynamic part and the asperity contact part. In the current model, the friction coefficient for asperity contact is a parameter chosen by model user, and is 0.1 by default. The friction coefficient for hydrodynamic part is generally much smaller than 0.1, except at near contact area where shear stress can be quite big due to small local clearance. So generally friction is relatively small when the side force is supported solely by hydrodynamic pressure. When asperity contact occurs, friction force generally becomes much bigger.

First a sample friction force trace almost without asperity contact is shown in figure 5-33. In this example, the speed is 3500rpm and load is 700mbar. To prevent asperity contact from happening, the waveheight is chosen to be 0.1um and the splash is chosen to be 2um. The figure shows that friction force reaches maximum value near mid-stroke when sliding speed is big, which is a clear feature of hydrodynamic friction.

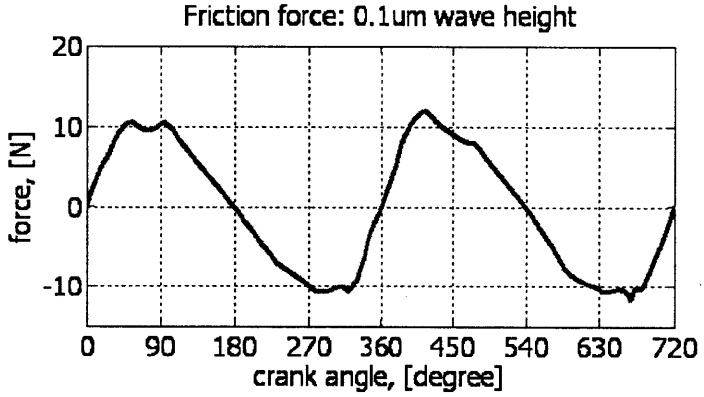

Figure 5-33: Friction force with no asperity contact

It is interesting to see when asperity contact will occur, that is when hydrodynamic pressure force is not enough to support the load. Intuitively reducing oil supply will tend to give more asperity contact. This point will be illustrated in next section. Another important parameter is the surface waveheight. Figure 5-34 shows a frictional force trace where asperity contact occurs. The speed is 3500rpm, load is 700mbar, splash is 4um and nominal clearance is 10um. From the figure we can see initially as the wave height increaess from 1um to 5um, the friction force almost stays the

same, having almost no asperity contact. When the waveheight is 8um, the result shows a lot of asperity contacts, especially during early expansion stroke. The reason is during piston slap, as discussed in previous section, the only oil available is the oil originally between the skirt and liner. For this case where the skirt is on the thrust side for upper compression stroke, the thrust side skirt has become quite dry as it approaches TDC. Then during piston slap, the surface wave penetrates the oil film and thus solid-solid contact occurs, giving high friction.

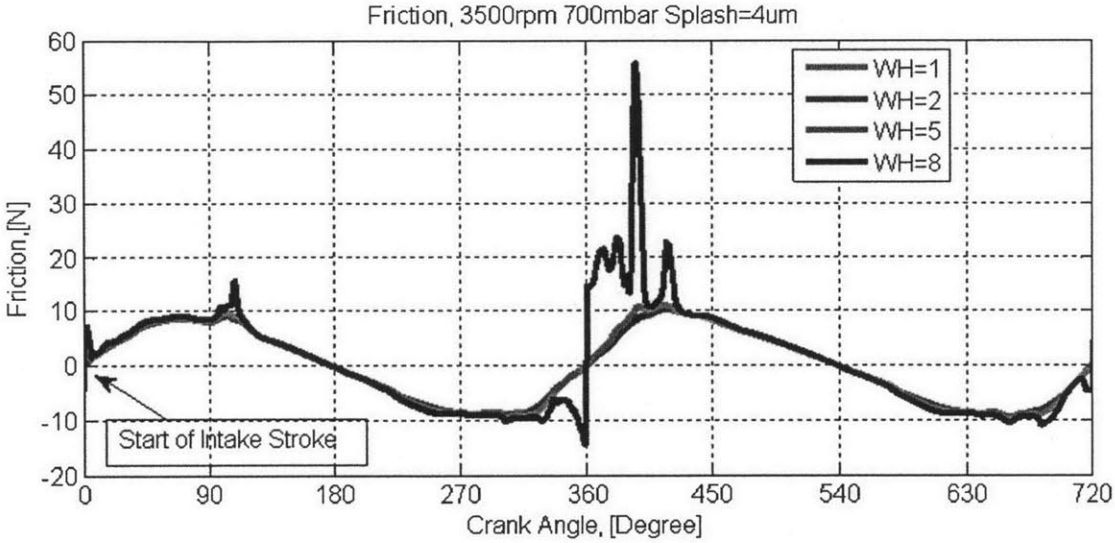

Figure 5-34: Friction force with different wave height

5.4 Parametric Study

This section illustrates the effects of some interesting parameters. These parametric studies are also aimed at further validating the model.

5.4.1 Structural Compliance

The structural deformations of the skirt and the liner make the model much harder to solve. Hence it deserves to see how they can influence the results.

Figure 5-35 shows the effect of skirt structural compliance. For this example, the liner is assumed to be rigid. In this example, the results of three skirts with different structural compliance are illustrated. Skirt 1 is rigid with no deformation. The other two skirts are soft with one skirt (skirt 3) being softer than the other one(skirt 2). All the other parameters are the same. The upper left panel shows the piston lateral displacements for these three cases. It is easy to see that softer skirt will give larger lateral movement, since the lateral movement includes skirt deformation as part of it.

The upper right panel shows the thrust side skirt deformations for the two soft skirts at 380 degree crank angle. We can see the central lower region of the skirt is softer and due to this deformation, the skirt will have a large area that can interact with the liner. The lower panel shows the corresponding hydrodynamic pressure distributions at 380 degree crank angle for these three cases. Note that the side forces for all the cases are the same. The left figure shows the result of skirt 1. Due to skirt ovality and barrel shape, only the center area of the skirt is able to interact with the liner and generate hydrodynamic pressure. The middle figure shows the result of skirt 2. This skirt deforms in the middle and hence allows a larger area of pressure generation. The right figure shows the result of skirt 3. This skirt has such a big deformation in the center area that the minimum clearance points actually occur at the sides. Hence there are two peaks of the hydrodynamic pressure as shown in the figure. Since the total force being carried is the same, as the skirt gets softer, there are larger areas that can generate hydrodynamic pressure and the peak pressure decreases accordingly.

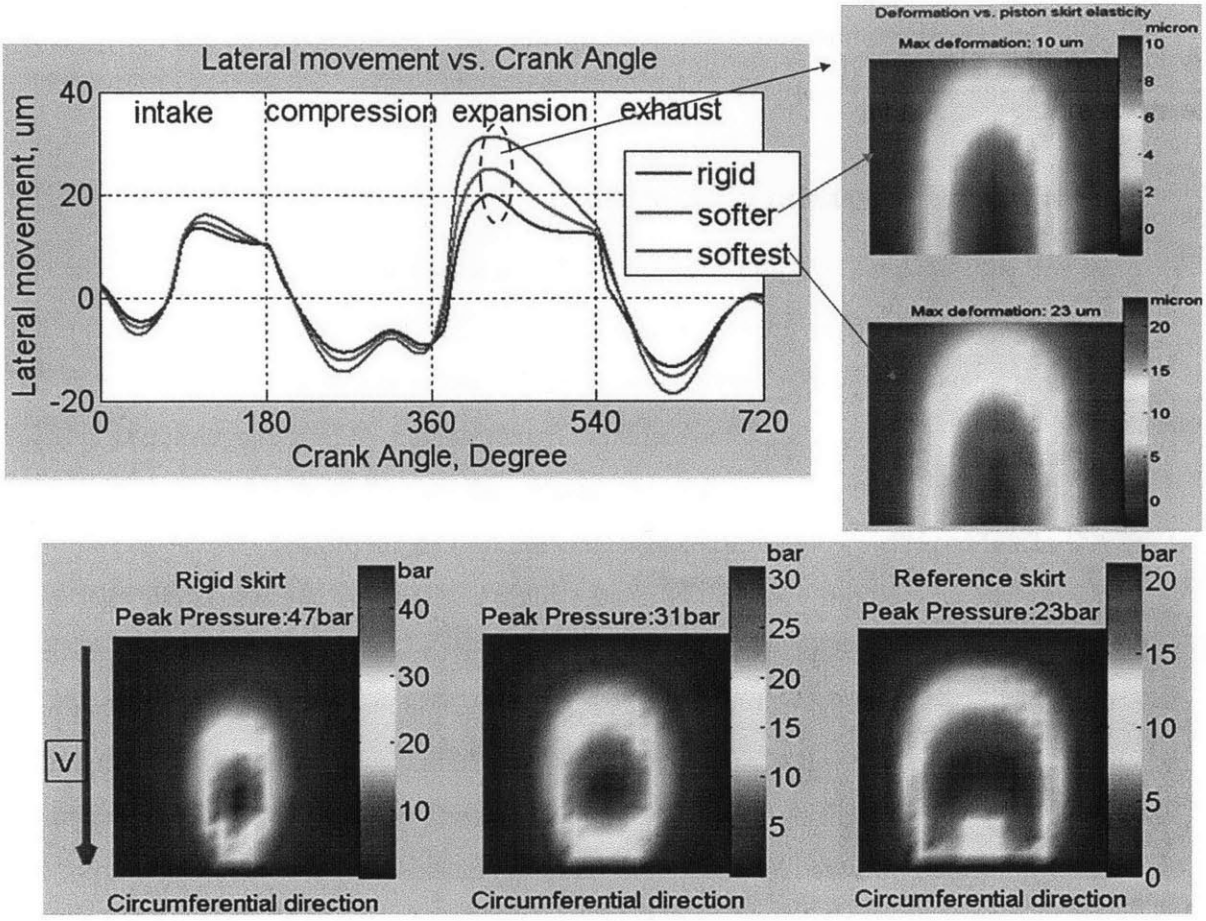

Figure 5-35: Effect of skirt structural compliance

The effect of the liner compliance is similar. Generally, the structural compliance of the surfaces allows the two surfaces to conform better. On the other hand, the piston lateral displacement also increases since there is more room to move.

5.4.2 Speed and Load

As described before, the side force acting on piston from the pin increases as engine speed increases. So higher speed increases the side force for intake stroke, exhaust stroke and the lower portion of compression stroke. On the other hand, higher engine load will increase the side force during expansion stroke, pushing piston harder to the liner. For heavy duty diesel engine, the load is so high that during the whole compression stroke the piston is pushed on the anti-thrust side.

The competition of speed and load during upper compression stroke has already been discussed in previous sections.

5.4.3 Oil Boundary Condition

For skirt lubrication, the oil boundary condition is very important. With sufficient oil, solid-solid contact may not occur and friction will be low. With limited oil, asperity contact may happen and contributes both to friction and wear. Also, the trade-off between friction, wear and noise should be considered. Thus, the difficulty lies in that with such a large skirt how to supply sufficient oil to the desired area while maintaining proper control of oil consumption and engine noise.

As the skirt slides over the liner, the inlet boundary is the bottom of the skirt during down stroke and the inlet boundary is the top of the skirt during up stroke. As a starting point, we will do a parametric study, assuming we can supply whatever amount of oil at the inlet boundary as we wish. To make the scenario simple enough, we assume at the inlet boundary, we supply the same oil film thickness along circumferential direction. We also assign the same boundary oil film thickness both for up stroke and down stroke. Figure 5-36 shows the model predicted frictional force with different boundary oil film thickness(OFT). As expected, the friction reduces with more oil supply. And when the boundary oil film thickness is sufficiently large, it's effect on friction becomes small.

Figure 5-37 shows the effect of oil boundary condition on piston secondary motion and pressure generation. The upper panel shows the piston lateral displacements with three different boundary OFTs. First, with more oil supply, the lateral displacement becomes smaller. It is reasonable since thicker oil between the skirt and liner allows the skirt to move less. Also, when oil supply becomes very thin, a lot of oscillations can be seen from the figure. As expected, the oil film has a cushioning effect, reducing oscillations and making the piston secondary motion smoother. The lower panel shows the thrust side pressure generated between the skirt-liner interface at 380 degree crank angle. For this example, both the 5um OFT supply and the 25um OFT supply gives purely hydrodynamic pressure generation. The 25um OFT case has a large area of

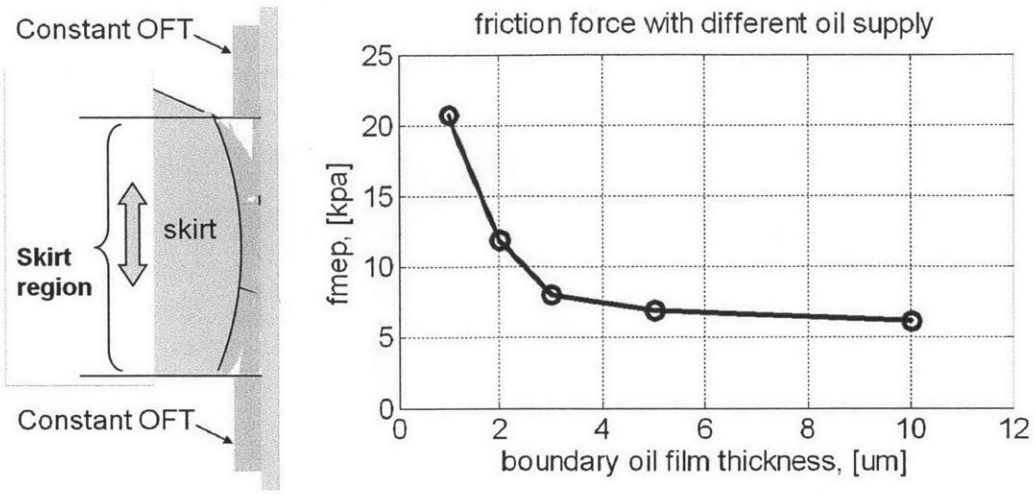

Figure 5-36: Effect of OFT on friction

pressure generation and thus smaller peak pressure. For 1um OFT supply, it can be seen that asperity contact actually occurs.

The amount of oil supply also affects the piston tilt angle. Figure 5-38 illustrates the snapshot of the model predicted piston position and pressure generation between the skirt and liner during late expansion stroke. The crank angle is 450 degree. Still, the blue lines are the liner, the black lines are the skirt position without deformation and the red lines are the actual deformed skirt position. We can clearly see how the oil supply can affect the tilt. With more oil supply, there are more oil coming into the skirt-liner interface from the bottom inlet boundary. The thicker the oil supply, the easier to generate hydrodynamic pressure and lift the skirt. So in this example, while the 1um OFT supply gives almost zero tilt angle, the 10um OFT supply gives a quite negative tilt angle.

The parametric studies above indicate that the oil boundary condition can significantly change the lubrication situation. However, it does not answer the question of how to determine the oil boundary condition. In a real engine, it may be very hard to have desired oil supply. As described in chapter 3, during down stroke, the bottom of the skirt is the inlet boundary and the amount of oil supply is determined by the oil film thickness on the liner before skirt, which may depend on the detailed features of splash and/or oil cooling jet. During up stroke, the oil supply comes from the

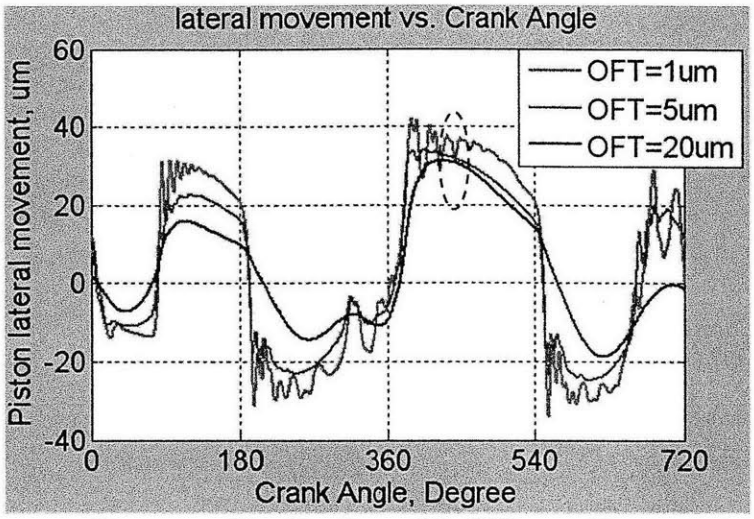

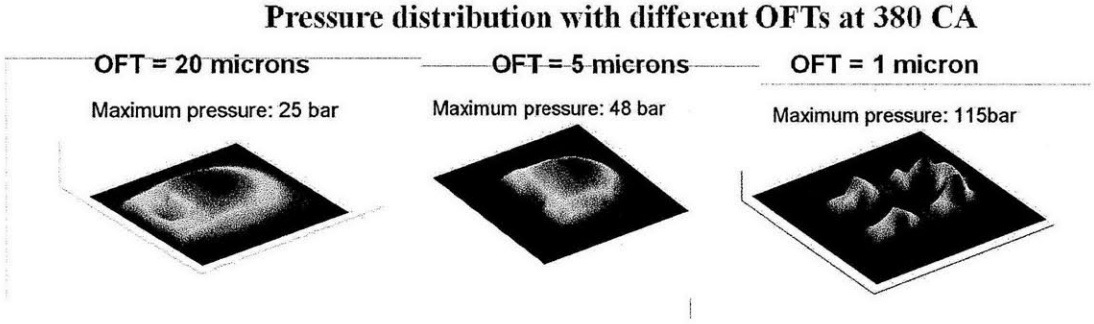

Figure 5-37: Effect of OFT on piston lateral displacement

skirt chamfer. In the example below, instead of arbitrarily assign the boundary oil supply, a more realistic treatment is applied. The oil transport between the skirt and its surroundings are included in to model in order to properly define the oil boundary condition for the skirt region. In this treatment, there is a chamfer oil release model that supplies oil to the skirt region during upstroke, as described in chapter 3. And during downstroke, the inlet oil boundary condition is determined by the oil left from previous upstroke and the splash. In this example, the splash is assumed to be uniformly distributed on the liner.

Figure 5-39 illustrates the model predicted friction with different splash and nominal clearance. As expected, with more splash, friction decreases. It is also interesting to see that in this range the friction decreases as nominal clearance increases. It is reasonable since generally tighter clearance means more likely to have solid-solid

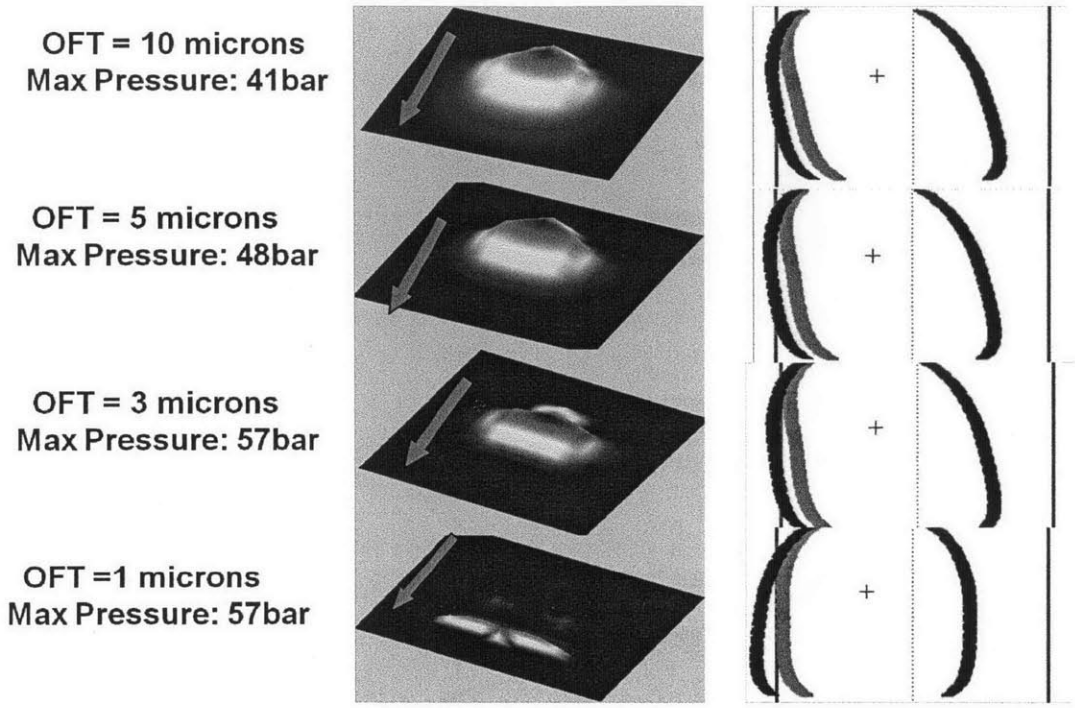

Figure 5-38: Effect of OFT on piston tilt

contact and more likely to have forces on both sides.

5.4.4 Waveheight

The tooling marks on piston skirt make the surface rougher. The wave height of the tooling marks affects how easy solid-solid contact may occur. Generally speaking, larger wave height means more likely to have asperity contact and leads to larger friction, as shown in figure 5-40. Other parameters for this example are: 4um splash to the liner and 10um nominal clearance. The engine is still the two-dimensional LIF engine.

Although it is easy to see larger wave height generally gives larger friction, the exact wave height may be hard to determine. Since the coating material are usually soft and aims at break in, the wave height is not a constant. And the wave height for different region of the skirt may be different as well. At regions where contact happen, the wearing process may remove the peaks of the tooling marks and make the surface smoother.

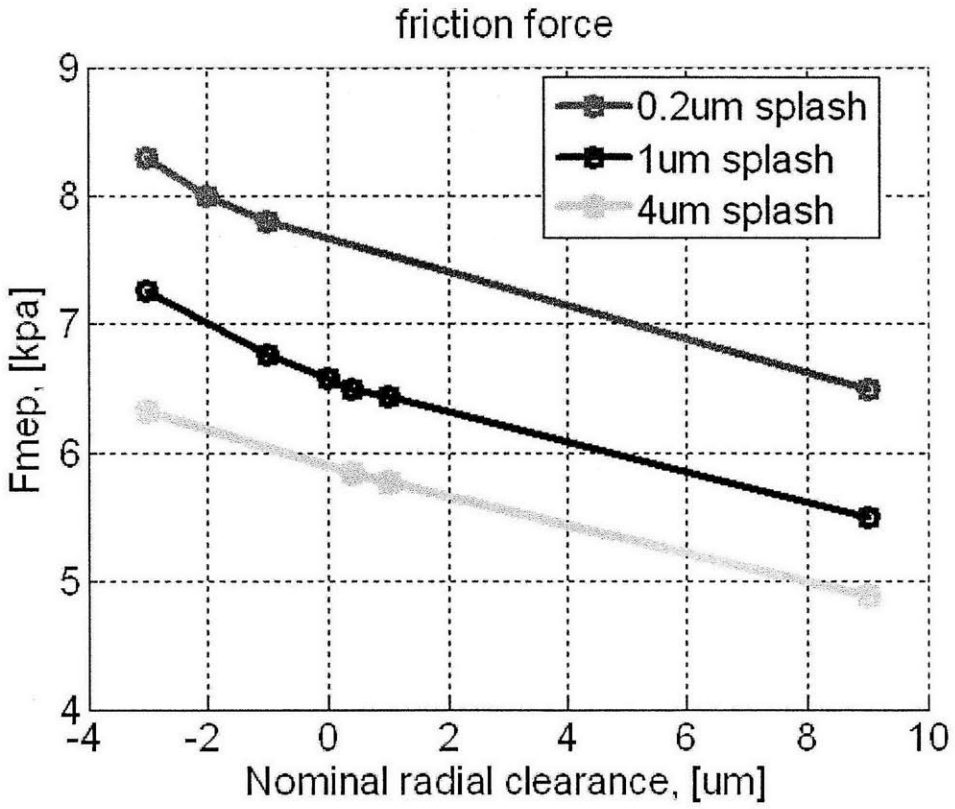

Figure 5-39: Friction with different splash and nominal clearance

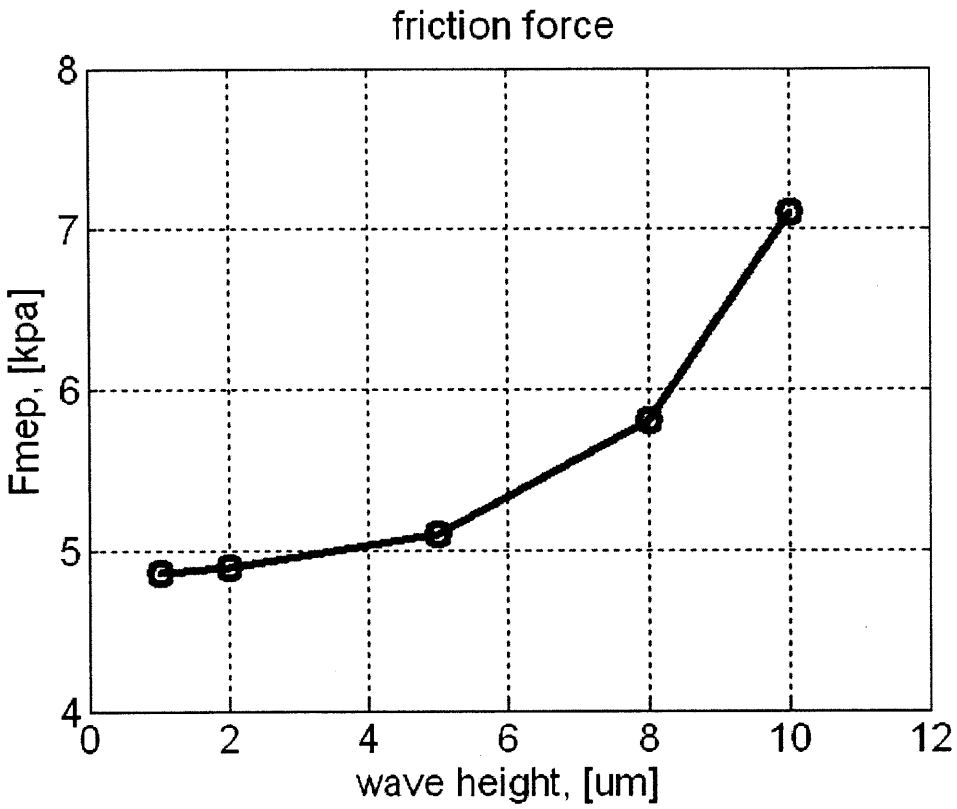

Figure 5-40: Friction with different waveheight

5.5 Direct Simulation Method

To consider the effect of micro surface geometry such as surface tooling marks, two methods can be applied. One way is to use average Reynolds Equation which uses flow factors to estimate the effect of surface micro structures on lubrication flows. The other way is to directly capture the surface waves by using very fine grid. Although the direct simulation method may be time consuming, in theory it is capable to capture the local features at near contact region such as inter-asperity cavitation and might be able to give more accurate estimation of friction at near contact region than average method. Since the average method can not capture the local geometry, it can not get the local pressure precisely. Figure 5-41 shows a snapshot of the inter-asperity cavitation predicted by direct simulation method during piston slap at 380 degree crank angle. In this case, due to the presence of surface tooling marks and thin oil film, cavitation occurs between the surface waves.

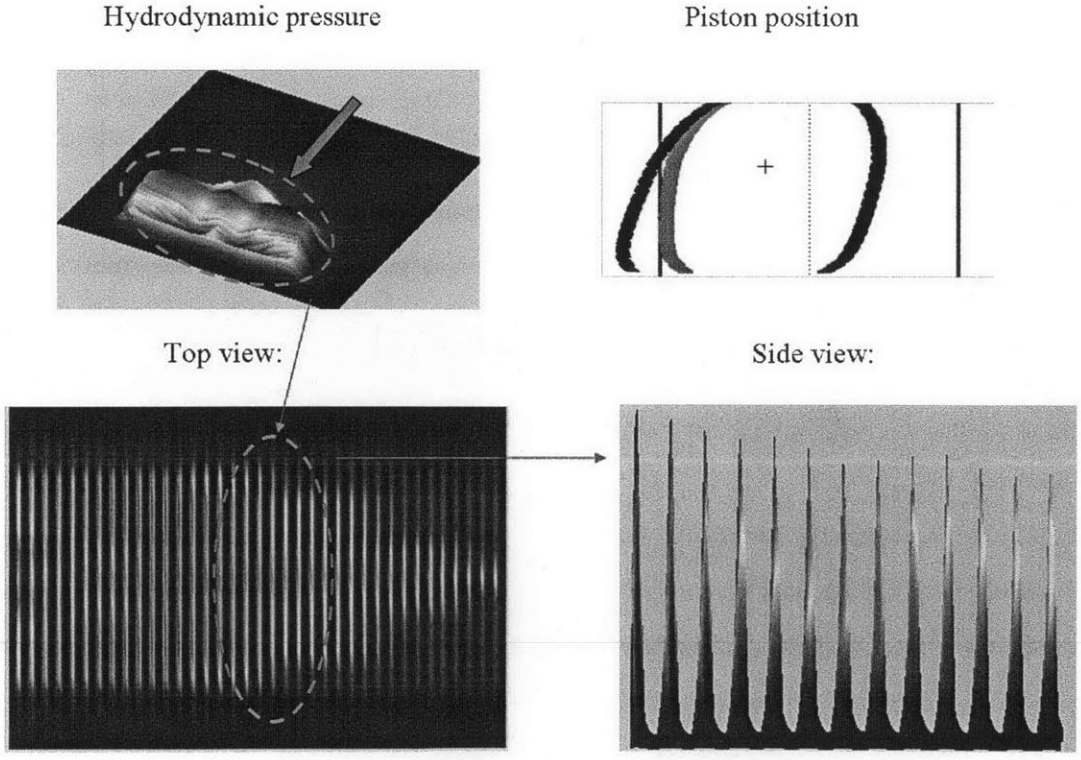

Figure 5-41: Inter-asperity cavitation predicted by direct simulation method

There is another problem of average model that can be handled better by direct simulation method. As discussed before, the hydrodynamic pressure is generated to fulfill mass conservation for each control volume. Except the squeezing effect, the hydrodynamic pressure is generated in order to balance the couette flow. At near contact region, the local clearance is very small and hence the interface conductivity is very small, thus requiring very high pressure gradient to transfer a given amount of oil mass. So at near contact region, it is possible to generate very high hydrodynamic pressure in order to balance oil mass. In reality the local curvature may be smooth and the high pressure only occurs over a small area and the resulting force is not big. However in average model the high pressure is assumed to apply for the whole control volume, and unrealistically high force may occur sometimes. This unrealistically high force will make the numerical scheme hard to converge. In some sense, this problem happens because the grid is not fine enough to capture the local clearance and pressure profile. Hence the direct simulation model seems to provide a solution, although it might be a time consuming one. From this point of view, the direct simulation method deserves further investigation.

Another potential application and improvement of the direct simulation method is the simulation of worn surfaces, since this method allows easy manipulation of surface profile. For example, if the direct simulation method predicts certain asperity contacts, then it might be interesting to see whether the solid-solid contact may disappear if the corresponding asperities are removed from the profile.

Chapter 6

Conclusions

This chapter discusses the conclusion on this thesis work. The first part summarizes the entire thesis work and the second part proposes some potential future work following this thesis work.

6.1 The Lubrication Model Developed in this Thesis Work

The piston skirt lubrication problem affects the friction, wear and oil consumption and deserves a thorough study. It involves hydrodynamic pressure generation coupled with surface elastic deformations, making the problem nonlinear. The model developed in this thesis work successfully integrates these important factors and the oil transport model. The model also proves to be robust and efficient.

To calculate the hydrodynamic lubrication, the model includes both the average method and the direct simulation method. The average method uses average Reynolds Equation with flow factors to estimate the effect of surface micro structures on lubrication flows. The direct simulation method uses very fine grid to directly capture the surface geometry. Although the direct simulation method may be time consuming, in theory it is capable to capture the local features at near contact region such as inter-asperity cavitation.

The model starts from the piston primary motion. The side force and driving moment for piston secondary motion are calculated from the dynamics and kinematics of each component of the power cylinder system. Then within the skirt-liner interface where side force and moment are mainly balanced, a lubrication solver is developed to calculate the hydrodynamic pressure generation with given boundary condition and surface geometry. To account for the situation of solid-solid contact, an asperity contact sub model is also developed which works for the case with triangular surface tooling marks. In order to properly define the oil boundary condition of the lubrication solver, the oil transport between skirt and its surroundings are studied and modeled. In the current model, the oil accumulation within chamfer due to oil control ring scraping during down stroke and oil release from the chamfer are considered. The oil exchange between skirt lubrication region and the liner region below the skirt are also included, making the main picture of oil transport complete. At the top level, a globally convergent Newton's method is applied to solve the nonlinear system. For the skirt lubrication solver, the partial film phenomenon makes the problem very complex. At partial film region the oil fraction of the partial film area needs to be resolved while at full film region the hydrodynamic pressure distribution is the unknown. The dynamics of the interface between full film region and partial film region must be properly taken care of to maintain the mass conservation. Because of the piston secondary dynamics, not only the partial film region changes with time, separation and reattachment phenomenon may also occur, further complicating the problem. In the model, a function mapping local variables such as pressure, oil fraction and clearance to local state is proposed to handle these phenomena. Then the corresponding equations are constructed based on mass conservation. With this physics-based algorithm, the model provides more realistic description of the lubrication situation.

6.2 Piston Dynamics and Oil Transport

The piston lateral movement is essentially driven by the combination of inertia component and combustion pressure component. This point is interestingly illustrated by

the competition of the two components during late compression stroke, with inertia driving piston to thrust side and combustion pressure driving piston to anti-thrust side.

The main oil transport can be characterized by oil accumulation in piston chamfer during down stroke mainly due to oil ring scraping, and oil flowing out from chamfer to lower skirt region during early up stroke due to inertia. After the whole down stroke, the piston chamfer contains a thick oil puddle at BDC. Although inertia tends to drive oil out of chamfer even at lower down stroke, the liner moves upward relative to the skirt and tends to drag the oil back to the chamfer. So the main oil release from chamfer is more likely to happen during lower upstroke. The oil puddle tends to flood the upper skirt region. Then as the skirt moves upward, sliding over the liner, it will also leave a sheet of oil on the liner. The oil film thickness left on liner may depends on the minimum clearance through which the oil passes and the availability of oil. For anti-thrust side, the clearance between skirt and liner is small due to piston secondary motion; hence the oil film left on the liner is generally relatively thinner. On the other hand, the oil puddle held on upper skirt area of anti-thrust side is consumed slower. So it may leave an oil film on the liner to a higher position.

6.3 Future Work

There are several opportunities for improvement to the thesis work. The model predictions can be further compared with the floating liner engine measurements. Of course such comparison is challenging since it is hard to make sure the model and the test engine have the same running parameters. And it may need careful analysis and thinking to interpret the result. Nevertheless, such comparison can help gain better understanding of both the model and the experiment.

Another potential topic is the asperity contact model. The current model assumes the surface tooling mark to be horizontal with triangular shape. While this is usually the case, nowadays there are people interested in more complex surface micro profile. For example, with different angle, the surface tooling marks may change the oil

transport on skirt.

The oil splash to the liner may also deserve further study. The model results show that the oil splashed onto the liner can directly change the lubrication situation during upper down stroke. Also, the current model does not include the oil exchange between the chamfer and the oil ring groove and the oil release from the drain hole. The development of sub models for more accurately tracking these oil transport would be very interesting and useful.

Bibliography

[1] Knoll, G.D. and Peeken, H,J, Dydrodynamic Lubrication of Piston Skirts, Journal of Lubrication Technology, Transaction of the ASME, 104, 504-509, 1982.

[2] H.G. Elrod. A cavitation algorithm, Journal of Lubrication Technology, 103(3):350–354, 1981.

[3] Patir, N. and Cheng, H.S., An Average Flow model for Determining Effects of Three-Dimensional Roughness on Partial Hydrodynamic Lubrication, Journal of Lubrication Technology, Transactions of the ASME, 100, 12-17, 1978.

[4] Zhu, D., Cheng, H., S., Arai, T. and Hamai, K., A Numerical Analysis for Piston Skirts in Mixed Lubrication. Part I: Basic Modeling, Journal of Tribology, Transactions of the ASME, 114(3), 553-562, 1992.

[5] Zhu, D., Hu, Y.Z., Cheng, H. S., Arai, T. and Hamai, K., A Numerical Analysis for Piston Skirts in Mixed Lubrication. Part II: Deformation Considerations, Journal of Tribology, Transactions of the ASME, 115, 125-133, 1993.

[6] Dursunkaya, Z., Keribar, R. and Ganapathy, V., A Model of Piston Secondary Motion and Elastohydrodynamic Skirt Lubrication, Journal of Tribology, Transactions of the ASME, 116(4), 777-785, 1994.

[7] Heywood, J. B., Internal Combustion Engine Fundamentals, McGraw-Hill, 1998.

[8] Wong, V.W., Tian, T., Lang, H., Ryan, J.P., Sekiya, Y., Kobayashi, Y. and Aoyama, S., A Numerical Model of Piston Secondary Motion and Piston Slap

in Partially Flooded Elastohydrodynamic Skirt Lubrication, SAE Paper 940696, 1994.

[9] Tripp, J.H., Surface Roughness Effects in Hydrodynamic Lubrication: the Flow Factor Method, Journal of Lubrication Technology, Transactions of the ASME, 105, 458-465, 1983.

[10] Oh, K.P., Li, C.H. and Goenka, P.K., Elastohydrodynamic Lubrication of Piston Skirts, Journal of Tribology, Transactions of the ASME, 109, 356-362, 1987.

[11] Harp, S.R. and Salant, R.F., An Average Flow Model of Rough Surface Lubrication with Inter-Asperity Cavitation, Journal of Tribology, Transactions of the ASME, 123 (1), 134-143, 2001.

[12] Payvar, P. and Salant, R.F., Computational methodfor cavitation in a wavy mechanical seal, Journal of Tribology, Transactions of the ASME, 114 (1), 199-204, 1992.

[13] McClure Fiona, Numerical Modeling of Piston Secondary Motion and Skirt Lubrication in Internal Combustion Engines, PhD Thesis, Massachusetts Institute of Technology, C.ambridge, USA, 2007.

[14] Li, Y., Multiphase Oil Transport at Complex Micro Geometry, PhD Thesis, Massachusetts Institute of Technology, C.ambridge, USA, 2011.

[15] R. S. Dwyer-Joyce, D A Green, P Harper, R Lewis, S Balakrishnan, P D King, H Rehanejat and S Howell-Smith, The measurement of liner-piston skirt oil film thickness by an ultrasonic means, SAE paper 2006-01-0648, 2006.

[16] Tesuya Kimura, Kazuki Takahashi and Shigeru Sugiyama, Development of a piston secondary motion analysis program with elastically deformable piston skirt, SAE paper 1999-01-3303, 1999.

[17] Gunter Offner, Hubert M Herbst and Hans H priebsch, A methodology to simulate piston secondary movement under lubricated contact conditions, SAE paper 2001-01-0565.

[18] S H Mansouri and V W Wong, Effects of piston design parameters on piston secondary motion and skirt-liner friction, SAE paper 2004-01-2911. 2004.

[19] Patankar, S.V., Numerical Heat Transfer and Fluid Flow, Hemisphere/McGraw-Hill, Washington DC, 1980.

[20] LinkLeVeque, Randall J., Finite-volume methods for hyperbolic problems, Cambridge, New York: Cambridge University Press, 2002.

[21] H.K. Versteeg and W. Malalasekera, An introduction to computational fluid dynamics : the finite volume method, Harlow, Essex, England : Longman Scientific & Technical ; New York : Wiley, 1995.

[22] Randall J. LeVeque, Numerical methods for conservation laws, Basel ; Boston : Birkhuser Verlag, 1992.

[23] Greenwood, J. A. and Tripp, J., The Contact of Two Nominally Flat Surfaces, Proc. Inst. Mech. Engrs., 185, 625-633, 1971.

[24] Przesmitzki Steve, Characterization of oil transport in the power cylinder of internal combustion engines during steady state and transient operation, PhD thesis, Massachusetts Institute of Technology, 2008.

[25] Bayada, G., Martin, S. and Vazquez, C., An Average Flow Model of the Reynolds Roughness Including a Mass-Flow Preserving Cavitation Model, Journal of Tribology, Transactions of the ASME, 127 (4), 793-802, 2005.

[26] Harp, S.R. and Salant, R.F., An Average Flow Model of Rough Surface Lubrication with Inter-Asperity Cavitation, Journal of Tribology, Transactions of the ASME, 123 (1), 134-143, 2001.

[27] Duyar, M., Bell, D. and Perchanok, M., A Comprehensive Piston Skirt Lubrication Model Using a Mass Conserving EHL Algorithm, SAE Paper 2005-01-1640, 2005.

[28] Dwyer-Joyce, R.S., Green, D.A., Harper, P., Lewis, R., Balakrishnan, S., King, P.D., Rahnejat, H., and Howell-Smith, S., The Measurement ofLiner-Piston Skirt Oil Film Thickness by an Ultrasonic Means, SAE Paper 2006-01 -0648, 2006.

[29] Rebecca M Hoffman, Agus Sudjianto, Xiaoping Du and Joseph Stout, Robust piston design and optimization using piston secondary motion analysis, SAE paper 2003-01-0148, 2003.

[30] Zheng-Dong Ma and Noel C Perkins, An efficient Multibody dynamics model for Internal combustion engine systems, Multibody system dynamics 2003.

[31] Patrick Ragot and Martin Rebbert, Investigation of crank offset and its influence on piston and piston ring friction behavior based on simulation and testing, SAE paper 2007-01-1248, 2007.

[32] Kenji Sato, Kinya Fujii, Makoto Ito and Shinsuke Koda, Application to engine development of friction analysis by piston secondary motion simulation in consideration of cylinder block bore distortion, SAE paper 2006-01-0428, 2006.

[33] Prashant Patel, Zissimos P. Mourelatos and Parasshah, A Comprehensive Method for Piston Secondary Dynamics and Piston-Bore Contact, SAE paper 2007-01-1249, 2007.

[34] Zafer Dursunkaya and Rifat Keribar, Simulation of secondary dynamics of articulated and conventional piton assemblies. SAE paper 920484, 1992.

[35] Benoist Thirouard, Characterization and modeling of the fundamental aspects of oil transport in the piston ring pack of internal combustion engines, PhD thesis, Massachusetts Institute of Technology, 2001.

[36] Vokac Adam, An experimental study of the oil evolution in critical piston ring pack regions and the effects of piston and ring designs in an internal combustion engine utilizing two-dimensional laser induced fluorescence and the impact on maritime economics, S.M. thesis, Massachusetts Institute of Technology, 2004.

[37] McGrogan Sean, Modeling and simulation of oil transport for studying piston deposit formation in IC engines, S.M. thesis, Massachusetts Institute of Technology, 2007.